SPATIAL AND TEMPORAL PATTERNS OF VEGETATION DISTURBANCES

IN GREAT SMOKY MOUNTAINS NATIONAL PARK

by

JIAYING HE

(Under the Direction of Marguerite Madden)

ABSTRACT

Forest ecosystems in Great Smoky Mountains National Park (GRSM) have long been affected by natural and human disturbances. Insect outbreaks and fires are the major disturbances affecting forest ecosystems in GRSM with interactions between each other. This manuscript-style thesis research explores these types of forest disturbances occurred in GRSM with two case studies. The first manuscript explores the spatial and temporal patterns of eastern hemlock (*Tsuga canadensis* L.) defoliation caused by hemlock woolly adelgid (HWA, *Adelges tsugae*) infestation in GRSM. Hemlock trees play an ecologically vital role in the eastern United States including GRSM. However, they have been facing a rapid infestation by the non-native HWA discovered in the park circa 2002. Moreover, the severe and persistent Chimney Tops 2 Fire occurred in November 2016 also put forest ecosystems in GRSM under threats. The second manuscript examines the spatial variations and driving factors affecting burn severity of the 2016 Chimney Tops 2 Fire in GRSM. The methodology and results from this project will support National Park Service forest management and insect control policies for the GRSM.

KEY WORDS: Great Smoky Mountains National Park, vegetation disturbances, remote sensing

SPATIAL AND TEMPORAL PATTERNS OF VEGETATION DISTURBANCES

IN GREAT SMOKY MOUNTAINS NATIONAL PARK

by

JIAYING HE

B.E., Wuhan University, 2012

A Master Thesis Submitted to the Graduate Faculty of The University of Georgia in Partial Fulfillment of the Requirements for the Degree

MASTER OF SCIENCE

ATHENS, GEORGIA

2018

SPATIAL AND TEMPORAL PATTERNS OF VEGETATION DISTURBANCES

IN GREAT SMOKY MOUNTAINS NATIONAL PARK

by

JIAYING HE

Major Professor: Marguerite Madden

Committee: Lan Mu
Sergio Bernardes

Electronic Version Approved:

Suzanne Barbour
Dean of the Graduate School
The University of Georgia
December 2018

ACKNOWLEDGEMENTS

First and foremost, I would like to express my deep gratitude to Dr. Marguerite Madden for supporting my study and research wholeheartedly as my major advisor during my master's study at Department of Geography, the University of Georgia. Thanks to Marguerite, I had the honor to join the big family of Center for Geospatial Research and enjoyed my work there. I would also like to thank my committee members Dr. Lan Mu and Dr. Sergio Bernardes for their kind help and suggestions during the process of my thesis research.

TABLE OF CONTENTS

LIST OF FIGURES

LIST OF TABLES

CHAPTER 1

INTRODUCTION AND LITERATURE REVIEW

1.1 Introduction

Climate change has resulted in severe impacts on biodiversity, ecosystem functioning and services through increasing temperatures, rising carbon dioxide levels, and growing number of extreme weather events since the 20th century (Staudinger et al., 2012; Blunden et al., 2018). Long-term datasets collected from the 1960s have shown that Earth's land surface temperature has increased approximately 0.17°C per decade (Blunden et al., 2018). Global warming can further increase the intensity and frequency of extreme events such as droughts, floods and heat waves (Trenberth et al., 2013; Stott, 2016). Specifically, droughts and heat stress induced by climate change, and climate-mediated processes like wildfire and infestations of invasive insects, have the potential to amplify forest mortality throughout the world (Allen et al., 2010).

Covering nearly one third of the total land area on the Earth with over 80% of the terrestrial biodiversity, forest ecosystems play a vital role in preserving soil and water resources, maintaining biodiversity and contributing to sustainable development (Aerts & Honnay, 2011). However, forests are currently suffering from strong pressure generated by increasing frequency and intensity of disturbances related to human activities and climate change such as wildland fire, insect outbreaks, droughts and wind storms (Hansen et al., 2013; Trumbore et al., 2015; Seidl et al., 2017). From 2000 to 2012, forest losses of about 2.3 million km^2 have been identified all over the world based on satellite observations (Hansen et al., 2013). In particular, the tropics have experienced the highest rates of forest loss caused by intensive forestry, followed by the loss of the boreal forests related to fire and forestry practices (Hansen et al., 2013).

Although human activities such as forestry and shifting agriculture are the primary drivers of forest loss globally (Curtis et al., 2018), natural disturbances such as insect outbreaks and wildfire also exert strong impacts on the forests in temperate North America (van Lierop et al., 2015). These forest disturbances not only cause massive mortality of plants and animals, but also influence the climate conditions in return by altering the carbon storage, hydrologic cycle, surface energy fluxes, etc. (Bonan, 2008). In addition, climate change could interact with pathogens, insects and fire to further impact the spatial distribution and phenology of tree species (Sturrock et al., 2011). Thus, monitoring of forest disturbance spatiotemporal patterns is of great importance for maintaining healthy forest ecosystems under climate change conditions.

1.2 Research Questions and Objectives

This Master's research utilizes remote sensing imagery to examine spatial and temporal patterns of vegetation disturbances in GRSM forests caused by insect outbreaks and fires, which are the major disturbance sources in the park. Dead trees caused by insect infestation have the potential to increase fire risks by providing fuels that support burning (Jenkins et al., 2008). In addition, insect outbreaks can affect post-fire severity levels in forests (Meigs et al., 2016). Remote sensing methods have the capability to detect both types of disturbances effectively for forest ecosystems. Specifically, this thesis examines two case studies are examined in GRSM: eastern hemlock defoliation caused by HWA and post-fire burn severity of the 2016 Chimney Tops 2 Fire. Both case studies can provide resource agencies such as the GRSM National Park Service (NPS) and U. S. Forest Service (USFS) with a complete methodology and results for long-term monitoring of forest disturbances and can assist the forest management and health protection at the broad spatiotemporal scale.

Chapter 2 (the first manuscript) focuses on geospatial analysis to quantify and map the spatial-temporal patterns of eastern hemlock defoliation in GRSM. The results of this study can be used to assess the overall effectiveness of control measures and to identify key locations for hemlock protection. They can also be used to support modeling and prediction of HWA risks. Two research questions are addressed in this chapter:

(1) How are the eastern hemlock disturbances caused by HWA in GRSM distributed in space and time?

(2) What regions in GRSM have the greatest decline or long disturbance of eastern hemlock?

Chapter 3 (the second manuscript) computes and maps the spatial variation of burn severity after the 2016 Chimney Tops 2 Fire and examines the factors influencing the severity distribution. The results of this study can assist the post-fire restoration efforts of the forest ecosystems in GRSM. This chapter addresses the following three research questions:

(1) How is burn severity distributed in GRSM after the 2016 fire?

(2) How does the fire impact the habitats of different vegetation species?

(3) What environmental factors affected the distribution of burn severity in this fire?

In summary, this thesis plans to achieve the following objectives:

(1) To analyze the spatiotemporal patterns of hemlock disturbances in GRSM;

(2) To identify the key time and locations of HWA infestation for future control and protection efforts;

(3) To map the burn severity for the 2016 fire in GRSM;

(4) To examine the vegetation species affected by the fire; and

(5) To identify the factors influencing the variance of burn severity.

1.3 Study Area

GRSM is located in Tennessee and North Carolina and encompasses approximately 2114.18 km^2 within the southern portion of the greater Appalachian Mountains (Figure 1.1). Among the oldest mountains in the world, the formation of the Southern Appalachian Mountains within which the GRSM lies can be dated back to perhaps 200 ~ 300 million years ago. Originally established in 1934, GRSM was designated as an International Biosphere Reserve by United Nations in 1976 and a World Heritage Site by United Nations Educational, Scientific and Cultural Organization (UNESCO) in 1983 in recognition of its unique and abundant natural resources (World Heritage Centre, 2018). Now with over nine million visitors annually, GRSM is known as the most visited park in the United States (U.S.).

Figure 1.1 The Great Smoky Mountains National Park straddling the boundary between Tennessee and North Carolina in the eastern U.S.

With elevations ranging between 267 and 2025 m in the park, it is believed that the heterogeneous geology and topographic features affect the distribution of the various species (Whittaker, 1956). The central massif of GRSM is surrounded by mountain valleys which reach as low as 256 m on the western side along most of the park boundary. A steep terrain of narrow ridges and rocky coves can also be found all over the park resulting in the relative short distances between elevation extremes (6 ~ 12 km), except for a few places that are mainly composed of metamorphosed and sedimentary rock covered with fields, grassland and some forest vegetation (Fridley, 2009). Throughout GRSM, temperature and lapse rate decreases as elevation increases while precipitation and humidity increase as the elevation rises. All of the above climate patterns will also be influenced by the microclimate conditions in certain areas (Busing et al., 2005).

1.4 Literature Review

1.4.1 Forest Disturbances in Great Smoky Mountains National Park (GRSM)

As part of the southern Appalachian Mountains in the eastern U.S., Great Smoky Mountains National Park (GRSM) once served as a place of refuge for plant and animal species during the last Ice Age and now is one of the most biodiverse regions in the world (Walker, 1991; Jenkins, 2007). GRSM contains more than 100,000 species with at least 5,400 plants, 450 vertebrates, 76,000 invertebrates and 20,000 fungi species, according to the All Taxa Biological Inventory developed based on expert knowledge (Sharkey, 2001). The flora and fauna species in GRSM are of great importance for maintaining the ecological integrity and ecosystem services of the southern Appalachian Mountains and the southeastern U.S. (Walker, 1991; Vandermast, 2005). In addition to the rich diversity of plant species, GRSM contains one of the largest old growth forests in the eastern U.S. (Jenkins, 2007).

Forests in GRSM have experienced a long history of both natural and anthropogenic disturbances (Pyle, 1985). Paleorecords suggest that fire occurred regularly in GRSM forests over the past 4,000 years (Fesenmyer & Christensen, 2010). Having lived in this region for thousands of years, Native Americans burned the forests and grasses for gaming and hunting purposes with relatively minimal impacts on the local ecosystems. The settlement of the Europeans in this region in the 1700s then became an important disturbance that influenced the vegetation communities in GRSM (Pyle, 1985). The impacts were still minimal in the beginning for cutting trees for building settlements and small area farming. The logging and farming activities during the 1800s and 1900s, however, was so extensive that over half the area of the park was cleared with severe loss of species until the establishment of GRSM in 1934 (Pyle, 1985).

In spite of the current protected status, forests in GRSM are also threatened by pathogenic fungi, insect outbreaks, fire and other disturbances (Jenkins, 2007). Accidentally introduced into North America in the early 1890s, chestnut blight (*Cryphonectria parasitica* Barr) wiped out American chestnut (*Castanea dentata*), a dominant species in GRSM forest communities, in the 1930s (Whittaker 1956). Balsam woolly adelgid (*Adelges piceae*), first discovered in 1956 in the Appalachians, has caused serious mortality of the only fir species in GRSM, Frasier fir (*Abies fraseri*) (Jenkins, 2007; Taylor, 2012). More recently, hemlock woolly adelgid (HWA, *Adelges tsugae*) has become a serious threat to the eastern hemlock (*Tsuga canadensis* L.) forests in GRSM since 2002.

In addition to fungus and insect infestations, GRSM forests experience both prescribed fires and two lightning-ignited fires per year, on average (NPS, 2018a). In particular, the Chimney Tops 2 Fire, one of many in the Fall of 2016 fire season in GRSM, has not only affected local forest ecosystems in GRSM, but also led to human deaths, injuries and severe damages in the developed areas of Gatlinburg, Tennessee. Other processes like tornados and catastrophic winds can also lead to damages on the forests, which could take decades for the ecosystems to recover

(Peterson, 2000; Allen et al., 2012; Bernardes & Madden, 2016). This research focuses on examining the impacts of recent disturbance events on GRSM forests, particularly the HWA infestation of hemlock forests and the Chimney 2 Tops Fire, as examples of remote sensing and geospatial analyses of broad-scale forest disturbances related to spatial and temporal patterns of forest damage.

Eastern Hemlock and Hemlock Woolly Adelgid

Known as “redwood of the East", eastern hemlock (*Tsuga canadensis* L.), or Canadian hemlock, is a slow-growing but long-lived evergreen coniferous tree species native to the eastern North America (Figure 1.2; Ward et al., 2004). Within the U.S., eastern hemlock forests are dominated throughout the northeastern U.S., extending from lower Quebec and the Canadian Maritime Provinces to the north, Michigan and the Appalachian Mountains to the west and stretching south to northern Georgia and Alabama. Specifically, they cover about 3.24 km^2 within GRSM, more than in any other parks (NPS, 2018b). The eastern hemlock normally require 250 ~ 300 years to mature and can live up to 800 years (Godman & Lancaster, 1990). It can grow more than 45 m tall with trunks measuring 2 m in diameter (Brisbin, 1970).

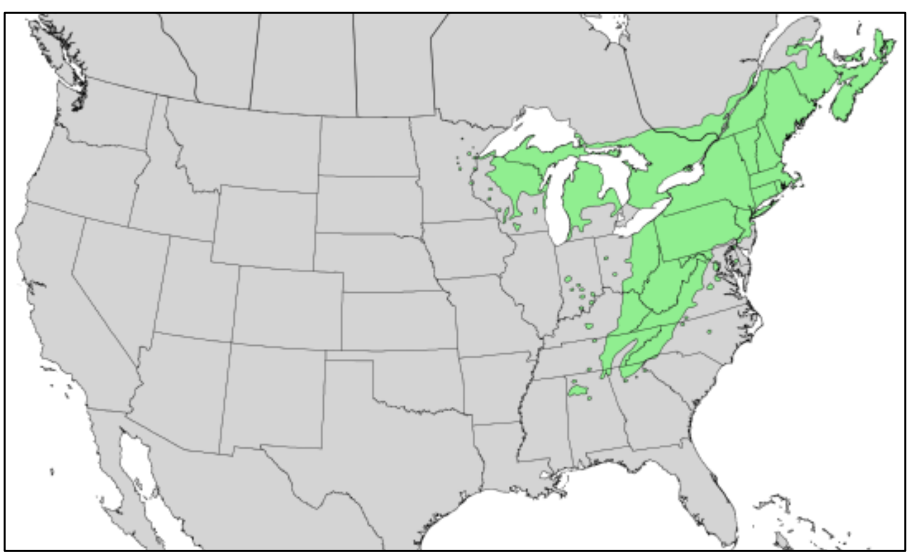

Figure 1.2 Eastern hemlock distribution in North America (Little & USGS, 1971)

Typically locating at elevations ranging from 600 m to 1800 m, eastern hemlock often occupies the area near streams and within cove or valley formations on lower protected slopes and terraces (Godman & Lancaster, 1990; Jenkins, 2007). It can also be found at higher elevations within or near northern hardwood forest community types. Eastern hemlock is generally confined to humid continental climates and mainly ranges in areas with constantly moist soil due to its sensitivity to drought and wind exposure (Benvie, 2000). During the growing season, the habitats of eastern hemlock typically have an average annual precipitation from 740 mm to more than 1270 mm. The habitats in the north can have average temperatures from -12°C to 16°C, while in the south the average temperature can reach 6°C (Godman & Lancaster, 1990). Its habitats are usually influenced by topographic features like slope and aspect, since they have the potential to affect soil moisture content and surface temperature (Orwig et al., 2002; Marks, 2012).

As one of the most common species in GRSM, eastern hemlock plays an essential role in forest and riparian ecosystems by providing a unique micro-habitat for local wildlife and maintaining the rich biodiversity of animal and plant species (NPS, 2018b). The heterogeneous vertical structure of mature hemlock forest stands also provides habitats for hundreds of vertebrate species (Ward et al., 2004). Its dense evergreen foliage reaching to the forest floor can maintain the cool and moist microclimates critical to the survival of cold-water species and stabilizes hydrologic budgets (Ward et al., 2004; Stadler et al., 2005). The thermal cover and forage provided by hemlock forests can also be utilized by various mammal and bird species, such as white-tailed deer and black-throated green warbler (Ward et al., 2004).

Though eastern hemlock has a long lifecycle, its population has declined rapidly across the eastern U.S. due to the infestation of hemlock wooly adelgid (HWA, *Adelges tsugae*), a small invasive insect native to Japan and probably China (Godman & Lancaster, 1990; Orwig et al., 2002; Clark et al., 2012). Although hemlock species in Japan are no longer significantly injured by HWA because of the host resistance and arthropod predators, they are now threatened by an increasing population of HWA in the North America (Letheren et al., 2017). The HWA can have two complete parthenogenetic wingless generations, winter and spring generations, on hemlock every year. Feeding at the needle junctions of hemlock, HWA can feed off the nutrients and then cause the needles to desiccate (Figure 1.3). The HWA can thus lead to serious needle loss, prevent the production of new apical buds and finally kill hemlock trees within three to five years (McClure & Salom, 2001). Since HWA has no natural predators within the U.S., it has become necessary for researchers and forest managers to intervene and control the spread of HWA considering the significance of eastern hemlock in protecting the ecosystems (Bonneau et al., 1999; Soehn et al., 2005).

Figure 1.3 Eastern hemlock infested by HWA (Credit: Connecticut Agricultural Experiment Station Archive, U.S.)

The HWA was first found in the northeastern U.S. in the 1950s and then spread along the Appalachian regions to the southeast from the late 1990s to early 2000s (Havill et al., 2016). The spreading rate of the HWA has reached 15.6 km per year in the southern areas since the 1990s and can be even higher in warmer years (Evans & Gregoire, 2007). By 2016, HWA had infested hemlock forests in most eastern US counties from Maine to Georgia (Figure 1.4). First discovered in GRSM in 2002, HWA then became widespread within the park and caused severe hemlock defoliation and death in both overstory and understory levels of the forests (Johnson et al., 2005; Krapfl et al., 2011). Specifically, the mortality rates of understory hemlock trees tend to be higher than those of the overstory ones (Krapfl et al., 2011). Though significant changes of species composition in the hemlock forests due to HWA infestations have not been identified, it is highly possible that hemlock trees could disappear in GRSM and thus influence the successional vegetation patterns in the forest ecosystems (Krapfl et al., 2011).

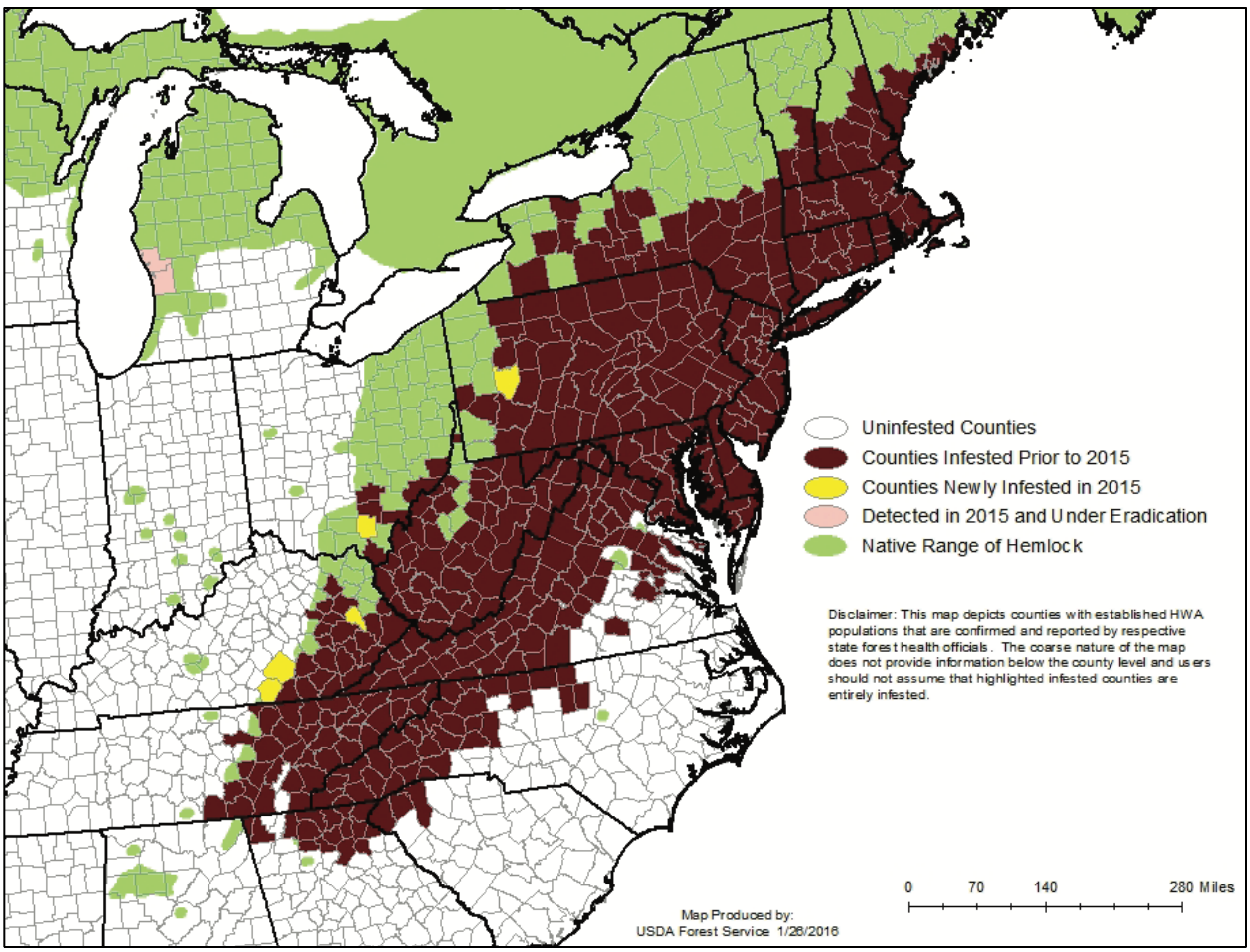

Figure 1.4 HWA distribution map in U.S. counties in 2015 (Havill et al., 2016)

Three types of treatments, including foliar treatments, systemic treatments and release of predator beetles, have been conducted by the NPS to kill the adelgids and control their dispersions in the hemlock forests of GRSM (NPS, 2018c). These treatments can be generally categorized into chemical and biological controls (Havill et al., 2016). Specifically, foliar treatments are applied to hemlock trees at accessible regions mainly with a spray of insecticidal soap to kill the adelgids. Systemic treatments apply a systemic insecticide into the trunk or soil of those trees that are not easily accessible by humans. Though effective, these chemical controls only last from a few months up to five years and require repeated treatments (Havill et al., 2016; NPS, 2018c). In addition, such "stand-alone" strategies are not viable for broad scale applications due to their costs and potential impacts on the environment (Abella, 2014; Havill et al., 2016). As a biologic control, predatory beetles have been released across the park since 2002, with a population greater than half a million reached by 2011 (NPS, 2018c). This method is under development with promising preliminary results (Havill et al., 2016; NPS, 2018c).

Although the site and climatic factors driving HWA's widespread distribution are still unclear, the vulnerability of hemlock to HWA infestation varies in space (Rentch et al., 2009; Havill et al., 2016). In addition, effective implementation of these controls requires knowledge of hemlock defoliation locations in inaccessible regions. Thus, gaining a thorough understanding about the spatiotemporal patterns of hemlock defoliation can improve our understanding of the underlying drivers and assist the management efforts of eastern hemlock forests in GRSM.

Wildland Fires in GRSM

The southern Appalachian forests have a long history of regularly occurring wildfires as suggested by soil charcoal data (Fesenmyer & Christensen, 2010). The frequency of fires increased abruptly in the recent 1000 years, related to the activities of Native Americans in this region (Fesenmyer & Christensen, 2010). After the establishment of the park in 1934, fire suppression efforts have significantly reduced wildfire occurrences in the forests of the southern Appalachian Mountains (Flatley et al., 2013). Currently in GRSM, arson is the primary cause of fires in GRSM, while lighting strikes accounted for about 10% of fires. Lightning-ignited fires in GRSM usually occur in May or June, mainly at the low and mid-elevations, and especially where pine and oak forests predominate (Cohen et al., 2007; NPS, 2018a).

Referred to as the largest fire in GRSM's history, the Chimney Tops 2 Fire that occurred in November of 2016, lasted for six days from November 23 to 28 and burned about 69.36 km^2 in total with 44.37 km^2 inside the park (Figure 1.5; Klein et al., 2017). Starting from the Chimney Tops Mountain in the central area of the park, this fire then grew rapidly under strong winds and raged across the park to the developed Gatlinburg region in Tennessee. Merged with two other smaller fires, this fire resulted in 14 deaths, a million-dollars of economic loss in the Gatlinburg area of Tennessee, and a massive number of dead trees within GRSM. Although ignited by arson by two juveniles, the occurrence of this unusually severe fire was also impacted by the unusually low precipitation and warm temperatures in this region from mid-summer to fall, resulting in a tinder dry condition for the forests in GRSM (Klein et al., 2017). In addition, the newly fallen leaves in the autumn of 2016 that piled up on the forest floor also provided plenty of fuels for the fire and extremely high winds rapidly spread the fire from its point of ignition.

Figure 1.5 The Chimney Tops 2 Fire in GRSM on November 27, 2016 (Credit: Brett Bevill)

There is a long history of fire management in GRSM. Currently, two types of fire management zones are distinguished in GRSM for different management purposes (Figure 1.6; GRSM, 2010). For the purpose of protecting human life, property and sensitive resources, the first type, Interface Zone, has been established in the regions within and adjacent to the park boundary, which covers approximately 17% of the total park area. The remaining 83% of the park is identified as the Natural Zone, within which natural processes are allowed to occur. Particularly, wildland fires occurring naturally in this unit will be allowed to burn for resource benefits under proper conditions. The GRSM management team will also ignite prescribed fires to maintain healthy forest ecosystems.

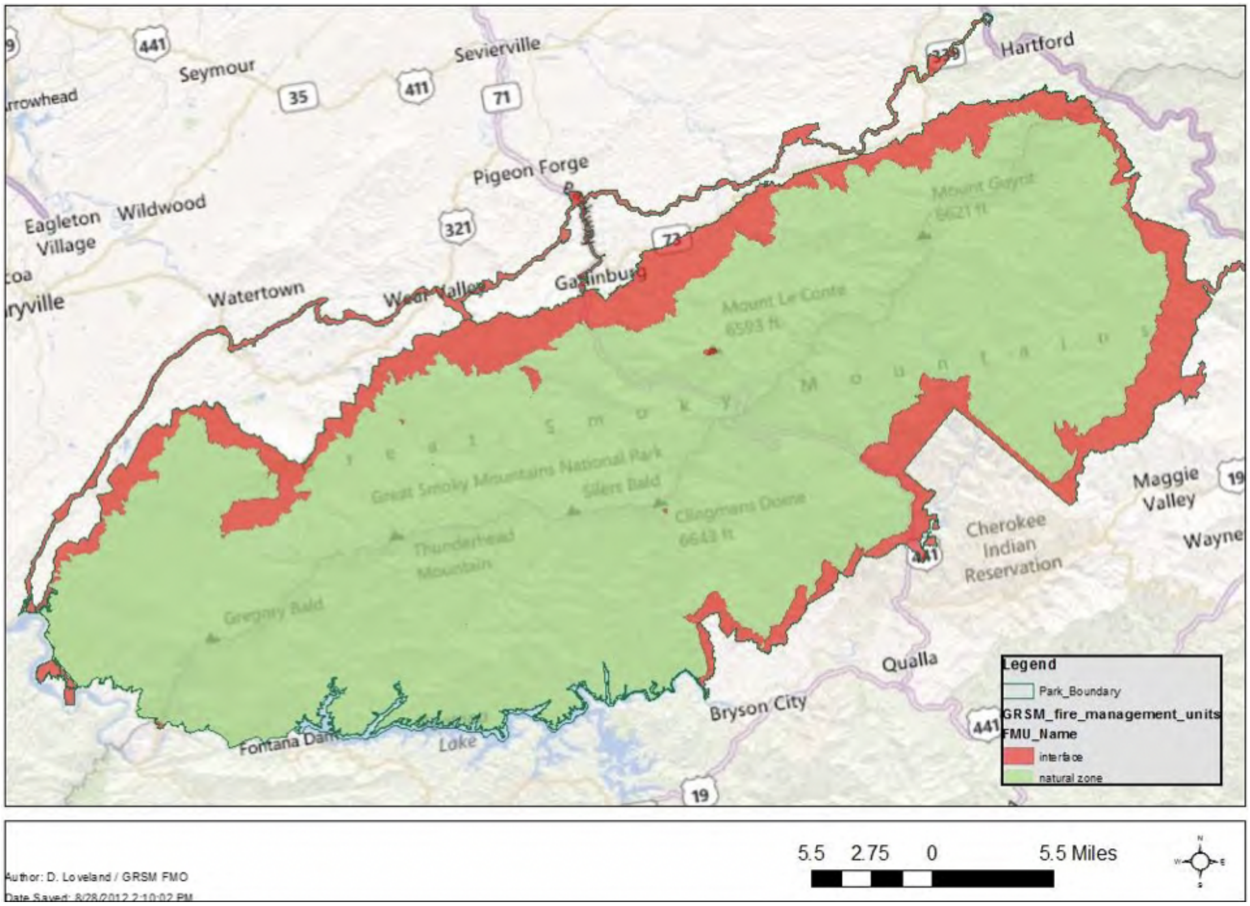

Figure 1.6 GRSM Fire Management Units (GRSM, 2010)

Fires are like a double-edged sword for the forest ecosystems. On one hand, wildland fires can alter the ecosystem functioning and services of forest and become dangerous for wildlife and human beings (Bonazountas et al., 2007; Thom & Seidl, 2016). While on the other hand, fires have the capability to maintain healthy forest ecosystems and to benefit the species by recycling the nutrients of dead trees (Tiedemann et al., 2000). Fire spread extent and severity could have different levels of negative impacts on the local ecosystems by influencing seed sources, vegetation mortality and even the biogeochemical cycles (Pyne et al., 1996; Certini, 2005; Cocke et al., 2005). The distribution of burn severity is largely dependent on the interactions between fires and environmental factors like fuel types, fuel moisture, topography and weather conditions (Pyne et al., 1996). Understanding the distribution of post-fire burn severity and environmental factors related to severity distribution can provide useful information for effective forest recovery management in GRSM.

1.4.2 Remote Sensing Applications in Environmental Studies

Remote sensing technology has been widely utilized in environmental and ecological applications due to its capability of collecting data with broad spatiotemporal coverage and continuity. In general, remote sensing can be defined as "the art and science of obtaining information about an object without being in direct physical contact with the object" (Reeves et al., 1975). To be more specific, it focuses on recording and analyzing the information of objects or phenomena from certain regions of the electromagnetic spectrum, including ultraviolet, visible, infrared and microwave spectral bands, using various sensors such as cameras, scanners, and lasers carried on platforms including handheld devices, towers, aircrafts and satellites (Jensen, 2007).

Particularly, multispectral remote sensors allow for the discrimination of different types of vegetation, rocks and soils, clear and turbid water, and selected man-made materials based on their different reflectance properties in the visible and infrared spectrum (Figure 1.7). With the development of remote sensing technologies over the past 45 years, multispectral remote sensors, such as Advanced Very High Resolution Radiometer (AVHRR) onboard National Oceanic and Atmospheric Administration (NOAA) satellites, Thematic Mapper (TM), Enhanced Thematic Mapper Plus (ETM+) and the Operational Land Imager (OLI) onboard Landsat satellites from National Aeronautics and Space Administration (NASA), and High Resolution Geometrical (HRG) instrument on SPOT 5 satellite from French Centre National d'Etudes Spatiales, among many others, have obtained a large amount of images to identify various ground objects, to acquire biophysical and land cover information and to examine their spatiotemporal trends at a broad scale (Running & Nemani, 1988; Cohen & Goward, 2004; Pettorelli et al., 2005; Tucker et al., 2005; Yuan & Bauer, 2007; Hansen et al., 2013). Compared to the relatively broad-band multispectral sensors, hyperspectral remote sensing sensors can capture hundreds of narrow-band spectral data. The use of hyperspectral imagery makes it possible to obtain more detailed spectral information for monitoring vegetation species and other ground objects (Figure 1.8), such as detecting forest health events caused by fire, insect infestation, invasive species, etc. (Treitz & Howarth, 1999; Koetz et al., 2008; Wang et al., 2010).

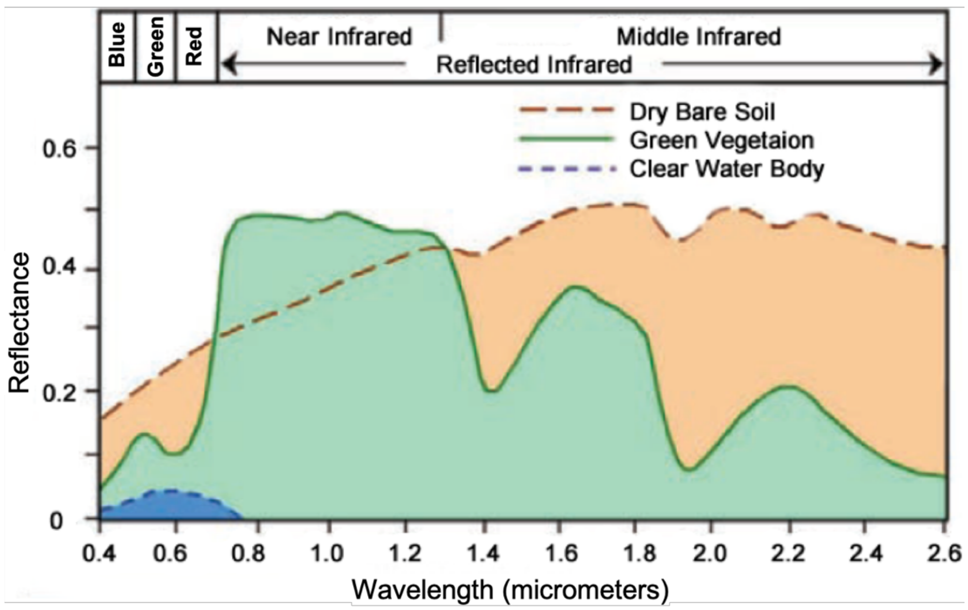

Figure 1.7 Spectral signatures for dry bare soil, green vegetation and clear water body (Govender et al., 2007)

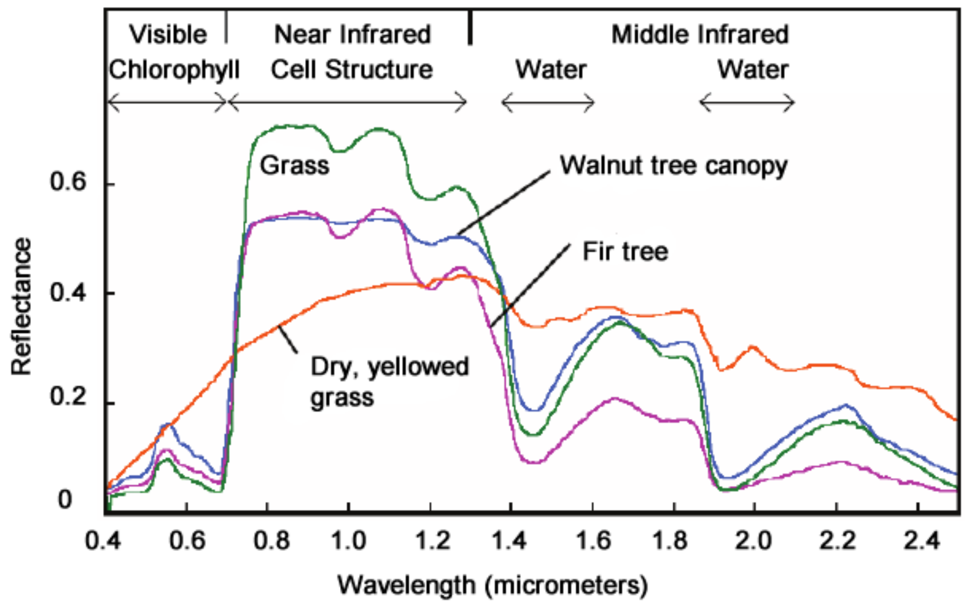

Figure 1.8 Surface reflectance spectra of different vegetation types (Govender et al., 2007)

In recent years, monitoring long-term forest dynamics and disturbances at broad spatiotemporal scales have become possible thanks to the large amount of open remote sensing satellite data provided by NASA (Kerr & Ostrovsky, 2003). Satellite images acquired at high temporal resolution such as daily Moderate Resolution Imaging Spectroradiometer (MODIS) data have been widely used to monitor the vegetation phenology for broad-scale agriculture and forest applications (Myneni et al., 2002; Zhang et al., 2003; Sakamoto et al., 2005; Verbesselt et al., 2010). With lower temporal frequency but higher spatial resolution, 30-m multispectral data collected by Landsat sensors have played the most important role in mapping vegetation cover change and using the derived surfaces in ecological models given their about 40-year record of data collection (Cohen & Goward, 2004; Hansen et al., 2013). Given similar spectral collection configurations and orbital parameters, data from both MODIS and Landsat sensors have been combined together for Earth observations to make full use of their spatial and temporal details.

First launched in 1972, Landsat satellite series has been the longest running satellite program for Earth observations. Ever since the USGS started to provide millions of Landsat scenes for free in

2008, Landsat satellites, particularly Landsat 4, 5, 7, and 8, have played an important role in providing data for broad scale studies and promoting the progress of scientific research in a variety of fields such as land use and land cover change, forest disturbances monitoring, wildland fires evaluation, and surface water extent estimation. Multispectral instruments onboard Landsat satellites, including TM on Landsat 4 and 5, ETM+ on Landsat 7, and OLI on Landsat 8, are designed to provide data with 30-m spatial resolution and 16-day revisiting time (Jensen, 2007; Jackson, 2009).

These instruments specifically capture reflective spectral bands covering visible, near infrared (NIR), and shortwave infrared (SWIR) portions of the electromagnetic spectrum (Figure 1.9; Jackson, 2009). In spite of the similar band designations among these sensors, ETM+ and OLI have improved radiometric resolution in data acquisition when compared to TM. However, the Scan Line Corrector failure of ETM+ sensor in 2003 resulted in scanline gaps in data collection and limited the usage of ETM+ data in scientific research. Specifically, the Landsat TM sensor has six reflective spectral bands, one thermal emissive band and one panchromatic band as listed in Table 1.1. The Landsat OLI sensor has eight reflective spectral bands and one panchromatic band, with one ultra-blue band and one cirrus band added for coastal and aerosol studies and atmospheric correction (Table 1.2).

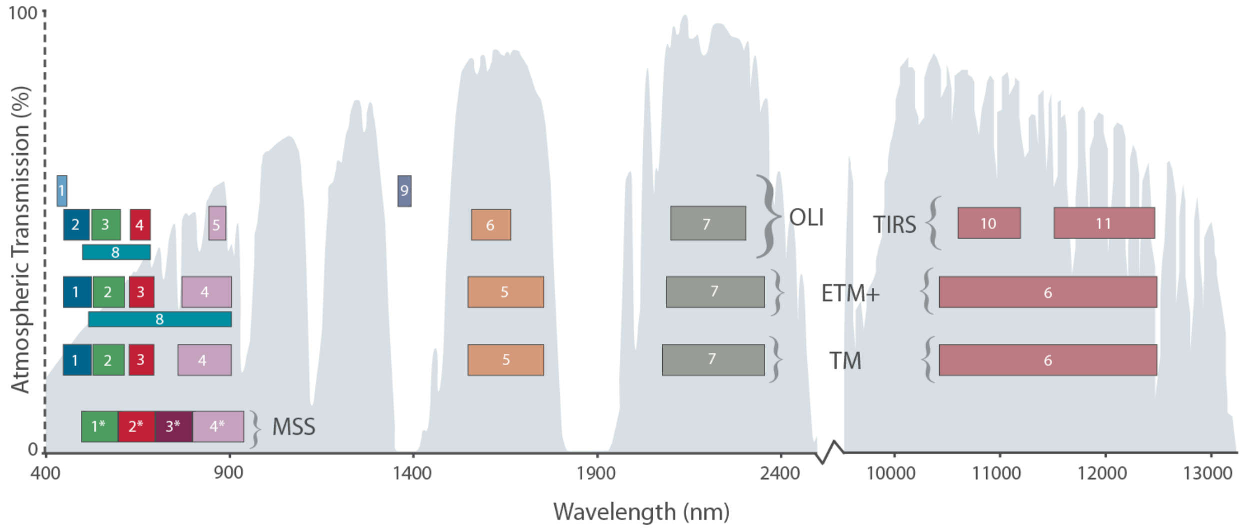

Figure 1.9 Comparison of Landsat TM, ETM+ and OLI spectral bands (Credit: NASA)

Table 1.1 Band designations of Landsat 5 TM sensor

Spectral Bands	Wavelength (micrometers)	Resolution (meters)
Band 1: Blue	0.45 - 0.52	30
Band 2: Green	0.52 - 0.60	30
Band 3: Red	0.63 - 0.69	30
Band 4: NIR	0.77 - 0.90	30
Band 5: SWIR 1	1.55 - 1.75	30
Band 6: Thermal Infrared	10.40 - 12.50	120
Band 7: SWIR 2	2.08 - 2.35	30
Band 8: Panchromatic	0.52 - 0.9	15

Table 1.2 Band designations of Landsat 8 OLI sensor

Spectral Bands	Wavelength (micrometers)	Resolution (meters)
Band 1: Ultra Blue	0.435 – 0.451	30
Band 2: Blue	0.452 - 0.512	30
Band 3: Green	0.533 - 0.590	30
Band 4: Red	0.636 - 0.673	30
Band 5: NIR	0.851 - 0.879	30
Band 6: SWIR 1	1.566 - 1.651	30
Band 7: SWIR 2	2.107 - 2.294	30
Band 8: Panchromatic	0.503 – 0.676	15
Band 9: Cirrus	1.363 – 1.384	30

The USGS has archived, processed and distributed multilevel Landsat satellite data acquired since 1972. Level-1 Landsat products delivered by USGS have been processed with radiometric calibration and geometric correction. Particularly, the standard terrain correction collection in level-1 products provides the digital number (DN) values with highest geometric accuracy with orthorectification processing using ground control points and DEM data. Then with properties provided in metadata, the top-of-atmospheric (TOA) radiance and reflectance values can then be calculated from DN data. In addition to level-1 products, USGS also provides on-demand level-2 surface reflectance products for TM, ETM+ and OLI data after applying radiometric calibration and atmospheric correction algorithms. Level-2 products of TM and ETM+ data are processed through the Landsat Ecosystem Disturbance Adaptive Processing System (LEDAPS) system for atmospheric correction, cloud masking and quality assessment (Masek et al., 2006), while OLI data are generated using the Landsat Surface Reflectance Code (LaSRC) system (Vermote et al., 2016). These two systems adopted different radiative transfer models, algorithms and input datasets for atmospheric correction, which could lead to the inconsistency of spectral signatures values in long-term data records.

1.4.3 Forest Disturbance Detection with Remote Sensing

Monitoring forest disturbance has always been a major concern in forest management due to the spatiotemporal limitations of on-site monitoring (Overpeck et al., 1990; Attiwill, 1994; Millar et al., 2007). In many cases, insect infestation has been a major cause of forest disturbances for decades and has had deep negative impacts on the health condition of ecosystems (Ayres & Lombardero, 2000; Czerwinski, 2012). The development of satellite sensors has allowed for improved measurements of forest extent and change at various spatial and temporal scales (Boyd & Danson, 2005). Specifically, the NASA Earth Observing System (EOS) including optical sensors on board satellites have systematically collected comprehensive global imagery on a regular schedule for decades. For example, Hansen et al. (2008) integrated MODIS and Landsat images to monitor Congo forest cover and change from 1990 and 2000. Masek et al. (2013) have mapped the forest disturbances and examined their temporal trends during 1985 ~ 2005 for the U.S. using Landsat TM and ETM+ archive data. Archived since 1984, Landsat TM and ETM+ data with a 16-day temporal resolution and 30-m spatial resolution are suitable for capturing the spatial details of vegetation characteristics and assessing long-term trends of land cover changes (Cohen & Goward, 2004; Meigs et al., 2011).

As a simple spectral transformation of various bands, vegetation indices calculated by band ratios are designed to enhance the detection of the contribution of vegetation properties and can be used to monitor seasonal, annual, and long-term variations of vegetation structural, phenological, and biophysical parameters (Huete et al., 2002). As the most commonly used index, Normalized Difference Vegetation Index (NDVI) calculated with NIR and red bands has been widely applied using Landsat data to measure the vegetation greenness and disturbance patterns globally (Maselli, 2004; Pettorelli et al., 2005; Tucker et al., 2005; Spruce et al., 2011; Fensholt et al., 2012). NDVI is calculated using the formula below:

$$NDVI = \frac{\rho_{NIR} - \rho_{Red}}{\rho_{NIR} + \rho_{Red}},$$

where ρ_{NIR} and ρ_{Red} are surface reflectances of the NIR and red spectral bands. Since NDVI tends to saturate in high biomass regions, Enhanced Vegetation Index (EVI) has been designed and adopted to improve vegetation monitoring with a combination of blue, red and NIR bands (Huete et al., 2002; Sims et al., 2008; Bernardes & Madden, 2016). EVI can be calculated using the following formula:

$$EVI = 2.5 \times \frac{\rho_{NIR} - \rho_{Red}}{\rho_{NIR} + (6 \times \rho_{Red} - 7.5 \times \rho_{Blue}) + 1},$$

where ρ_{NIR}, ρ_{Red} and ρ_{Blue} are surface reflectances of the NIR, red and blue spectral bands. Other indices like Soil and Atmospheric Resistant Vegetation Index (SARVI) and Normalized Difference Moisture Index (NDMI) also show good performances in mapping forest disturbances in different ecosystems (Maingi & Luhn, 2005; Goodwin et al., 2008). Normalized Burn Ratio (NBR), a metric calculated with NIR and SWIR bands, is originally developed to capture the impacts of fire on vegetation communities (García & Caselles, 1991). Existing research also suggests the effectiveness of NBR in detecting other forest disturbances like insect outbreaks, due to its sensitivity to low intensity disturbance events (Cohen et al., 2010; Kennedy et al., 2010). The formula of NBR is presented as:

$$NBR = \frac{\rho_{NIR} - \rho_{SWIR}}{\rho_{NIR} + \rho_{SWIR}},$$

where ρ_{NIR} and ρ_{SWIR} are surface reflectances of the NIR and SWIR spectral ranges. In addition, by deriving three linear combinations (Brightness, Greenness, and Wetness) of spectral bands related to biophysical properties, Tasseled Cap (TC) transformation can reduce the volume and improve the interpretability of multispectral data, and thus is commonly used to assist vegetation classification and disturbance monitoring efforts (Crist, 1985; Dymond et al., 2002; Zhang et al., 2002; Healey et al., 2005).

When considering change detection analysis with Landsat data, image differencing, Principle Component Analysis (PCA) and Change Vector Analysis are among the most widely used methods for measuring change with images from two different dates (Czerwinski, 2012). To analyze the spatial variation of landscape changes with temporal details, trend analysis methods dealing with multi-temporal remote sensing data have been developed. Masek et al. (2008) mapped the disturbance and early recovery of North American forest using the temporal change in a Tasseled-Cap “Disturbance Index” for the 1990-2000 Landsat record. Eastman et al. (2009)

applied Theil-Sen slope to calculate the pixel-level median slope of an image time series to estimate the long-term trend. Huang et al. (2010) designed a Vegetation Change Tracker algorithm to map forest disturbance in eastern U.S. from 1984 to 2006. Kennedy et al. (2010) developed a trajectory-based temporal segmentation algorithm combining both regression-based and point-to-point fitting of spectral indices as a function of time to capture abrupt and gradual change of forest disturbance and recovery.

1.4.4 Fire Severity Estimation with Remote Sensing

Fire severity, or burn severity, was originally proposed to describe the ecological impacts of fire intensity, which describes the energy released from organic matter during different physical phases of combustion (Keeley, 2009). In spite of the interchangeable use of these terms in some existing studies, they represent different post-fire impacts regarding the temporal scale and the properties they describe (Lentile et al., 2006; Keeley, 2009). In particular, considering both short- and long-term fire impacts, burn severity describes more attributes related to fire severity and ecosystem responses when compared to fire severity (Lentile et al., 2006; Keeley, 2009). Fire management efforts for forest ecosystems require accurate monitoring of post-fire burn severity and enhanced understanding of environmental factors driving burn severity distribution (Malmström, 2010; Jenkins et al., 2011; Francos et al., 2016).

Deriving empirical relationships between remote sensing spectral indices and field severity measurements is the most commonly used method for broad scale estimation of burn severity across different types of ecosystems. Different from remote sensing indices developed based on spectral information, field measurements of burn severity such as composite burn index (CBI) are usually designed to represent a much broader set of attributes considering not only organic matter loss, but also ecosystem responses (Keeley, 2009). Existing studies have identified strong relationships between spectral indices like NDVI and burn severity measured with post-fire biomass loss (Keeley, 2009). NBR shows significant relationship with field measurements and has been widely utilized in monitoring and quantifying burn severity in different ecosystems (Rogan & Franklin, 2001; Roy et al., 2006; Stow et al., 2007).

For example, Brewer et al. (2005) compared six methods of burn severity mapping including indices, PCA and Artificial Neural Network and identified NBR-based empirical method as the most effective one for the 2000 fire season in the Northern Rocky Mountains and Northern Great Plains. Developed based on NBR, differenced NBR (dNBR) and Relative dNBR (RdNBR) were used as alternative ways for mapping severity (Miller & Thode, 2007; Wimberly & Reilly, 2007). Other metrics such as change in leaf area index (LAI; Boer et al., 2008) were also developed to capture certain aspects of fire severity.

In addition to empirical fitting with spectral indices, inversion methods with radiative transfer models (RTM) have shown their effectiveness in assessing burn severity within certain ranges (Chuvieco et al., 2006; De Santis & Chuvieco, 2007). For example, De Santis and Chuvieco (2007) compared both types of methods in Mediterranean forests and found that RTM based methods have higher accuracy for estimating CBI values in high severity and unburned areas than the empirical ones. Although NBR-based indices have their limitations in interpreting fire-related biophysical changes and mapping burning perimeters (Cocke et al., 2005; Boer et al., 2008), they are still considered to be among the most effective methods in assessing forest burn severity in many applications (Chang et al., 2016).

Spatial variation of burn severity is under the control of environmental factors such as fuel types, topography and weather conditions across the landscape through their impacts on fire intensity and duration (Pyne et al., 1996; Dillon et al., 2011; Estes et al., 2017). Types of vegetation fuels are critical for the distribution of burn severity in forest ecosystems, since they can affect flammability and fuel loads and thus influence fire intensity and duration (Pyne et al., 1996).

Specifically, the LANDFIRE program maintained by USFS uses Landsat data to map the spatial distribution of major fuel types across the entire country to support wildfire studies and fire risk modeling (Rollins, 2009). Topography and weather conditions also exert strong impacts on the severity distribution in multiple ways. On one hand, they can influence the accumulation of fuels that support burning by altering vegetation distribution and productivity and controlling local energy and water balances for vegetation growth (Barbour, 1999; Dillon et al., 2011). On the other hand, they can affect the microclimatic conditions of fire weathers and thus influence the fuel moisture content (Pyne et al., 1996). U.S. National Fire Danger Rating System (NFDRS) and Canadian Forest Fire Danger Rating System (CFFDRS) have developed specific indices to quantify weather conditions for fire potential evaluation.

Impacts of these factors on post-fire burn severity vary by different ecosystems and locations. Wimberly & Reilly (2007) found strong linkages between burn severity and pre-fire vegetation types, topography, changes in species richness in the southern Appalachians using Landsat TM and ETM+ imagery. Birch et al. (2015) examined the fires in central Idaho and western Montana forests and suggested that vegetation and topographic factors tended to influence burn severity the most. Kane et al. (2015) identified seven factors, including time since previous fire, actual evapotranspiration, climatic water deficit, burning index, slope, and solar radiation to explain burn severity variance for the Rim fire occurred in the western U.S. Another study by Chang et al. (2016) also identified topographic factors and daily humidity as the determinative factors affecting burn severity for forests in northeastern China.

1.5 Thesis Structure

This manuscript-style thesis is comprised of four chapters containing two manuscripts, which will be submitted for publication in peer-reviewed journals. The first chapter introduces background information of this research, research questions and objectives to be addressed, study area and related literature review. The second chapter, which is the first manuscript, aims to explore the defoliation pattern of eastern hemlock forests in GRSM using a temporal segmentation algorithm and Landsat time series imagery. The third chapter, which is the second manuscript, focuses on evaluating the burn severity in GRSM after the 2016 Chimney Tops 2 Fire and explores the environmental factors affecting the burn severity distribution. Finally, the fourth chapter summarizes this thesis and discusses the next steps of work.

References

Abella, S. R. (2014). Impacts and Management of Hemlock Woolly Adelgid in National Parks of the Eastern United States. Southeastern Naturalist, 13(6), 16–45.

Aerts, R., & Honnay, O. (2011). Forest restoration, biodiversity and ecosystem functioning. BMC Ecology, 11(1), 29.

Allen, C. D., Macalady, A. K., Chenchouni, H., Bachelet, D., McDowell, N., Vennetier, M., Kitzberger, T., Rigling, A., Breshears, D. D., Hogg, E. H., Gonzalez P., Fensham, R., Zhang Z., Castro, J., Demidova, N., Lim, J., Allard, G., Running, S. W., Semerci, A., & Cobb, N. (2010). A global overview of drought and heat-induced tree mortality reveals emerging climate change risks for forests. Forest Ecology and Management, 259(4), 660–684.

Allen, M. S., Thapa, V., Arévalo, J. R., & Palmer, M. W. (2012). Windstorm damage and forest recovery: Accelerated succession, stand structure, and spatial pattern over 25 years in two Minnesota forests. Plant Ecology, 213(11), 1833–1842.

Attiwill, P. M. (1994). The disturbance of forest ecosystems: the ecological basis for conservative management. Forest Ecology and Management, 63(2–3), 247–300.

Ayres, M. P., & Lombardero, M. J. (2000). Assessing the consequences of global change for forest disturbance from herbivores and pathogens. Science of The Total Environment, 262(3), 263–286.

Barbour, M. G. (1999). Terrestrial plant ecology. Benjamin/Cummings series in the life sciences. (3rd ed.). Menlo Park, Calif. SE - 1 volume (various pagings): illustrations, maps; 24 cm.: Benjamin/Cummings.

Benvie, S. (2000). The encyclopedia of North American trees. Firefly Books.

Bernardes, S., & Madden, M. (2016). Vegetation Disturbance and Recovery Following a Rare Windthrow Event in the Great Smoky Mountains National Park. In the International

Archives of the Photogrammetry, Remote Sensing and Spatial Information Sciences (Vol. XLI-B8, pp. 571–575).

Birch, D. S., Morgan, P., Kolden, C. A., Abatzoglou, J. T., Dillon, G. K., Hudak, A. T., & Smith, A. M. S. (2015). Vegetation, topography and daily weather influenced burn severity in central Idaho and western Montana forests. Ecosphere, 6(1), art17.

Blunden, J., Arndt, D. S., Hartfield, & Sánchez-Lugo, G., Eds. (2018). State of the Climate in 2017. Bulletin of the American Meteorological Society, 99(8).

Boer, M. M., Macfarlane, C., Norris, J., Sadler, R. J., Wallace, J., & Grierson, P. F. (2008). Mapping burned areas and burn severity patterns in SW Australian eucalypt forest using remotely-sensed changes in leaf area index. Remote Sensing of Environment, 112(12), 4358–4369.

Bonan, G. B. (2008). Forests and Climate Change: Forcings, Feedbacks, and the Climate Benefits of Forests. Science, 320(5882), 1444 LP-1449.

Bonazountas, M., Kallidromitou, D., Kassomenos, P., & Passas, N. (2007). A decision support system for managing forest fire casualties. Journal of Environmental Management, 84(4), 412–418.

Bonneau, L., Shields, K., & Civco, D. (1999). Using satellite images to classify and analyze the health of hemlock forests infested by the hemlock woolly adelgid. Biological Invasions, 1985(McClure 1989), 255–267.

Boyd, D. S., & Danson, F. M. (2005). Satellite remote sensing of forest resources: three decades of research development. Progress in Physical Geography, 29(1), 1–26.

Brewer, C. K., Winne, J. C., Redmond, R. L., Opitz, D. W., & Mangrich, M. V. (2005). Classifying and Mapping Wildfire Severity: A Comparison of Methods. Photogrammetric Engineering & Remote Sensing, 71(11), 1311–1320.

Brisbin, R. L. (1970). Eastern hemlock (Tsuga canadensis (L.) Carr.). FS-239, 239.

Busing, R. T., Stephens, L. A., & Clebsch, E. E. C. (2005). Climate data by elevation in the Great Smoky Mountains: a database and graphical displays for 1947-1950 with comparison to long-term data. US Geological Survey.

Certini, G. (2005). Effects of fire on properties of forest soils: a review. Oecologia, 143(1), 1–10.

Chang, Y., Zhu, Z., Feng, Y., Li, Y., Bu, R., & Hu, Y. (2016). The spatial variation in forest burn severity in Heilongjiang Province, China. Natural Hazards, 81(2), 981–1001.

Chuvieco, E., Riaño, D., Danson, F. M., & Martin, P. (2006). Use of a radiative transfer model to simulate the postfire spectral response to burn severity. Journal of Geophysical Research: Biogeosciences, 111(G4).

Clark, J. T., Fei, S., Liang, L., & Rieske, L. K. (2012). Mapping eastern hemlock: Comparing classification techniques to evaluate susceptibility of a fragmented and valued resource to an exotic invader, the hemlock woolly adelgid. Forest Ecology and Management, 266, 216–222.

Cocke, A. E., Fulé, P. Z., & Crouse, J. E. (2005). Comparison of burn severity assessments using Differenced Normalized Burn Ratio and ground data. International Journal of Wildland Fire, 14(2), 189.

Cohen, D., Dellinger, B., Klein, R., & Buchanan, B. (2007). Patterns in lightning-caused fires at Great Smoky Mountains National Park. Fire Ecology, 3(2), 68–82.

Cohen, W. B., & Goward, S. N. (2004). Landsat's Role in Ecological Applications of Remote Sensing. BioScience, 54(6), 535–545.

Cohen, W. B., Yang, Z., & Kennedy, R. (2010). Detecting trends in forest disturbance and recovery using yearly Landsat time series: 2. TimeSync - Tools for calibration and validation. Remote Sensing of Environment, 114(12), 2911–2924.

Crist, E. P. (1985). A TM Tasseled Cap equivalent transformation for reflectance factor data. Remote Sensing of Environment, 17(3), 301–306.

Curtis, P. G., Slay, C. M., Harris, N. L., Tyukavina, A., & Hansen, M. C. (2018). Classifying drivers of global forest loss. Science, 361(6407), 1108–1111.

Czerwinski, C. (2012). Forest Change Detection and Mapping in Gatineau Park, Québec, 1987 to 2010 using Landsat imagery.

De Santis, A., & Chuvieco, E. (2007). Burn severity estimation from remotely sensed data: Performance of simulation versus empirical models. Remote Sensing of Environment, 108(4), 422–435.

Delcourt, P. A., & Delcourt, H. R. (1998). The Influence of Prehistoric Human-Set Fires on Oak-Chestnut Forests in the Southern Appalachians. Castanea, 63(3), 337–345.

Dillon, G. K., Holden, Z. A., Morgan, P., Crimmins, M. A., Heyerdahl, E. K., & Luce, C. H. (2011). Both topography and climate affected forest and woodland burn severity in two regions of the western US, 1984 to 2006. Ecosphere, 2(12), art130.

Dymond, C. C., Mladenoff, D. J., & Radeloff, V. C. (2002). Phenological differences in Tasseled Cap indices improve deciduous forest classification. Remote Sensing of Environment, 80(3), 460–472.

Eastman, R. J., Sangermano, F., Ghimire, B., Zhu, H., Chen, H., Neeti, N., Cai, Y., Machado, E. A. & Crema, S. C. (2009). Seasonal trend analysis of image time series. International Journal of Remote Sensing, 30(10), 2721–2726.

Estes, B. L., Knapp, E. E., Skinner, C. N., Miller, J. D., & Preisler, H. K. (2017). Factors influencing fire severity under moderate burning conditions in the Klamath Mountains, northern California, USA. Ecosphere, 8(5).

Evans, A. M., & Gregoire, T. G. (2007). A geographically variable model of hemlock woolly adelgid spread. Biological Invasions, 9(4), 369–382.

Fensholt, R., & Proud, S. R. (2012). Evaluation of earth observation based global long term vegetation trends: Comparing GIMMS and MODIS global NDVI time series. Remote Sensing of Environment, 119, 131–147.

Fesenmyer, K. a, & Christensen, N. L. (2010). Reconstructing Holocene fire history in a southern Appalachian forest using soil charcoal. Ecology, 91(3), 662–670.

Flatley, W. T., Lafon, C. W., Grissino-Mayer, H. D., & LaForest, L. B. (2013). Fire History and Its Relation to Climate and Land Use in Three Southern Appalachian Landscapes in the Eastern U.S. Ecological Applications, 23(6), 130328164915002.

Francos, M., Úbeda, X., Tort, J., Panareda, J. M., & Cerdà, A. (2016). The role of forest fire severity on vegetation recovery after 18 years. Implications for forest management of Quercus suber L. in Iberian Peninsula. Global and Planetary Change, 145, 11–16.

Fridley, J. D. (2009). Downscaling Climate over Complex Terrain: High Finescale (<1000 m) Spatial Variation of Near-Ground Temperatures in a Montane Forested Landscape (Great Smoky Mountains). Journal of Applied Meteorology and Climatology, 48(5), 1033–1049.

García, M. J. L., & Caselles, V. (1991). Mapping burns and natural reforestation using thematic Mapper data. Geocarto International, 6(1), 31–37.

Godman, R. M., & Lancaster, K. (1990). Tsuga canadensis (L.) Carr. eastern hemlock. Silvics of North America, 1(1), 604–612.

Goodwin, N. R., Coops, N. C., Wulder, M. A., Gillanders, S., Schroeder, T. A., & Nelson, T. (2008). Estimation of insect infestation dynamics using a temporal sequence of Landsat data. Remote Sensing of Environment, 112(9), 3680–3689.

Govender, M., Chetty, K., & Bulcock, H. (2007). A review of hyperspectral remote sensing and its application in vegetation and water resource studies. Water Sa, 33(2).

GRSM (2010). Great Smoky Mountains National Park Fire Management Plan. National Park Service.

Hansen, M. C., Roy, D. P., Lindquist, E., Adusei, B., Justice, C. O., & Altstatt, A. (2008). A method for integrating MODIS and Landsat data for systematic monitoring of forest cover and change in the Congo Basin. Remote Sensing of Environment, 112(5), 2495–2513.

Hansen, M. C. C., Potapov, P. V, Moore, R., Hancher, M., Turubanova, S. A. a, Tyukavina, A., Thau, D., Stehman, S. V., Goetz, S. J., Loveland, T. R., Kommareddy, A., Egorov, A., Chini, L., Justice, C. O., & Townshend, J. R. G. (2013). High-Resolution Global Maps of 21st-Century Forest Cover Change. Science, 342 (November), 850–854.

Havill, N. P., Vieira, L. C., & Salom, S. M. (2016). Biology and Control of Hemlock Woolly Adelgid. USDA Forest Service Publication FHTET-2014-05. USDA Forest Service Publication FHTET-2014-05. Revised June 2016., (June).

Healey, S. P., Cohen, W. B., Zhiqiang, Y., & Krankina, O. N. (2005). Comparison of Tasseled Cap-based Landsat data structures for use in forest disturbance detection. Remote Sensing of Environment, 97(3), 301–310.

Huang, C., Goward, S. N., Masek, J. G., Thomas, N., Zhu, Z., & Vogelmann, J. E. (2010). An automated approach for reconstructing recent forest disturbance history using dense Landsat time series stacks. Remote Sensing of Environment, 114(1), 183–198.

Huete, A., Didan, K., Miura, T., Rodriguez, E. P., Gao, X., & Ferreira, L. G. (2002). Overview of the radiometric and biophysical performance of the MODIS vegetation indices. Remote Sensing of Environment, 83(1–2), 195–213.

Jackson, M. W. (2009). Earth Observing Platforms and Sensors. In Manual of Remote Sensing, Third Ed., Vol. 1.1 (p. 520 p.). Bethesda, Maryland: American Society for Photogrammetry and Remote Sensing.

Jenkins, M. A. (2007). Vegetation Communities of Great Smoky Mountains National Park. Southeastern Naturalist, 6, 35–56.

Jenkins, M. J., Hebertson, E., Page, W., & Jorgensen, C. A. (2008). Bark beetles, fuels, fires and implications for forest management in the Intermountain West. Forest Ecology and Management, 254(1), 16–34.

Jenkins, M. A., Klein, R. N., & McDaniel, V. L. (2011). Yellow pine regeneration as a function of fire severity and post-burn stand structure in the southern Appalachian Mountains. Forest Ecology and Management, 262(4), 681–691.

Jensen, J. R. (2007). Remote sensing of the environment: an earth resource perspective. Prentice Hall series in geographic information science (2nd ed.). Upper Saddle River, NJ SE - xvi, 592 pages, [48] pages of plates: illustrations (some color), maps (some color) ; 29 cm.: Pearson Prentice Hall.

Johnson, K., Taylor, G., & Remaley, T. (2005). Managing hemlock woolly adelgid and balsam woolly adelgid at Great Smoky Mountains National Park. In Third symposium on hemlock woolly adelgid in the Eastern United States. Forest Health Technology Enterprise Team, Morgantown, WV, USDA Forest Service, FHTET-2005-01 (Vol. 384).

Kane, V. R., Cansler, C. A., Povak, N. A., Kane, J. T., McGaughey, R. J., Lutz, J. A., Churchill, D. J., & North, M. P. (2015). Mixed severity fire effects within the Rim fire: Relative importance of local climate, fire weather, topography, and forest structure. Forest Ecology and Management, 358, 62–79.

Keeley, J. E. (2009). Fire intensity, fire severity and burn severity: A brief review and suggested usage. International Journal of Wildland Fire, 18(1), 116–126.

Kennedy, R. E., Yang, Z., & Cohen, W. B. (2010). Detecting trends in forest disturbance and recovery using yearly Landsat time series: 1. LandTrendr — Temporal segmentation algorithms. Remote Sensing of Environment, 114(12), 2897–2910.

Kerr, J. T., & Ostrovsky, M. (2003). From space to species: Ecological applications for remote sensing. Trends in Ecology and Evolution, 18(6), 299–305.

Klein, R. N. J., Paxton, E. W., & Wood, J. M. (2017). Southern Appalachian / Piedmont Fire Effects Monitoring Annual Report, 2016. National Park Service.

Koetz, B., Morsdorf, F., der Linden, S., Curt, T., & Allgöwer, B. (2008). Multi-source land cover classification for forest fire management based on imaging spectrometry and LiDAR data. Forest Ecology and Management, 256(3), 263–271.

Krapfl, K. J., Holzmueller, E. J., & Jenkins, M. a. (2011). Early impacts of hemlock woolly adelgid in Tsuga canadensis forest communities of the southern Appalachian Mountains. Journal of the Torrey Botanical Society, 138(1), 93–106.

Lentile, L. B., Holden, Z. A., Smith, A. M. S., Falkowski, M. J., Hudak, A. T., Morgan, P., Lewis, S. A., Gessler, P. E., & Benson, N. C. (2006). Remote sensing techniques to assess active fire characteristics and post-fire effects. International Journal of Wildland Fire, 15(3), 319–345.

Letheren, A., Hill, S., Salie, J., Parkman, J., & Chen, J. (2017). A little bug with a big bite: Impact of hemlock woolly adelgid infestations on forest ecosystems in the eastern USA and potential control strategies. International Journal of Environmental Research and Public Health, 14(4), 8–10.

Little, E. L. & USGS (1971). USGS Geosciences and Environmental Change Science Center: Digital Representations of Tree Species Range Maps from "Atlas of United States Trees" by Elbert L. Little, Jr.

Maingi, J. K., & Luhn, W. M. (2005). Mapping Insect-Induced Pine Mortality in the Daniel Boone National Forest, Kentucky Using Landsat TM and ETM+ Data. GIScience &

Remote Sensing, 42(3), 224–250.

Malmström, A. (2010). The importance of measuring fire severity-Evidence from microarthropod studies. Forest Ecology and Management, 260(1), 62–70.

Marks, T. (2012). Analysis of hemlock-topography relationships in southwest Wisconsin. Western Illinois University.

Masek, J.G., Vermote, E.F., Saleous N.E., Wolfe, R., Hall, F.G., Huemmrich, K.F., Gao, F., Kutler, J., and Lim, T-K. (2006). A Landsat surface reflectance dataset for North America, 1990–2000. IEEE Geoscience and Remote Sensing Letters 3(1):68-72.

Masek, J. G., Huang, C., Wolfe, R., Cohen, W., Hall, F., Kutler, J., & Nelson, P. (2008). North American forest disturbance mapped from a decadal Landsat record. Remote Sensing of Environment, 112(6), 2914–2926.

Masek, J. G., Goward, S. N., Kennedy, R. E., Cohen, W. B., Moisen, G. G., Schleeweis, K., & Huang, C. (2013). United States Forest Disturbance Trends Observed Using Landsat Time Series. Ecosystems, 16(6), 1087–1104.

McClure, M. S., & Salom, S. (2001). Hemlock Wooly Adelgid. Forest Health Technology Enterprise Team. US Forest Service Publication FHTET--2001--03. Morgantown, WV.

Meigs, G. W., Kennedy, R. E., & Cohen, W. B. (2011). A Landsat time series approach to characterize bark beetle and defoliator impacts on tree mortality and surface fuels in conifer forests. Remote Sensing of Environment, 115(12), 3707–3718.

Meigs, G. W., Zald, H. S., Campbell, J. L., Keeton, W. S., & Kennedy, R. E. (2016). Do insect outbreaks reduce the severity of subsequent forest fires? Environmental Research Letters, 11(4), 45008.

Millar, C. I., Stephenson, N. L., & Stephens, S. L. (2007). Climate change and forests of the future: managing in the face of uncertainty. Ecological Applications, 17(8), 2145–2151.

Miller, J. D., & Thode, A. E. (2007). Quantifying burn severity in a heterogeneous landscape with a relative version of the delta Normalized Burn Ratio (dNBR). Remote Sensing of Environment, 109(1), 66–80.

Myneni, R. B., Hoffman, S., Knyazikhin, Y., Privette, J. L., Glassy, J., Tian, Y., Wang, Y., Song, X., Zhang, Y., Smith, G. R., Lotsch, A., Friedl, M., Morisette, J., T., Votava, P., Nemani, R. R., & Running, S. W. (2002). Global products of vegetation leaf area and fraction absorbed PAR from year one of MODIS data. Remote Sensing of Environment, 83(1–2), 214–231.

National Park Service. (2018a) Great Smoky Mountains, Wildland Fire. Retrieved from: https://www.nps.gov/grsm/learn/nature/wildlandfire.htm

National Park Service. (2018b) Great Smoky Mountains, Nature & Science. Retrieved from: https://www.nps.gov/grsm/learn/nature/index.htm

National Park Service. (2018c) Great Smoky Mountains, Hemlock Woolly Adelgid. Retrieved from: https://www.nps.gov/grsm/learn/nature/hemlock-woolly-adelgid.htm

Orwig, D., Foster, D., & Mausel, D. (2002). Landscape patterns of hemlock decline in New England due to the introduced hemlock woolly adelgid. Journal of Biogeography, 1475–1487.

Overpeck, J. T., Rind, D., & Goldberg, R. (1990). Climate-induced changes in forest disturbance and vegetation. Nature, 343(6253), 51.

Peterson, C. J. (2000). Damage and recovery of tree species after two different tornadoes in the same old growth forest: A comparison of infrequent wind disturbances. Forest Ecology and Management, 135(1–3), 237–252.

Pettorelli, N., Vik, J. O., Mysterud, A., Gaillard, J.-M., Tucker, C. J., & Stenseth, N. C. (2005). Using the satellite-derived NDVI to assess ecological responses to environmental change. Trends in Ecology & Evolution, 20(9), 503–510.

Pyle, C. (1985). Vegetation Disturbance History of Great Smoky Mountains National Park: An Analysis of Archival Maps and Records.

Pyne, S. J., Andrews, P. L., & Laven, R. D. (1996). Introduction to Wildland Fire (Second Edi). John Wiley & Sons, Inc.

Reeves, R. G., Anson, A., & Landen, D. (1975). Manual of remote sensing. Falls church, Virginia: American Society of Photogrammetry.

Rentch, J., Fajvan, M. A., Evans, R. A., & Onken, B. (2009). Using dendrochronology to model hemlock woolly adelgid effects on eastern hemlock growth and vulnerability. Biological Invasions, 11(3), 551–563.

Rollins, M. G. (2009). LANDFIRE: A nationally consistent vegetation, wildland fire, and fuel assessment. International Journal of Wildland Fire, 18(3), 235–249.

Rogan, J., & Franklin, J. (2001). Mapping wildfire burn severity in Southern California forests and shrublands using enhanced thematic mapper imagery. Geocarto International, 16(4), 91–106.

Roy, D. P., Boschetti, L., & Trigg, S. N. (2006). Remote sensing of fire severity: Assessing the performance of the normalized burn ratio. IEEE Geoscience and Remote Sensing Letters, 3(1), 112–116.

Running, S. W., & Nemani, R. R. (1988). Relating seasonal patterns of the AVHRR vegetation index to simulated photosynthesis and transpiration of forests in different climates. Remote Sensing of Environment, 24(2), 347–367.

Sakamoto, T., Yokozawa, M., Toritani, H., Shibayama, M., Ishitsuka, N., & Ohno, H. (2005). A crop phenology detection method using time-series MODIS data. Remote Sensing of Environment, 96(3–4), 366–374.

Seidl, R., Thom, D., Kautz, M., Martin-Benito, D., Peltoniemi, M., Vacchiano, G., Wild, J., Ascoli, D., Petr, M., Honkaniemi, J., Lexer, M. J., Trotsiuk, V., Mairota, P., Svoboda, M., Fabrika, M., Nagel, T. A., & Reyer, C. P. O. (2017). Forest disturbances under climate change. Nature Climate Change, 7(6), 395.

Sharkey, M. J. (2001). The all taxa biological inventory of the Great Smoky Mountains National Park. Florida Entomologist, 556–564.

Sims, D. A., Rahman, A. F., Cordova, V. D., El-Masri, B. Z., Baldocchi, D. D., Bolstad, P. V, Flanagan, L. B., Goldstein, D. D., Hollinger, D. Y., Misson, L., Monson, R. K., Oechel, W. C., Schmid, H. P., Wofsy, S. C., & Xu, L. (2008). A new model of gross primary productivity for North American ecosystems based solely on the enhanced vegetation index and land surface temperature from MODIS. Remote Sensing of Environment, 112(4), 1633–1646.

Soehn, D., Taylor, G., Remaley, T., & Johnson, K. (2005). Draft environmental assessment of hemlock woolly adelgid control strategies in Great Smoky Mountains National Park. National Park Service, Great Smoky Mountains National Park, Gatlinburg, TN.

Souto, Dennis R. & Shields, Kathleen S. 2000. Overview of hemlock health. In: McManus, Katherine A.; Shields, Kathleen S.; Souto, Dennis R., eds. Proceedings: Symposium on sustainable management of hemlock ecosystems in eastern North America. Gen. Tech. Rep. NE-267. Newtown Square, PA: U.S. Department of Agriculture, Forest Service, Northeastern Forest Experiment Station. 76-80.

Spruce, J. P., Sader, S., Ryan, R. E., Smoot, J., Kuper, P., Ross, K., Prados D., Russell, J., Gasser, G., & McKellip, R. (2011). Assessment of MODIS NDVI time series data products for detecting forest defoliation by gypsy moth outbreaks. Remote Sensing of Environment, 115(2), 427–437.

Stadler, B., Müller, T., Orwig, D., & Cobb, R. (2005). Hemlock Woolly Adelgid in New

England Forests: Canopy Impacts Transforming Ecosystem Processes and Landscapes. Ecosystems, 8(3), 233–247.

Staudinger, M. D., Grimm, N. B., Staudt, A., Carter, S. L., Stuart III, F. S., Kareiva, P., Ruckelshaus, M., & Stein, B. A. (2012). Impacts of climate change on biodiversity, ecosystems, and ecosystem services: technical input to the 2013 National Climate Assessment. Washington, D.C.

Stott, P. (2016). How climate change affects extreme weather events. Science, 352(6293), 1517 LP-1518.

Stow, D., Petersen, A., Rogan, J., & Franklin, J. (2007). Mapping Burn Severity of Mediterranean-Type Vegetation Using Satellite Multispectral Data. GIScience & Remote Sensing, 44(1), 1–23.

Sturrock, R. N., Frankel, S. J., Brown, A. V, Hennon, P. E., Kliejunas, J. T., Lewis, K. J., Worrall, J. J., & Woods, A. J. (2011). Climate change and forest diseases. Plant Pathology, 60(1), 133–149.

Taylor, G. (2012). Forest health monitoring summary Great Smoky Mountains National Park. Natural Resource Data Series NPS/APHN/NRDS-2012/378, 378, 1–13.

Thom, D., & Seidl, R. (2016). Natural disturbance impacts on ecosystem services and biodiversity in temperate and boreal forests. Biological Reviews of the Cambridge Philosophical Society, 91(3), 760–781.

Tiedemann, A. R., O. Klemmedson, J., & Bull, E. L. (2000). Solution of forest health problems with prescribed fire: Are forest productivity and wildlife at risk? Forest Ecology and Management, 127(1), 1–18.

Treitz, P. M., & Howarth, P. J. (1999). Hyperspectral remote sensing for estimating biophysical parameters of forest ecosystems. Progress in Physical Geography, 23(3), 359–390.

Trenberth, K. E., Dai, A., van der Schrier, G., Jones, P. D., Barichivich, J., Briffa, K. R., & Sheffield, J. (2013). Global warming and changes in drought. Nature Climate Change, 4, 17.

Trumbore, S., Brando, P., & Hartmann, H. (2015). Forest health and global change. Science, 349(6250), 814 LP-818.

Tucker, C. J., Pinzon, J. E., Brown, M. E., Slayback, D. A., Pak, E. W., Mahoney, R., Vermote, E. F., & El Saleous, N. (2005). An extended AVHRR 8-km NDVI dataset compatible with MODIS and SPOT vegetation NDVI data. International Journal of Remote Sensing, 26(20), 4485–4498.

van Lierop, P., Lindquist, E., Sathyapala, S., & Franceschini, G. (2015). Global forest area disturbance from fire, insect pests, diseases and severe weather events. Forest Ecology and Management, 352, 78–88.

Vandermast, D. B. (2005). Disturbance and long-term vegetation change in the high-elevation deciduous forests of Great Smoky Mountains National Park. University of North Carolina at Chapel Hill.

Verbesselt, J., Hyndman, R., Newnham, G., & Culvenor, D. (2010). Detecting trend and seasonal changes in satellite image time series. Remote Sensing of Environment, 114(1), 106–115.

Vermote, E., Justice, C., Claverie, M., & Franch, B. (2016). Preliminary analysis of the performance of the Landsat 8/OLI land surface reflectance product. Remote Sensing of Environment, 185, 46–56.

Walker, S. L. (1991). Great Smoky Mountains: The Splendor of the Southern Appalachians. Camelback Design Group.

Wang, J., Sammis, T. W., Gutschick, V. P., Gebremichael, M., Dennis, S. O., & Harrison, R. E. (2010). Review of satellite remote sensing use in forest health studies. The Open Geography Journal, 3, 28–42.

Ward, J. S. J. S., Montgomery, M. E., Cheah, C. a. S.-J., Onken, B. P., & Cowles, R. S. (2004). Eastern Hemlock Forests: Guidelines to Minimize the Impacts of Hemlock Woolly Adelgid. NA-TP-03–04, USDA Forest Service, Northeastern Area State and Private Forestry, Morgantown, WV, 32.

Ward, J. S., Montgomery, M. E., Cheah, C. A. J., Onken, B. P., & Cowles, R. S. (2004). Eastern hemlock forests: guidelines to minimize the impacts of hemlock woolly adelgid. NA-TP-03-04. US Department of Agriculture, Forest Service, Northeastern Area State & Private Forestry, Morgantown, WV. 27 P., 1–27.

Whittaker, R. H. (1956). Vegetation of the Great Smoky Mountains. Ecological Monographs, 26(1), 2–80.

Wimberly, M. C., & Reilly, M. J. (2007). Assessment of fire severity and species diversity in the southern Appalachians using Landsat TM and ETM+ imagery. Remote Sensing of Environment, 108(2), 189–197.

World Heritage Centre. (2018). Great Smoky Mountains National Park. Retrieved from: https://whc.unesco.org/en/list/259

Yuan, F., & Bauer, M. E. (2007). Comparison of impervious surface area and normalized difference vegetation index as indicators of surface urban heat island effects in Landsat imagery. Remote Sensing of Environment, 106(3), 375–386.

Zhang, X., Schaaf, C. B., Friedl, M. A., Strahler, A. H., Gao, F., & Hodges, J. C. F. (2002). MODIS tasseled cap transformation and its utility. In IEEE International Geoscience and Remote Sensing Symposium (Vol. 2, pp. 1063–1065 vol.2).

Zhang, X., Friedl, M. A., Schaaf, C. B., Strahler, A. H., Hodges, J. C. F., Gao, F., Reed, B. C., & Huete, A. (2003). Monitoring vegetation phenology using MODIS. Remote Sensing of Environment, 84(3), 471–475.

CHAPTER 2

SPATIAL AND TEMPORAL PATTERNS OF EASTERN HEMLOCK DEFOLIATION CAUSED BY HEMLOCK WOOLLY ADELGID INFESTATION IN GREAT SMOKY MOUNTAINS NATIONAL PARK[1]

[1] He, Jiaying, et al. To be submitted to *Photogrammetric Engineering & Remote Sensing*

Abstract

Eastern hemlock (*Tsuga canadensis* L.) plays an ecologically vital role in forest ecosystems of eastern United States. Within Great Smoky Mountains National Park (GRSM), hemlock forests provide a unique habitat for many flora and fauna species that thrive in cool, shaded aquatic or terrestrial landscapes. However, hemlock trees are currently threatened by the non-native hemlock woolly adelgid (HWA, *Adelges tsugae*) discovered in the park circa 2002. A variety of controls have been conducted to prevent the rapid loss of hemlock trees caused by the infestation of HWA. However, the performances of these control efforts are largely limited when compared to the dramatic loss of trees throughout the park. In this study we aim to gain a thorough understanding of hemlock defoliation caused by HWA in GRSM at the broad spatiotemporal scale, using National Aeronautics and Space Administration (NASA) Earth Observing System (EOS) data. We use Landsat 5 Thematic Mapper (TM) and Landsat 7 Enhanced Thematic Mapper Plus (ETM+) imagery acquired during leaf-off conditions from 1991 to 2011 to construct temporal trajectories of hemlock disturbance. Then we apply a temporal segmentation algorithm, LandTrendr, to identify pixel-based defoliation trends and to evaluate the health condition of eastern hemlock in GRSM. The methodology and results from this project can inform National Park Service forest management and insect control policies for the GRSM.

2.1 Introduction

The Great Smoky Mountains National Park (GRSM) is one of the most biodiverse regions in the world and the largest virgin forest landmass in the United States (U.S.; Jenkins 2007). Containing at least 1,300 native plant species, 1,570 species of flowering plants and 4,000 species of non-flowering plants, GRSM plays an important role in preserving flora and fauna diversity and maintaining ecological integrity of the southern Appalachian Mountains (Walker, 1991). Forest ecosystems in GRSM has long been threatened by natural or human disturbances (Pyle, 1985). In particular, biotic disturbances caused by fungi and insects are major drivers for forest defoliation in GRSM during the recent decades. Chestnut blight (*Cryphonectria parasitica*), introduced to the U.S. in the early 1900s, has wiped out the majority of American chestnuts (*Castanea dentate*) in GRSM by the late 1930s (Taylor, 2012). By the 1970s, balsam woolly adelgid (*Adelges picea*) has led to the death of about 80 ~ 90% mature Fraser fir (*Abies fraseri*) throughout GRSM (Taylor, 2012). More recently, eastern hemlock (*Tsuga canadensis*) forests in GRSM are also at risk due to the infestation of hemlock woolly adelgid (HWA, *Adelges tsugae*) since 2002 (Krapfl et al., 2011).

Known as “redwood of the East", eastern hemlock is a slow-growing but long-lived coniferous tree native to the eastern North America (Ward et al., 2004). Within the U.S., hemlock trees have been found throughout New York, New England area, Pennsylvania, extending from New Jersey to the Appalachian Mountains in the west side and stretching to the northern Georgia and Alabama in the south (Figure 2.1). Eastern hemlock trees usually require approximately 250 to 300 years to mature and can live up to 800 years (Godman & Lancaster, 1990). In general, they can reach heights of about 25 to 30 m with trunk diameter at breast height of about 0.6 ~ 1 m (Brisbin, 1970). Having grown in GRSM for more than 400 years, eastern hemlock is the dominant species in many sites (Johnson et al., 2000). These old-growth hemlock trees cover more than 3.2 km^2, while younger trees growing for about 75 ~ 100 years occupy about another 360 km^2 land area throughout the park (NPS, 2018).

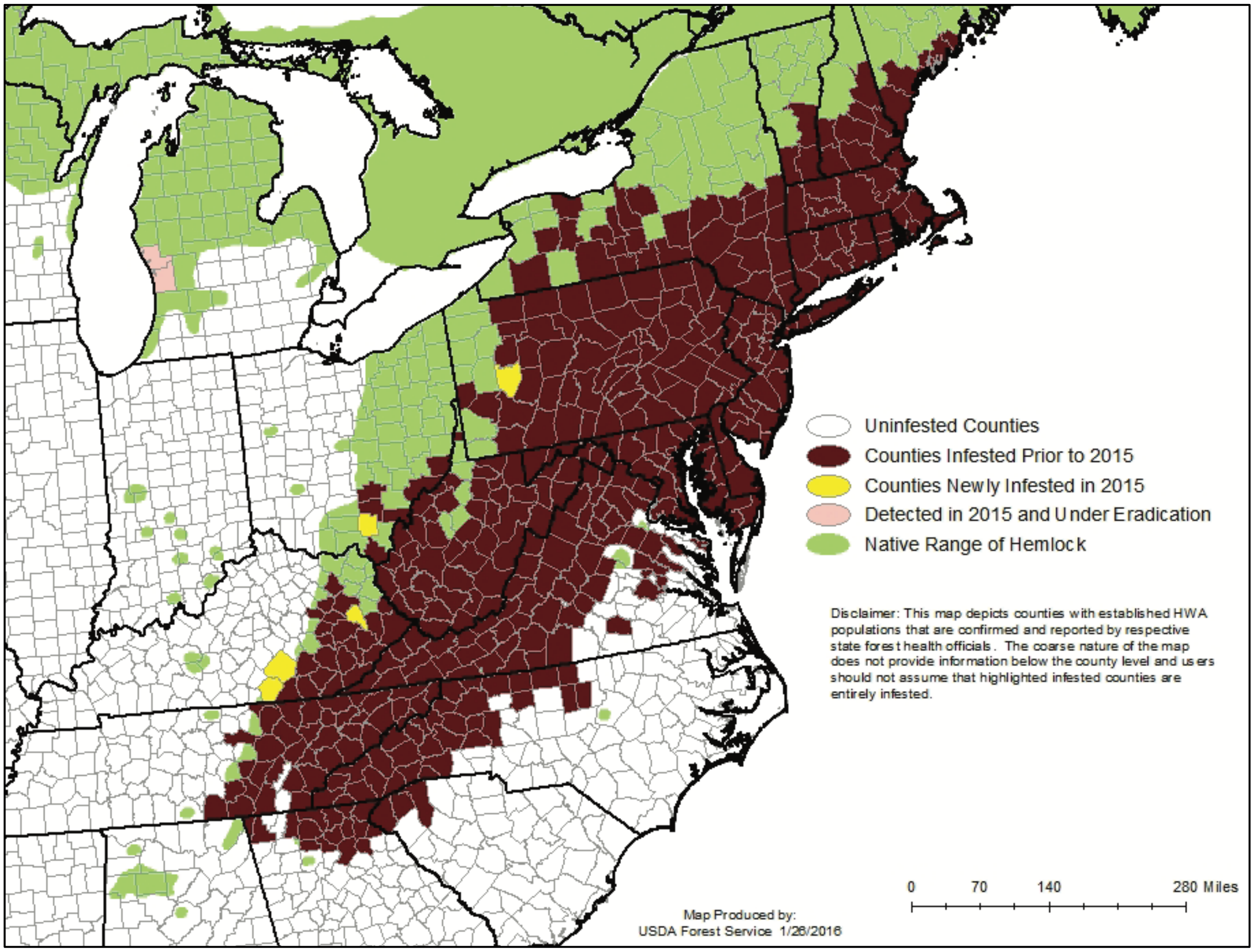

Figure 2.1 HWA distribution map in U.S. counties in 2015 (Havill et al., 2016)

As one of the most common species in GRSM, eastern hemlock plays an essential role in the local forest and riparian ecosystems by providing a unique micro-habitat for wildlife and maintaining the rich biodiversity of animal and plant species (NPS, 2018). The heterogeneous vertical structure of hemlock forests provides mature stands for hundreds of vertebrate species (Ward et al., 2004). The dense evergreen foliage reaching to the forest floor from hemlocks can stabilizes hydrologic budgets and maintain the cool and moist microclimates, which are critical to the survival of cold-water species (Ward et al., 2004; Stadler et al., 2005). The thermal cover and forage provided by hemlock trees can also benefit various mammal and bird species, such as white-tailed deer (*Odocoileus virginianus*) and black-throated green warbler (*Dendroica virens*) (Ward et al., 2004).

Despite of its ecological importance, eastern hemlock has declined rapidly across the eastern U.S. due to the infestation of HWA (Godman & Lancaster, 1990; Orwig et al., 2002; Clark et al., 2012). First discovered in GRSM in 2002, HWA became widespread and caused severe hemlock defoliation and death in both overstory and understory levels of the forests (Johnson et al., 2005; Krapfl et al., 2011). Previous studies identified negative impacts of HWA induced hemlock mortality on the local biodiversity, hydrologic processes and ecosystem stability (Ford & Vose, 2007; Letheren et al., 2017). Existing treatments such as biological and chemical methods were conducted in GRSM to control the infestation of HWA and to decrease the mortality of eastern hemlock. However, due to the lack of knowledge about factors driving HWA population and large-scale distribution patterns of hemlock mortality, treatments of hemlock defoliation throughout the park are difficult to conduct and their performances are quite limited (Letheren et al., 2017). Thus, to assist the effective management and protection of eastern hemlock forests in future, it is of great importance to gain a thorough understanding about the spatiotemporal patterns of hemlock decline caused by HWA in GRSM.

The development of remote sensing technology over the past 45 years makes it possible for tracking ecosystem disturbances on Earth in broad spatiotemporal scales. Having been archived since 1972, multispectral remote sensing imagery collected by Landsat satellites provide consistent Earth observations with a 16-day temporal coverage and 30-m spatial resolution. Vegetation indices extracted from Landsat spectral bands, such as Normalized Difference Vegetation Index (NDVI; Maselli, 2004), Normalized Burn Ratio (NBR; García & Caselles, 1991) and Soil and Atmospheric Resistant Vegetation Index (SARVI; Maingi & Luhn, 2005), have been widely used to monitor the spatiotemporal patterns of biophysical parameters and disturbance events across different ecosystems (Huete et al., 2002; Cohen & Goward, 2004). Tasseled Cap (TC) transformation, which derives three components (Brightness, Greenness and Wetness) with linear combinations of spectral bands, has also been commonly applied for capturing spectral properties of vegetation communities and identifying forest disturbances (Crist, 1985; Healey et al., 2005). A group of algorithms have been developed for mapping spatial and temporal disturbance patterns, including Seasonal Trend Analysis (Eastman et al., 2009), Vegetation Change Tracker (Huang et al., 2010) and LandTrendr (Kennedy et al., 2010).

Existing remote sensing studies in GRSM primarily focused on mapping the spatial distributions of overstory vegetation communities using both spectral and non-spectral information from aerial imagery (Welch et al., 2002; Madden et al., 2009; Kim et al., 2010). Allen and Madden (2009) developed 3D visualizations for HWA damage in GRSM based on the developed vegetation database (Welch et al., 2002; Madden et al., 2004). Strother et al. (2015) also applied Lightning Detection and Range (LiDAR) remote sensing data to measure tree heights in GRSM. In addition, NDVI time series data generated from coarse resolution Moderate Resolution Imaging Spectroradiometer (MODIS) data have captured phenological variability (Norman et al., 2017) and potential hemlock defoliation trend (Norman et al., 2013) in GRSM since 2000.

However, spatiotemporal patterns of hemlock decline have not been examined in detail with 30-m resolution Landsat imagery across the entire GRSM so far. This study aims to analyze the spatiotemporal patterns of HWA disturbances in eastern hemlock forests in GRSM, and to identify the key time and locations of defoliation to assist future pest control and protection efforts. Specifically, the following two research questions are addressed in this chapter: (1) How are the eastern hemlock disturbances caused by HWA in GRSM distributed in space and time? (2) What regions in GRSM have the greatest decline or long disturbance of eastern hemlock?

2.2 Datasets and Materials

2.2.1 GRSM Vegetation Database

This study utilizes the GRSM vegetation database to determine the spatial distribution of eastern hemlock forests in the study area. Developed by the Center for Geospatial Research (http://www.cgr.uga.edu/) at the University of Georgia in collaboration with NPS (Madden et al., 2004), this dataset provides detailed information about overstory and understory vegetation species and their distributions throughout the whole GRSM. Figure 2.2 shows a generalized overstory vegetation species (about 25 classes) summarized from over 100 classes of forest from the original dataset.

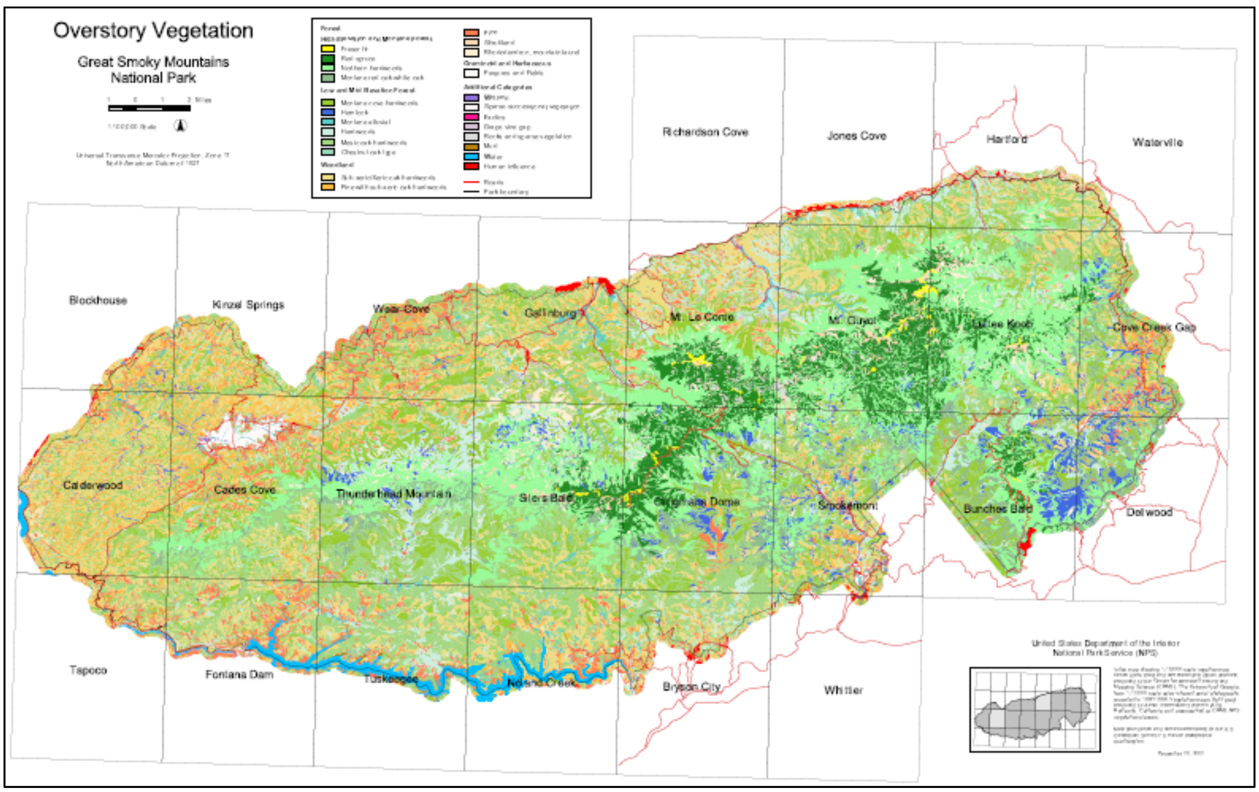

Figure 2.2 GRSM overstory vegetation map (Jordan 2002; Welch et al., 2002; Madden et al., 2004)

The overstory vegetation communities were classified to the Association level, which is the finest division from the National Vegetation Classification System protocol of the U.S.

Geological Survey (USGS) NPS Vegetation Mapping Program. Over 1000 color infrared aerial photographs were acquired a 1:12,000 scale and recorded with a Wild RC20 photogrammetric camera. Specifically, leaf-on photos in the fall were collected from 1997 to 1998 in late October since they display diverse colors to distinguish vegetation communities. These photos were then scanned at 800 dpi resulted in digital images, reaching about 0.4 m spatial resolution (Jordan 2002). Manual interpretation was used to map the overstory vegetation communities with these data. Supplementary data, including USGS National Aerial Photography Program (NAPP) Air Photos, USGS Topographic Maps, USGS Digital Orthophoto Quarter Quadrangles (DOQQs) and USGS level-2 Digital Elevation Model (DEM), were also integrated to generate the GRSM vegetation database.

2.2.2 Remote Sensing Imagery

Landsat 5 TM and Landsat 7 ETM+ 30-m level-2 surface reflectance data delivered by USGS were obtained from EarthExplorer (http://earthexplorer.usgs.gov/) to examine the long-term trend of eastern hemlock defoliation in GRSM. Processed with the Landsat Ecosystem Disturbance Adaptive Processing System (LEDAPS), this level-2 product provides surface reflectance values for each reflective spectral band after radiometric calibration, geometric correction and atmospheric correction (USGS, 2018). For atmospheric correction, LEDAPS processes level-1 Landsat data with MODIS atmospheric correction routines using water vapor, ozone, aerosol optical thickness, geopotential height and digital elevation as input parameters for the Second Simulation of a Satellite Signal in the Solar Spectrum (6S) radiative transfer models (Masek et al., 2006). Clouds and cloud shadows are also masked using the CFMask algorithm through this system.

To construct the temporal trend of eastern hemlock deforestation condition, Landsat tiles covering GRSM (Path 19 Row 35) from 1991 to 2011 were collected for data analysis. Images with limited cloud coverage were preferred. Specifically, only images in leaf-off conditions (November, December and next January) were selected to remove the impacts of understory broadleaf species on the reflectance of eastern hemlock. The pixel quality assessment data provided by level-2 data were then used to identify the clear pixels for data processing and analysis. The selected Landsat images for generating the time series are listed in Table 2.1.

Table 2.1 List of leaf-off Landsat 5 TM and Landsat 7 ETM+ imagery obtained for this study.

Year	Sensor	Landsat Scene ID	Acquisition Date	Date of Year	Cloud Coverage
1991	Landsat 5 TM	LT50190351991351XXX02	1991/12/17	351	1%
1992	Landsat 5 TM	LT50190351992322XXX02	1992/11/17	322	5%
1994	Landsat 5 TM	LT50190351994311AAA02	1994/11/07	311	0%
1995	Landsat 5 TM	LT50190351995330AAA02	1995/11/26	330	8%
1996	Landsat 5 TM	LT50190351996333XXX01	1996/11/28	333	9%
	Landsat 5 TM	LT50190351996349XXX01	1996/12/14	349	5%
1999	Landsat 5 TM	LT50190351999341XXX02	1999/12/07	341	30%
	Landsat 5 TM	LT50190351999357XXX02	1999/12/23	357	3%
2000	Landsat 5 TM	LT50190352000344XXX03	2000/12/09	344	25%
2001	Landsat 5 TM	LT50190352001314LGS01	2001/11/10	314	2%
	Landsat 5 TM	LT50190352001330LGS01	2001/11/26	330	14%
	Landsat 7 ETM+	LE70190352001338EDC00	2001/12/04	338	6%
2002	Landsat 5 TM	LT50190352002333LGS01	2002/11/29	333	0%
	Landsat 7 ETM+	LE70190352002341EDC00	2002/12/07	341	4%
2003	Landsat 5 TM	LT50190352003336GNC02	2003/12/02	336	18%
	Landsat 7 ETM+	LE70190352003360EDC01	2003/12/26	360	0%
2004	Landsat 5 TM	LT50190352004339GNC01	2004/12/04	339	0%
2005	Landsat 5 TM	LT50190352006024GNC01	2006/01/24	24	4%
2006	Landsat 5 TM	LT50190352006328GNC01	2006/11/24	328	0%
	Landsat 5 TM	LT50190352007027GNC01	2007/01/27	27	1%
2008	Landsat 7 ETM+	LE70190352008342EDC00	2008/12/07	342	9%
	Landsat 5 TM	LT50190352009032GNC01	2009/02/01	32	0%
2009	Landsat 5 TM	LT50190352009320GNC01	2009/11/16	320	0%
	Landsat 7 ETM+	LE70190352009344EDC00	2009/12/10	344	2%
2010	Landsat 7 ETM+	LE70190352010315EDC00	2010/11/11	315	0%
	Landsat 5 TM	LT50190352010323GNC01	2010/11/19	323	2%
2011	Landsat 5 TM	LT50190352011310EDC00	2011/11/06	310	4%

2.2.3 Auxiliary Dataset

Although detailed field measurements of eastern hemlock loss are not available for this research, we used the 30-m resolution global forest cover change data provided by Global Land Analysis & Discovery (GLAD; Hansen et al., 2013) as a reference for result evaluation and comparison. Developed with 30-m Landsat top-of-atmosphere reflectance data using decision tree method, GLAD data provides binary data of forest cover loss from 2000 to 2014, binary data of forest cover gain from 2000 to 2012, and the year of gross forest loss between 2000 and 2014.

2.3 Methodology

2.3.1 Identifying Eastern Hemlock Distribution in GRSM

Before examining the spatiotemporal trend of eastern hemlock decline, the eastern hemlock forest regions in GRSM were first determined using the overstory vegetation classification data from the GRSM vegetation database. Based on hemlock extent and canopy presence information from the overstory vegetation dataset, two types of eastern hemlock distribution were identified within GRSM: dominant hemlock region and mixed hemlock region. Here the vegetation communities with eastern hemlock coverage greater than 50% were identified as the dominant hemlock distribution type, while the vegetation communities with hemlock coverage within 20 ~ 50% were referred to as the hemlock mixed type.

2.3.2 Trajectory-based Algorithm LandTrendr

This study then applies a LandTrendr (http://landtrendr.forestry.oregonstate.edu) algorithm to analyze the spatial-temporal distributions of eastern hemlock defoliation in GRSM. LandTrendr is designed for mapping the temporal trend of forest disturbance through extraction of spectral-temporal trajectories (Kennedy et al., 2010). This algorithm is comprised of five successive steps: preprocessing, segmentation, change label mapping, spatial filtering and result validation. Using vegetation indices to represent vegetation greenness and to construct trajectories, it conducts pixel-by-pixel temporal segmentation for the trajectories and then simplifies the temporal trajectories to identify the trends of forest change.

Landsat data preprocessing

LandTrendr requires specific data formats for processing. Here we prepared three data files for each Landsat image listed in Table 2.1. A layer stack of the six surface reflectance bands for Landsat 5 and 7 was first generated. Then a layer stack of the three TC components was then calculated with the surface reflectance data and prepared in integer format. Both surface reflectance and TC component layer stacks were prepared using the ENVI software. LandTrendr also requires cloud mask data for each image. Here the quality assurance data provided by LEDAPS level-2 product were utilized to prepare the cloud mask data. Only "clear" pixels were assigned as "1" in the cloud mask data for LandTrendr processing, while other pixels were assigned as "0" to remove low-quality pixels such as clouds, shadows, snows and Landsat 7 Scan Liner Corrector (SLC) gaps. Although originally designed for highlighting burned area and estimating fire severity, NBR is found to have good performances in identifying forest disturbance trends due to its high sensitivity to low intensity disturbance events (Cohen et al., 2010; Kennedy et al., 2010; Meigs et al., 2011). Thus, here NBR was adopted as the index for constructing the trajectories and tracking the hemlock defoliation pattern.

Algorithm description

As the core part of the LandTrendr algorithm, temporal segmentation utilizes straight line segments to model the key features of a pixel's spectral time series while removing the impacts of noise (Kennedy et al., 2010). The detailed steps of segmentation are shown in Figure 2.3. The algorithm first constructs the pixel-by-pixel temporal trajectories and removes ephemeral spikes in the trend. Then potential vertices are identified using deviation from simple regression lines, with more vertices identified than needed. The excess vertices are then removed based on the low angle change. Next, a single path through the vertices is chosen using flexible fitting rules, and then segments are removed to create successively simplified models of the trajectory. Finally, the algorithm chooses the best-fit model and records segment details in the output data.

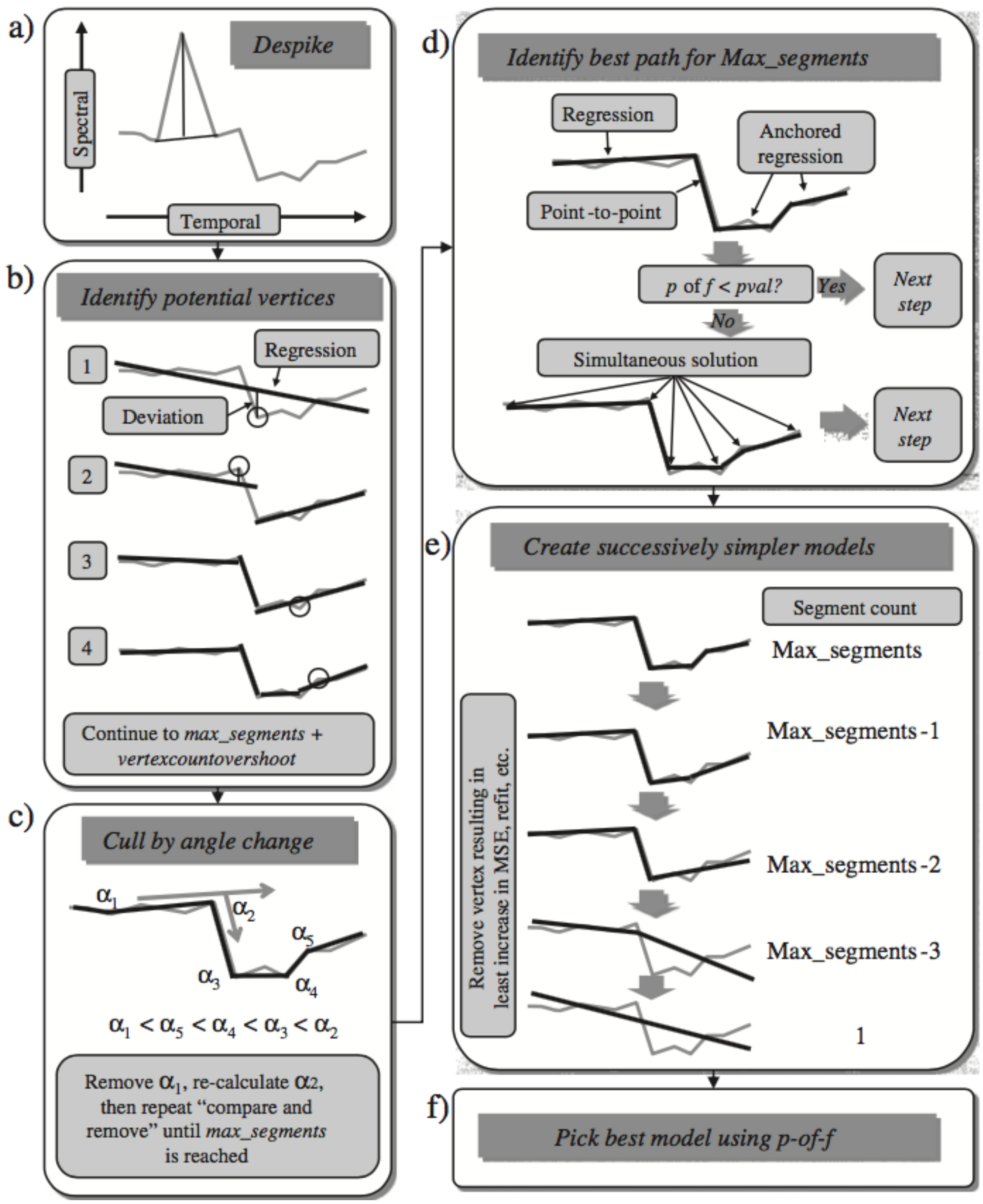

Figure 2.3 LandTrendr algorithm segmentation process (Kennedy et al., 2010): (a) removal of ephemeral spikes; (b) identification of potential vertices; (c) removal of excess vertices; (d) choice of a single path through the vertices; (e) removal of segments to create successively simplified models of the trajectory; (f) determination of the best-fit model.

After segmentation, the next step is change label mapping. This step interprets the segmentation results based on user-defined rules, and then creates maps that highlight important processes of vegetation loss and growth. For vegetation index like NBR, decreases of values represent loss of forest and increases of values suggest gain of forest. The outputs from change label mapping can provide the onset timing, duration and conditions of significant loss or recover processes at pixel level. Then to remove single-pixel noises in the results, a spatial filtering step is conducted to create patch-based maps.

In general, when running the algorithm, we first run the segmentation and labeling in an evaluation model to detect and fix any problematic issues related to data preparation, in order to generate stable results. Then, the code is run in a full segmentation mode, which creates fitted images considering original index, multiple bands and TC components. Next, change labeling and spatial filtering steps are conducted to generate final outputs.

2.3.2 Experiments with LandTrendr

The performance of LandTrendr is highly dependent on a variety of parameters related to segmentation, trajectory fitting, and change labeling in the algorithm. Specifically, three parameters "*pct_tree_loss1*", "*pct_tree_loss20*" and "*pct_tree_gain*" from the change labeling step have direct impacts when characterizing the forest cover changes based on the segmentation results. Here *"pct_tree_loss1"* specifies the minimum percent cover loss caused by disturbances within one year. Similar to "*pct_tree_loss1*", *"pct_tree_loss20"* is defined for a 20-year duration. In addition, *"pct_tree_gain"* represents the minimum cover gain to determine a segment growth. Fragal et al. (2016) tested several different combinations of these parameters to optimize the algorithm results. Thus, in this study we also explored different settings of these parameters as suggested by Fragal et al. (2016). The detailed parameter settings are summarized in Table 2.2.

Table 2.2 Parameter settings for LandTrendr experiments

Parameter	Group1	Group2	Group3	Group4	Group5
pct_tree_loss1	0.1	0.2	0.25	0.3	0.35
pct_tree_loss20	0.03	0.1	0.125	0.15	0.2
pct_tree_gain	0.05	0.15	0.2	0.25	0.3

2.3.3 Evaluation of Results

The source trajectories and the fitted trajectories were then compared to examine the trend of disturbance for these pixels. For each group of tests, we generated labeled change detection maps including: year of disturbance onset, duration of change and magnitude of disturbance. To assess the results, we calculated the confidence level of our results from all five groups of tests to estimate the confidence of detected change based on the method described in Fragal et al. (2016). For each group, we generated the change detection binary layers by assigning changed pixels to 1 and the rest to 0. Then for each pixel, a confidence index ranging from 0 to 1 was calculated as the normalized sum of results from all five groups using the following equation:

$$Confidence\ Index = \frac{\sum_{i=0}^{N} x_i}{N},$$

where N represents the total number of groups, i represents each group and x_i is the binary value of each pixel in each group. In addition, GLAD forest cover loss data were used to examine and compare the spatial patterns of forest loss estimated with LandTrendr.

2.4 Results and Discussions

2.4.1 Distribution of eastern hemlock forests in GRSM

Eastern hemlock forests in GRSM are typically mixed with vegetation communities such as rhododendron, Southern Appalachian mixed hardwoods, montane alluvial hardwoods, etc. (Madden et al., 2004). According to the percent coverage of different species, we first summarized the major vegetation communities related to the two hemlock distribution types as listed in Table 2.3. The distribution of both hemlock dominant and hemlock mixed types were further mapped in Figure 2.4. The hemlock dominant region is sparsely spread within GRSM with a total area of 63.81 km^2. It primarily concentrates in the eastern side of the national park, around the Cataloochee Valley. With a larger coverage of 140.90 km^2 in GRSM, the hemlock mixed region is widely distributed in the western and mid parts of the park.

Table 2.3 Dominant and mixed hemlock regions with corresponding vegetation communities

Type	Overstory Vegetation Communities	Vegetation Class Code
Dominant hemlock region	Eastern Hemlock/Rhododendron	T, T/R, T/K
	E. Hemlock/ Southern Appalachian Mixed Mesic Acid Hardwoods	T/NHxA
	E. Hemlock/Yellow Birch/Rhododendron	T/NHxB, T/NHx
	Hemlock/ Montane Alluvial Hardwoods and Broad Valley Acid Code Hardwoods	T/MAL
	Red Spruce-Hemlock/Rhododendron	T/S
	S. Appalachian Cove Hardwoods	T/CHx, T/CHxA, T/HxL
	E. Hemlock - E. White Pine/ Rhododendron	T/PIs
Mixed hemlock region	Red Spruce-Hemlock/Rhododendron	S-T, S-T/R
	S. Appalachian Northern Hardwoods	NHx-T, NHxB-T, NHxR-T, NHxA-T,
	Montane Alluvial Hardwoods	MAL-T
	S. Appalachian Cove Hardwood Forests	CHx-T, CHxL-T, CHxA-T
	S. Appalachian Early Successional Hardwoods	HxL-T, HxB-T
	S. Appalachian Mixed Hardwood Forest	HxA-T
	E. Hemlock - E. White Pine/ Rhododendron	PIs-T

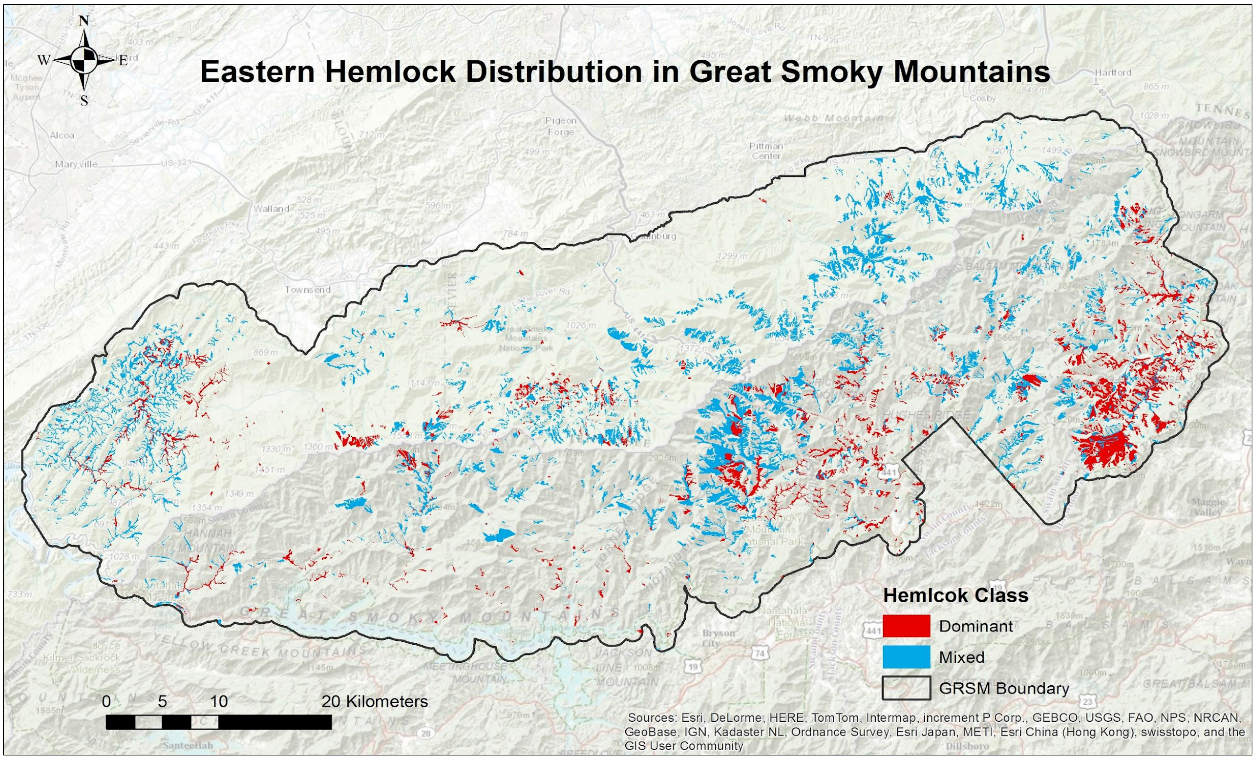

Figure 2.4 Spatial distribution of the hemlock dominant and hemlock mixed classes in GRSM (Welch et al., 2002; Madden et al., 2004)

2.4.2 Spatial and temporal patterns of hemlock defoliation in GRSM

We then constructed and fitted pixel-by-pixel spectral trajectories from 1991 to 2011 in the segmentation step of LandTrendr. The segments and significant vertices were generated primarily based on the NBR trends while considering the temporal trends of three surface reflectance bands and TC components. Figure 2.5 shows two examples of original and fitted trajectories of NBR for two hemlock forest sites in GRSM. The hemlock site in Figure 2.5 (a) shows consistent NBR values from 1991 to 2002 and decrease from 0.4 to 0.1 during 2003 to 2005. The NBR then tends to stay around 0.1 after 2006. Similarly, the fitted NBR trajectory in Figure 2.5 (b) shows that the western site has an NBR value reducing from 0.4 to 0.35 from 1991 to 2003. Then the value begins to drop rapidly during 2003 and 2004. Compared to the original NBR data, the fitted lines represent the general temporal changes in these sites very well and also remove the noises properly.

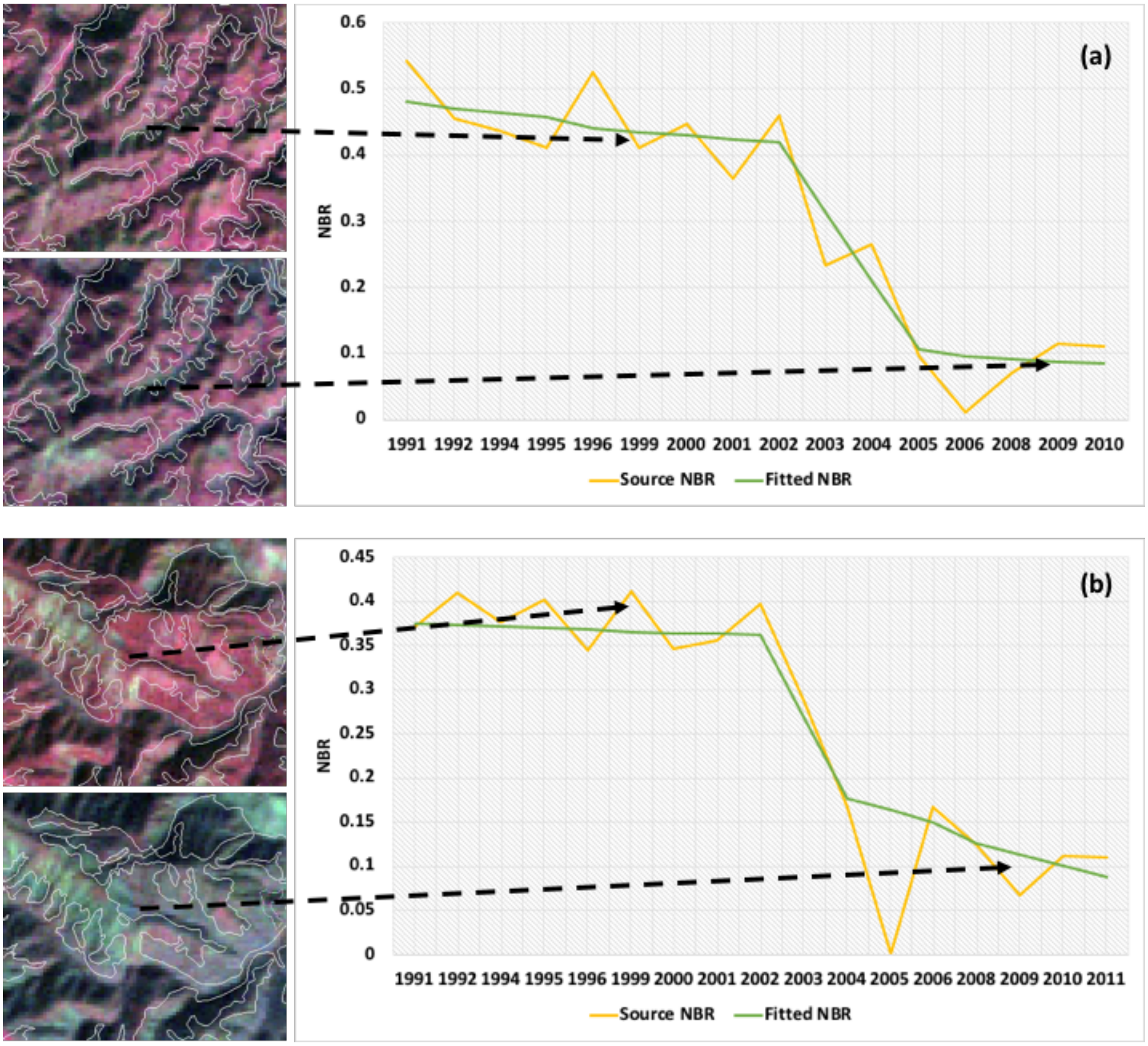

Figure 2.5 Temporal NBR trajectories of two hemlock forest sites in GRSM. In particular, (a) is from eastern GRSM and (b) is from western GRSM. Upper false color images show the original Landsat surface reflectance data before disturbance in 1999. Lower false color images show the original Landsat surface reflectance data after disturbance in 2009.

Based on the fitted trajectories, we then labeled the change classes using the five groups of parameter settings in Table 2.2. We further generated patch-based maps for different change classes through spatial filtering and examined the year of onset, magnitude and duration for these classes. Here we focus on the results and discussions for the following change classes: greatest disturbance, longest disturbance and longest discovery. The greatest disturbance change class in this study considers all the disturbance segments identified in the trajectories, without restrictions on the time period, duration length or magnitude. Compared to the greatest disturbances, we only consider the segments longer than four years as the longest disturbance change class. The greatest recovery class here considers all segments that indicate potential tree recovery in the 20-year time series, without any further restrictions. For each change class, we further assess the overall patterns (year of onset, duration, and magnitude) for hemlock dominant and hemlock mixed regions and show the detailed maps of certain regions. Since Group 5 is the most restrictive parameter set with the highest reliability when compared to other groups (Fragal et al., 2016), here we only discuss the results of Group 5 in detail.

For the greatest disturbance events, we summarized the area of each year of onset in Figure 2.6. For both hemlock dominant and mixed forests, the years of 1992, 2003 and 2006 show substantial large disturbance areas when compared to other years. Ever since the first discover of HWA in GRSM circa 2002, hemlock forests in GRSM were most severely disturbed in 2003 and 2006, with more than 6 km^2 and 8 km^2 forests affected, respectively. The 2003 disturbance influenced more hemlock dominant region than the mixed region, while the 2006 disturbance mainly occurred in the hemlock mixed region with an area of 5.4 km^2. Following 2003, the years of 2004 and 2005 also showed disturbances that covered less than 2 km^2. Prior to the infestation of HWA in GRSM, the year of 1992 was also detected as the onset year of defoliation in about 7.4 km^2 hemlock forest, because these pixels actually show a general decreasing trend during the entire 20-year time series (Figure 2.7). On one hand, this gradual trend could be caused by other gradual disturbances related to climate change (warming, drought, etc.) rather than HWA infestation. On the other hand, although the algorithm tries to minimize the noises in the time series, data quality and inconsistency in the 20-year period still have the potential to result in this pattern.

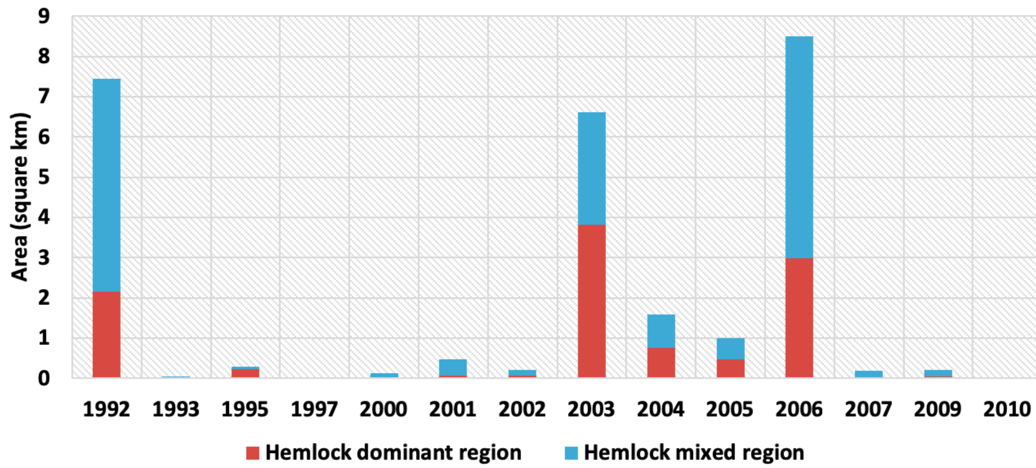

Figure 2.6 Year of onset of greatest disturbance events for hemlock forests in GRSM

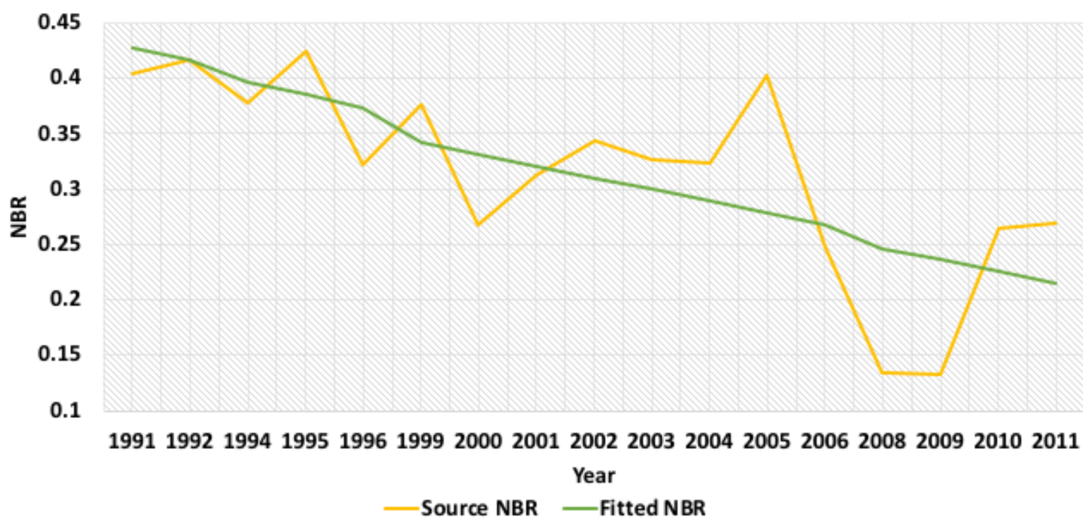

Figure 2.7 Source and fitted NBR trends for a site in hemlock forests with 1992 as the onset year of disturbance

Figure 2.8 shows an example of the affected hemlock forests in eastern GRSM. The disturbance events in this region mainly start in 2003 (yellow) and 2006 (cyan). We also examined the duration of greatest disturbance events in the study area as shown in Figure 2.8. Since we consider all the disturbance for this change class, greatest disturbance events mainly range from 1 to 9 years for within the hemlock forests in GRSM. Disturbance events lasting 1 year, 4 years and 6 years cover more than 3 km^2 in total for the hemlock forests. The 20-year disturbance is corresponding to the 1992 events shown in Figure 2.6, which is not the main focus of this study.

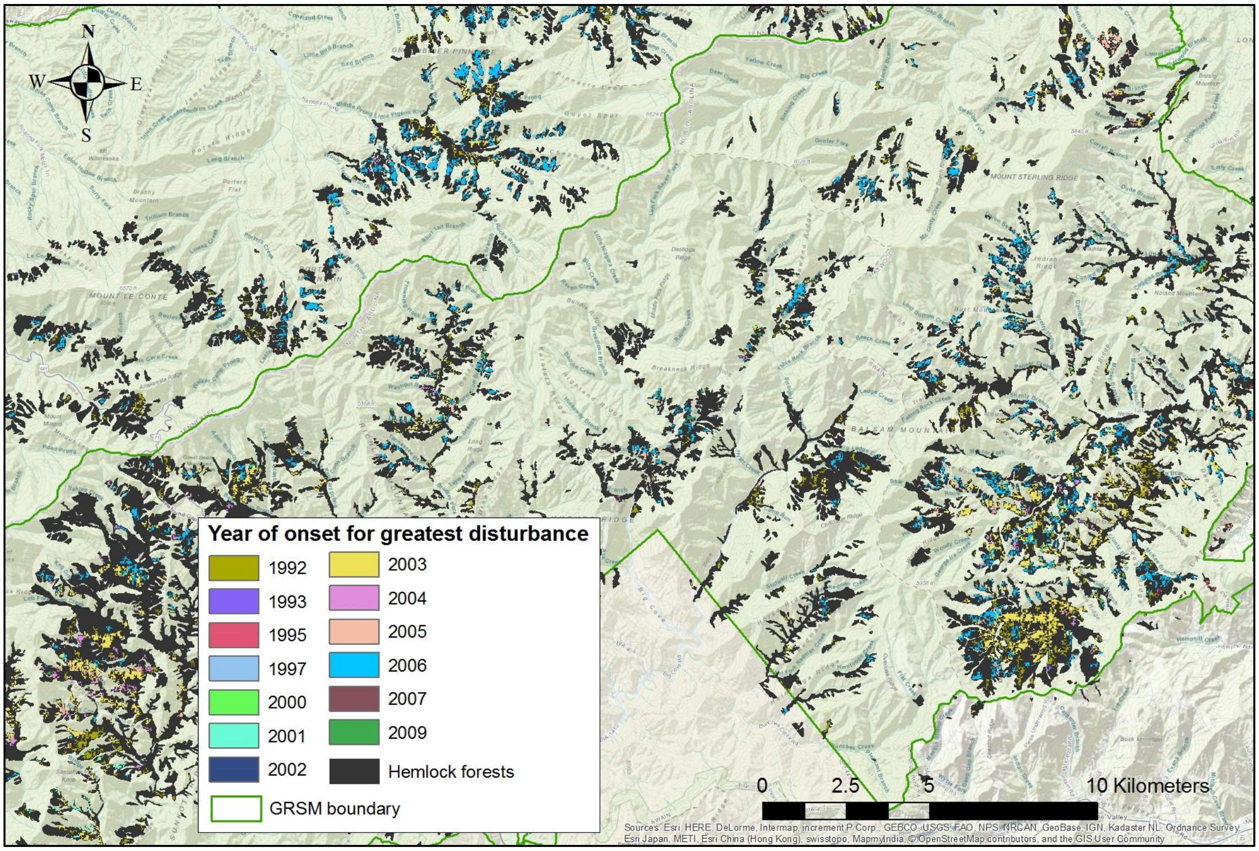

Figure 2.8 Year of onset of greatest disturbance events for hemlock forests in eastern GRSM

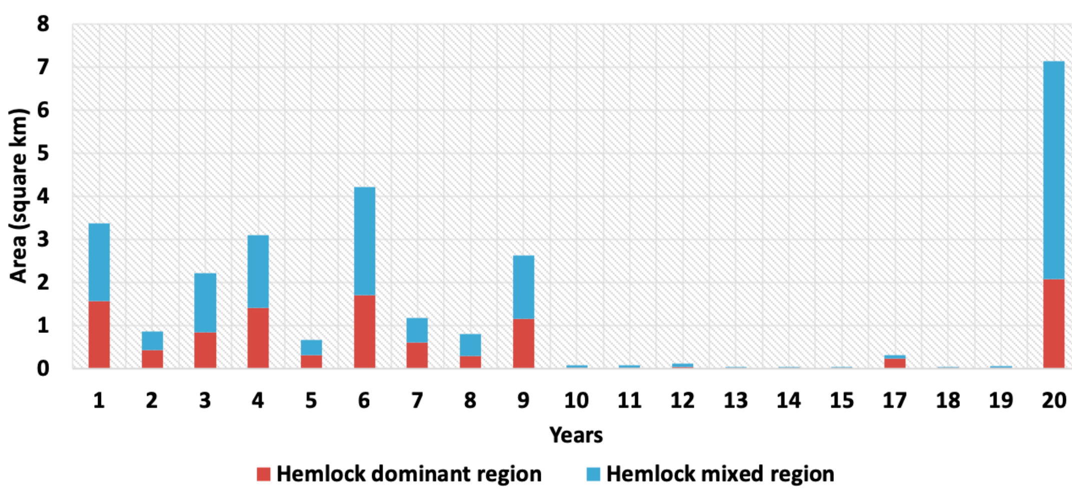

Figure 2.9 Duration of greatest disturbance events for hemlock forests in GRSM

For the longest disturbance events, we summarized the area of each year of onset in Figure 2.10. Different from the greatest disturbance events, the year of 2003 has many more disturbance events longer than four years when compared to other years, which occupies about 12.8 km^2

throughout the hemlock forests in GRSM. Following that, in 2004, about 7 km^2 hemlock regions started to experience forest loss that longer than four years. The years 2002, 2005 and 2006 also witnessed long-term hemlock disturbance covering about 4 km^2. Figure 2.11 mapped the onset year of longest disturbance type that affect hemlock forests in eastern GRSM.

For the greatest recovery events, we summarized the area of each year of onset in Figure 2.11. An area of approximately 2 km^2 of hemlock forests started to show recovery in 2009 and 2010. While other years indicated very limited recovery occurred. Figure 2.12 is an example of the recovered hemlock forests in eastern GRSM. The recovery of 2009 and 2010 are shown as light and dark green in the output map. Since the growth and succession of understory vegetation can affect the spectral signatures after the defoliation of overstory hemlock trees, this recovery pattern can be resulted from the detection of understory vegetation and does not represent the actual recovery of overstory hemlock forests. The year 1992 is also identified as the year of onset for the recovery of approximately 9.7 km^2 hemlock forests from 1991 to 2011. Similar to the 20-year gradual decline, this type of recovery can be caused by the algorithm itself or data quality, rather than the control efforts of HWA infestation in GRSM.

Compared to Group 5, the other 4 groups generate similar spatial and temporal patterns for these disturbance and recovery events of hemlock forests in GRSM, although they tend to identify larger areas of these events in general. Since the algorithm is only developed for imagery from Landsat 5 and 7, we have so far only constructed a 20-year time series with only Landsat 5 and 7 data without including Landsat 8 data acquired after 2014 in the data processing. This is because the original LandTrendr algorithm written in Interactive Data Language that we used here does not incorporate Landsat 8 data, and the SLC gaps in Landsat 7 data could affect the overall results if we simply include Landsat 7 data after 2012. Kennedy et al. (2018) recently implemented the algorithm for all Landsat data on the Google Earth Engine platform. In future, we will improve the results by combining Landsat 8 data in the analysis to monitor the hemlock defoliation condition in GRSM.

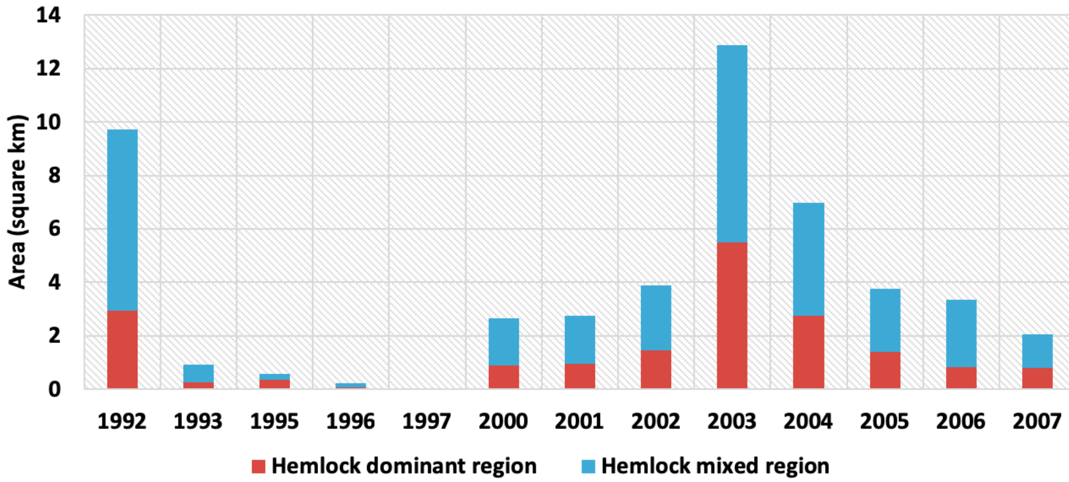

Figure 2.10 Year of onset of longest disturbance events for hemlock regions

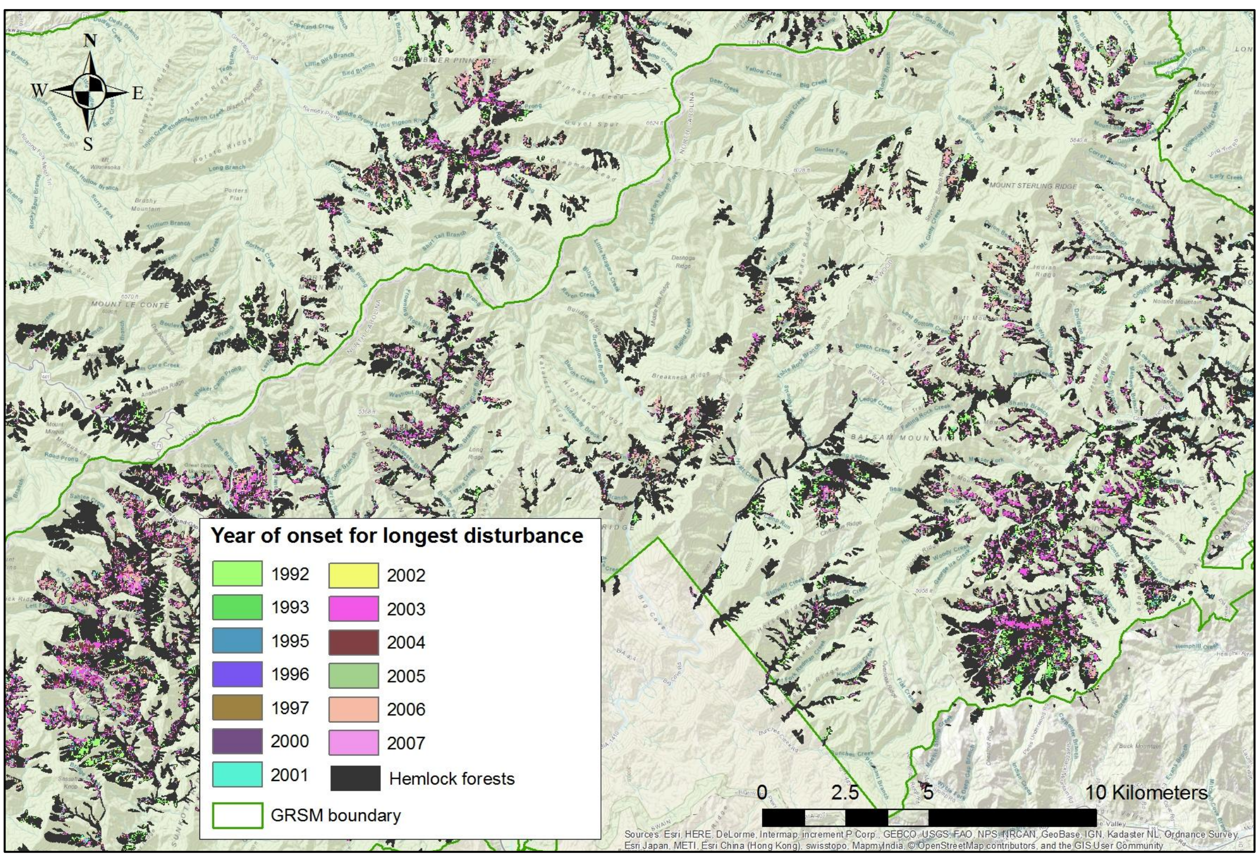

Figure 2.11 Year of onset of longest disturbance events in eastern GRSM

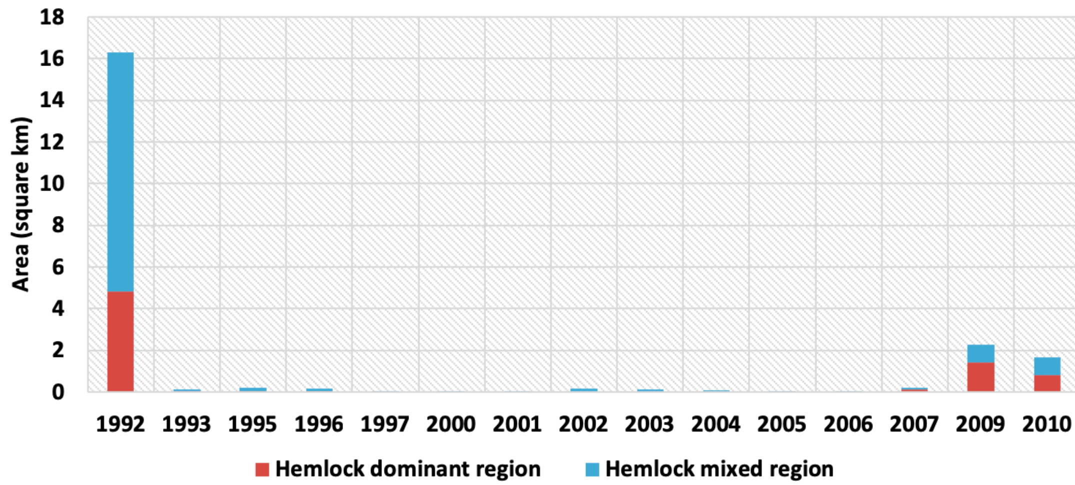

Figure 2.12 Year of onset of greatest recovery events for hemlock forests in GRSM

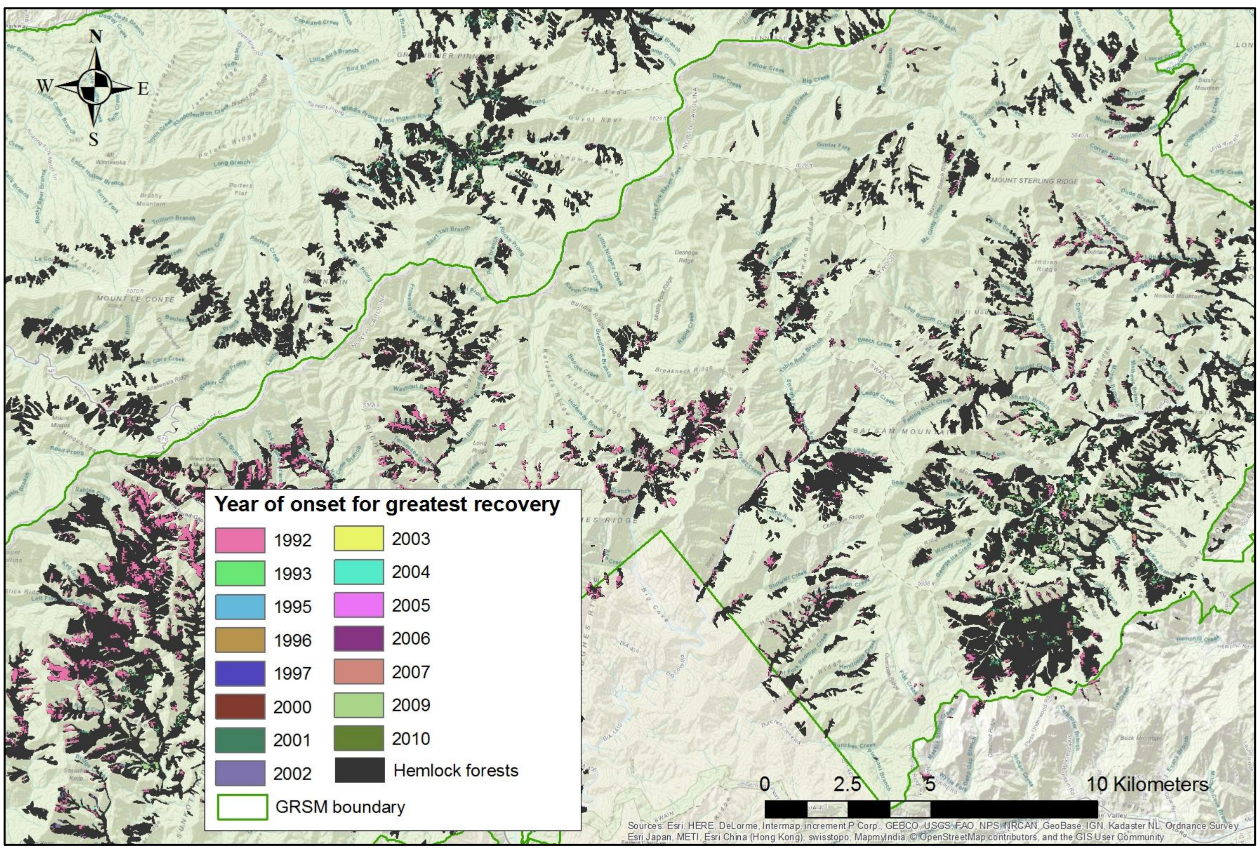

Figure 2.13 Year of onset of greatest recovery events in eastern GRSM

2.4.3 Result evaluation and comparison

To assess the overall performance of the loss and recovery results from LandTrendr, we further calculated the confidence index for the greatest disturbance and greatest recovery results from the five groups of tests. Since HWA infestation was first observed in GRSM circa 2002, we only focused on the pixels with year of onset after 2000 to assess the hemlock change caused by HWA. Figure 2.14 summarizes the confidence index for both disturbance and recovery for hemlock forests. Here disturbance refers to the greatest disturbance event and recovery refers to the greatest recovery event from the results. In general, about 8.2 km^2 hemlock dominant region and 10.7 km^2 hemlock mixed region are identified as hemlock loss with high confidence, while recovery occurred in approximately 2.3 km^2 of hemlock dominant region and 2.1 km^2 hemlock mixed region with high confidence. During the leaf-off period in this study, other coniferous species, such as rhododendrons and white pine, and understory vegetation species might stay active during the dates of our data collection. Due to the mixed canopy cover, this impact should be minimized as the study focused on areas previously identified as hemlock.

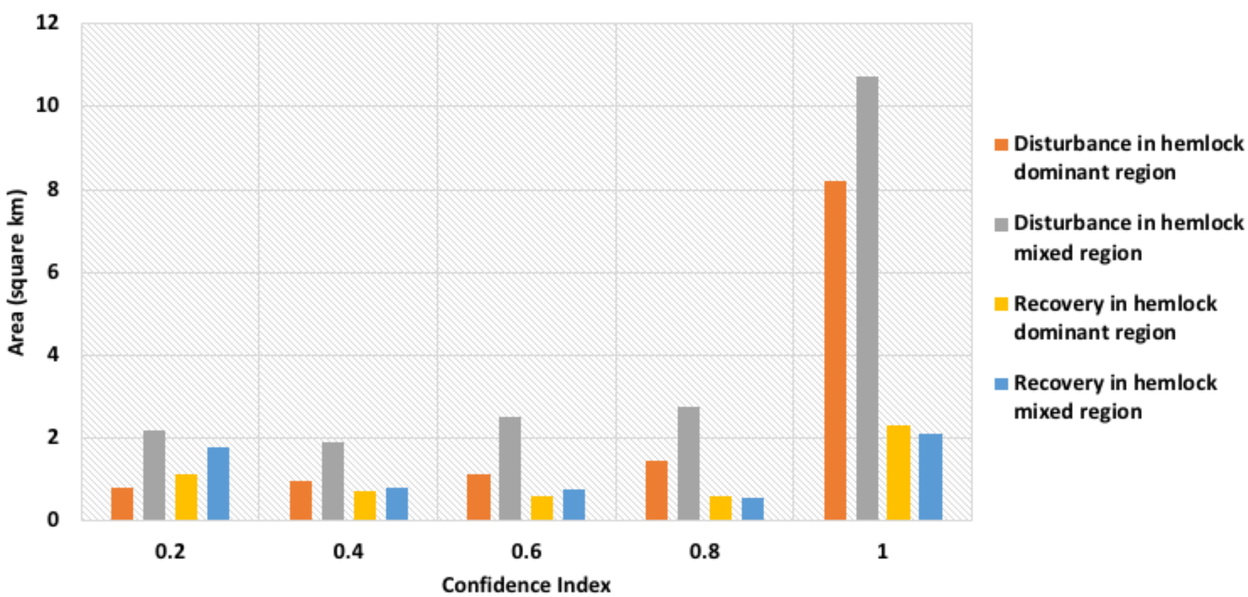

Figure 2.14 Confidence index values for post-2000 disturbance and recovery in the hemlock forests of GRSM

We also compared our results with the forest loss captured by GLAD dataset between 2001 and 2014. Figure 2.15 shows the area of tree cover loss captured in each year within the defined hemlock forests in GRSM. In general, the GLAD dataset underestimates the disturbance in hemlock forests when compared to our results. There is a significant loss within hemlock forests that is actually caused by the tornado outbreak across the Southeastern US in April 2011 (Bernardes & Madden, 2016; Figure 2.16), while other years like 2008 and 2004 only witnessed limited loss of tree cover in hemlock forests. The differences in results could be caused by the methods that are used to generate the GLAD data. Aiming at mapping the overall forest cover conditions, GLAD is developed based on the data acquired in leaf-on seasons, during which other mixed overstory and understory species could affect the spectral signals in the data. Focusing on the hemlock defoliation conditions, our study simply adopted data in leaf-off conditions to minimize the impacts from other species.

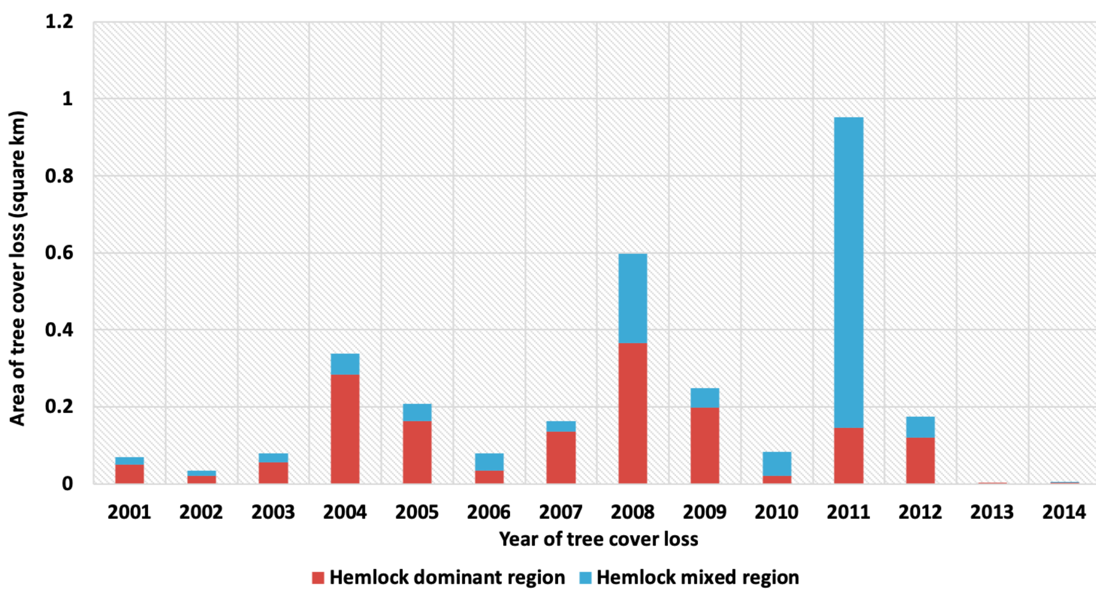

Figure 2.15 Yearly tree cover loss of hemlock forests in GRSM as from GLAD data

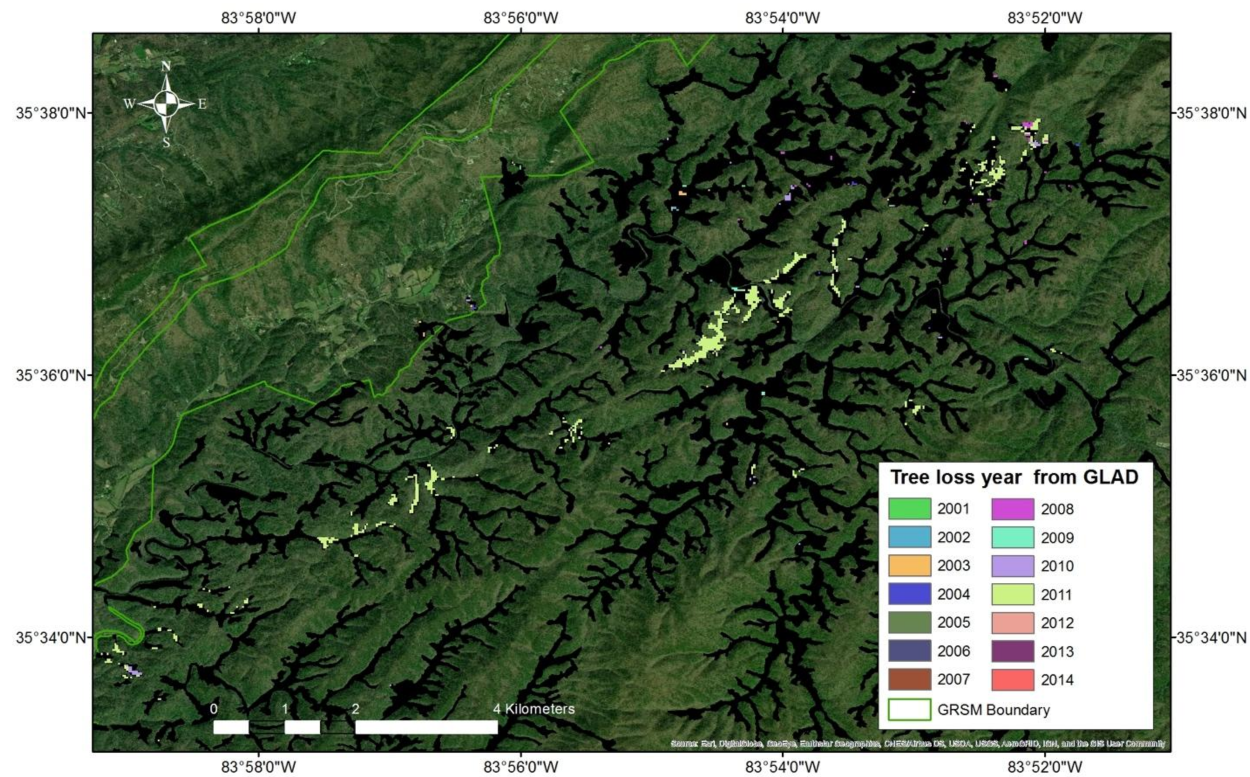

Figure 2.16 Yearly tree cover loss from GLAD data for hemlock forests in eastern GRSM

The algorithm used in this study has the capability of capturing the major disturbance events by examining the spatial and temporal patterns of spectral information. However, it also has its weaknesses. To represent forest disturbance conditions accurately, this method requires expert knowledge for parameter settings in the segmentation and change labeling steps. The performance of the segmentation step is largely impacted by the trajectory construction results, which depends on the proper removal of cloud and cloud shadow pixels. In addition, the information of spatially-adjacent pixels are only considered for spatial filtering, but not integrated into the segmentation step, which could affect the robustness of the results (Kennedy et al., 2010). Moreover, other drivers of disturbances in hemlock forests such as tornadoes and fires were not separated in our study, which could amplify the impacts of HWA on hemlock defoliation.

Although this algorithm can detect forest cover changes, the factors driving the change still need more knowledge and long-term monitoring of the study area. Our results also suggest gradual forest loss within the hemlock forests of GRSM, which could be driven by factors other than insect infestation. In addition to HWA, the health condition of eastern hemlock is also threatened by the stresses from drought, poor site conditions and other disease pests (Souto & Shields, 2000). Existing studies also have shown that changing climatic conditions, such as temperature extremes and drought, can affect the susceptibility of trees to insects and amplify the mortality of trees (Allen et al., 2010; Sturrock et al., 2011; Evans et al., 2013). As eastern hemlock is very sensitive to drought, it is also believed that drought can weaken the eastern hemlock and can increase the susceptibility of hemlock to HWA (Orwig & Foster, 1998). For more accurate evaluation of results, ground-based forest inventory data should be investigated in future to better understand the hemlock health conditions in GRSM.

2.4.4 Implications for hemlock management practices

Although previous studies have examined hemlock defoliation in other regions, this regional-scale analysis makes an initial effort in examining the overall spatiotemporal patterns of hemlock defoliation induced by HWA outbreaks in recent years. The 30-m forest change maps generated in this study also suggest potential management actions for hemlock forests within GRSM. The disturbance results map the extent of hemlock loss and assist the proper design of HWA control policies. Koch et al. (2006) predicted the future infestation of HWA in GRSM and found it most likely to occur in the northern portion of the park or near the roads and major trails. However, our results suggest that HWA infestation has been widely distributed across the hemlock forests in GRSM by 2011. Krapfl et al. (2011) previously observed significant hemlock loss caused by HWA infestation in GRSM with forest inventory data. Our results further quantify the yearly hemlock loss in GRSM, which could assist the evaluation of potential impacts of hemlock mortality on local ecosystems. In addition, the recovery results can help with tracking the long-term performance of existing control efforts.

2.5 Conclusions and Future Work

In summary, this study maps yearly hemlock defoliation caused by HWA infestation in GRSM at a fine spatial scale. By identifying the starting year and lasting period of substantial disturbance events of hemlock forests, our results provide an important context for ecosystem monitoring and insect control planning policies in GRSM. In particular, our results identify the hotspots of hemlock defoliation and recovery, which highlights the regions that requires HWA controls effects and further assessments of ecosystem impacts. In addition to the forest loss caused by HWA infestation, we also identified long-term gradual disturbances inside the park during the two decades (1991 ~ 2011), suggesting the need to examine additional driving factors of forest loss within GRSM. Accurate evaluation and consistent monitoring of hemlock mortality will continue to be significant for sustainable ecosystem management within GRSM. With the Landsat 8 satellite launched by NASA in 2013 and Sentinel-2A and 2B satellites launched by European Space Agency (ESA) in 2015 and 2017, broad-scale forest health monitoring will reach a new epoch with higher spatial and temporal resolution. In addition, considering the inconsistency of Landsat level-2 datasets caused by sensors and processing algorithms, the utilization of Landsat Analysis Ready Data developed by USGS can improve the performances of long-term disturbance studies.

References

Allen, H., & Madden, M. (2009). Geovisualization of Forest Dynamics: Hemlock Woolly Adelgid Damage in Great Smoky Mountains National Park. Vasa.

Allen, C. D., Macalady, A. K., Chenchouni, H., Bachelet, D., McDowell, N., Vennetier, M., Kitzberger, T., Rigling, A., Breshears, D.D., Hogg, E.H., Gonzalez, P., Fensham, R., Zhang, Z., Castro, J., Demidova, N., Lim, J.H., Allard, G., Running, S.W., Semerci, A., & Cobb, N.. (2010). A global overview of drought and heat-induced tree mortality reveals emerging climate change risks for forests. Forest Ecology and Management, 259(4), 660–684.

Bernardes, S., & Madden, M. (2016). Vegetation Disturbance and Recovery Following a Rare Windthrow Event in the Great Smoky Mountains National Park. In the International Archives of the Photogrammetry, Remote Sensing and Spatial Information Sciences (Vol. XLI-B8, pp. 571–575).

Brisbin, R. L. (1970). Eastern hemlock (Tsuga canadensis (L.) Carr.). FS-239, 239.

Clark, J. T., Fei, S., Liang, L., & Rieske, L. K. (2012). Mapping eastern hemlock: Comparing classification techniques to evaluate susceptibility of a fragmented and valued resource to an exotic invader, the hemlock woolly adelgid. Forest Ecology and Management, 266, 216–222.

Cohen, W. B., & Goward, S. N. (2004). Landsat's Role in Ecological Applications of Remote Sensing. BioScience, 54(6), 535–545.

Cohen, W. B., Yang, Z., & Kennedy, R. (2010). Detecting trends in forest disturbance and recovery using yearly Landsat time series: 2. TimeSync - Tools for calibration and validation. Remote Sensing of Environment, 114(12), 2911–2924.

Crist, E. P. (1985). A TM Tasseled Cap equivalent transformation for reflectance factor data. Remote Sensing of Environment, 17(3), 301–306.

Evans, B., Stone, C., & Barber, P. (2013). Linking a decade of forest decline in the south-west of Western Australia to bioclimatic change. Australian Forestry, 76(3–4), 164–172.

Eastman, R. J., Sangermano, F., Ghimire, B., Zhu, H., Chen, H., Neeti, N., Cai, Y., Machado, E. A. & Crema, S. C. (2009). Seasonal trend analysis of image time series. International Journal of Remote Sensing, 30(10), 2721–2726.

Ford, C. R., & Vose, J. M. (2007). Tsuga canadensis (L.) Carr. Mortality Will Impact Hydrologic Processes in Southern Appalachian Forest Ecosystems. Ecological Applications, 17(4), 1156–1167.

Fragal, E. H., Silva, T. S. F., & Novo, E. M. L. de M. (2016). Reconstructing historical forest cover change in the Lower Amazon floodplains using the LandTrendr algorithm. Acta Amazonica, 46(1), 13–24.

García, M. J. L., & Caselles, V. (1991). Mapping burns and natural reforestation using thematic Mapper data. Geocarto International, 6(1), 31–37.

Godman, R. M., & Lancaster, K. (1990). Tsuga canadensis (L.) Carr. eastern hemlock. Silvics of North America, 1(1), 604–612.

Hansen, M. C., Potapov, P. V, Moore, R., Hancher, M., Turubanova, S. A., Tyukavina, A., Thau, D., Stehman, S. V., Goetz, S. J., Loveland, T. R., Kommareddy, A., Egorov, A., Chini, L., Justice, C. O., Townshend, J. R. G. (2013). High-Resolution Global Maps of 21st-Century Forest Cover Change. Science, 342(6160), 850–853.

Healey, S. P., Cohen, W. B., Zhiqiang, Y., & Krankina, O. N. (2005). Comparison of Tasseled Cap-based Landsat data structures for use in forest disturbance detection. Remote Sensing of Environment, 97(3), 301–310.

Huang, C., Goward, S. N., Masek, J. G., Thomas, N., Zhu, Z., & Vogelmann, J. E. (2010). An automated approach for reconstructing recent forest disturbance history using dense Landsat time series stacks. Remote Sensing of Environment, 114(1), 183–198.

Huete, A., Didan, K., Miura, T., Rodriguez, E. P., Gao, X., & Ferreira, L. G. (2002). Overview of the radiometric and biophysical performance of the MODIS vegetation indices. Remote Sensing of Environment, 83(1–2), 195–213.

Jenkins, M. A. (2007). Vegetation Communities of Great Smoky Mountains National Park. Southeastern Naturalist, 6, 35–56.

Johnson, K. D., Hain, F. P., Johnson, K. S., & Hastings, F. (2000). Hemlock resources at risk in the Great Smoky Mountains National Park. In Proceedings: Symposium on Sustainable Management of Hemlock Ecosystems in Eastern North America. US Department of Agriculture, Forest Service, General Technical Report NE-267, Newtown Square, Pennsylvania (pp. 111–112).

Johnson, K., Taylor, G., & Remaley, T. (2005). Managing hemlock woolly adelgid and balsam woolly adelgid at Great Smoky Mountains National Park. In Third symposium on hemlock woolly adelgid in the Eastern United States. Forest Health Technology Enterprise Team, Morgantown, WV, USDA Forest Service, FHTET-2005-01 (Vol. 384).

Jordan, T. R. (2002). Softcopy photogrammetric techniques for mapping mountainous terrain: Great Smoky Mountains National Park. University of Georgia.

Kennedy, R. E., Yang, Z., & Cohen, W. B. (2010). Detecting trends in forest disturbance and recovery using yearly Landsat time series: 1. LandTrendr — Temporal segmentation algorithms. Remote Sensing of Environment, 114(12), 2897–2910.

Kennedy, R. E., Yang, Z., Gorelick, N., Braaten, J., Cavalcante, L., Cohen, W. B., & Healey, S. (2018). Implementation of the LandTrendr algorithm on Google Earth Engine. Remote Sensing, 10(5), 1–10.

Kim, M., Madden, M., & Xu, B. (2010). GEOBIA vegetation mapping in Great Smoky

Mountains National Park with spectral and non-spectral ancillary information. Photogrammetric Engineering & Remote Sensing, 76(2), 137–149.

Koch, F. H., Cheshire, H. M., & Devine, H. A. (2006). Landscape-Scale Prediction of Hemlock Woolly Adelgid, Adelges tsugae (Homoptera: Adelgidae), Infestation in the Southern Appalachian Mountains. Environmental Entomology, 35(5), 1313–1323.

Krapfl, K. J., Holzmueller, E. J., & Jenkins, M. a. (2011). Early impacts of hemlock woolly adelgid in Tsuga canadensis forest communities of the southern Appalachian Mountains. Journal of the Torrey Botanical Society, 138(1), 93–106.

Letheren, A., Hill, S., Salie, J., Parkman, J., & Chen, J. (2017). A little bug with a big bite: Impact of hemlock woolly adelgid infestations on forest ecosystems in the eastern USA and potential control strategies. International Journal of Environmental Research and Public Health, 14(4), 8–10.

Madden, M., Jordan, T., Kim, M., Allen, H., & Xu, B. (2009). Integrating remote sensing and GIS: From overlays to GEOBIA and geovisualization. Manual of Geographic Information Systems, 701–720.

Madden, M., Welch, R., Jordan, T., Jackson, P., Seavey, R., & Seavey, J. (2004). Digital Vegetation Maps for the Great Smoky Mountains National Park. Center for Remote Sensing and Mapping Science, Department of Geography, University of Georgia, US.

Maingi, J., & Luhn, W. (2005). Mapping insect-induced pine mortality in the Daniel Boone National Forest, Kentucky using Landsat TM and ETM+ data. GIScience & Remote Sensing, (3), 224–250.

Masek, J. G., Vermote, E. F., Saleous, N. E., Wolfe, R., Hall, F. G., Huemmrich, K. F., Gao, F., Kutler, J., Lim, T.-K. (2006). A Landsat surface reflectance dataset for North America, 1990-2000. IEEE Geoscience and Remote Sensing Letters, 3(1), 68–72.

Maselli, F. (2004). Monitoring forest conditions in a protected Mediterranean coastal area by the analysis of multiyear NDVI data. Remote Sensing of Environment, 89(4), 423–433.

Meigs, G. W., Kennedy, R. E., & Cohen, W. B. (2011). A Landsat time series approach to characterize bark beetle and defoliator impacts on tree mortality and surface fuels in conifer forests. Remote Sensing of Environment, 115(12), 3707–3718.

Norman, S., Hargrove, W., & Spruce, J. (2013). Highlights of satellite-based forest change recognition and tracking using the ForWarn System. USDA General Technical Report.

Norman, S. P., Hargrove, W. W., & Christie, W. M. (2017). Spring and Autumn Phenological Variability across Environmental Gradients of Great Smoky Mountains National Park, USA. Remote Sensing, 9(5), 407.

Orwig, D. A., & Foster, D. R. (1998). Forest response to the introduced hemlock woolly adelgid in southern New England, USA. Journal of the Torrey Botanical Society, 60–73.

Pyle, C. (1985). Vegetation Disturbance History of Great Smoky Mountains National Park: An Analysis of Archival Maps and Records.

NPS. (2018) Great Smoky Mountains, Nature & Science. Retrieved from https://www.nps.gov/grsm/learn/nature/index.htm

Souto, Dennis R. & Shields, Kathleen S. 2000. Overview of hemlock health. In: McManus, Katherine A.; Shields, Kathleen S.; Souto, Dennis R., eds. Proceedings: Symposium on sustainable management of hemlock ecosystems in eastern North America. Gen. Tech. Rep. NE-267. Newtown Square, PA: U.S. Department of Agriculture, Forest Service, Northeastern Forest Experiment Station. 76-80.

Stadler, B., Müller, T., Orwig, D., & Cobb, R. (2005). Hemlock Woolly Adelgid in New England Forests: Canopy Impacts Transforming Ecosystem Processes and Landscapes. Ecosystems, 8(3), 233–247.

Strother, C. W., Madden, M., Jordan, T. R., & Presotto, A. (2015). Applications Paper: Lidar Detection of the Ten Tallest Trees in the Tennessee Portion of the Great Smoky Mountains National Park. Photogrammetric Engineering & Remote Sensing, 81(5), 407–413.

Sturrock, R. N., Frankel, S. J., Brown, A. V, Hennon, P. E., Kliejunas, J. T., Lewis, K. J., Worrall, J.J., Woods, A. J. (2011). Climate change and forest diseases. Plant Pathology, 60(1), 133–149.

USGS. (2018). Landsat 4-7 Surface Reflectance (LEDAPS) Product.

Taylor, G. (2012). Forest health monitoring summary Great Smoky Mountains National Park. Natural Resource Data Series NPS/APHN/NRDS-2012/378, 378, 1–13.

Walker, S. L. (1991). Great Smoky Mountains: The Splendor of the Southern Appalachians. Camelback Design Group.

Ward, J. S., Montgomery, M. E., Cheah, C. A.-J., Onken, B. P., & Cowles, R. S. (2004). Eastern hemlock forests: guidelines to minimize the impacts of hemlock woolly adelgid. NA-TP-03-04. US Department of Agriculture, Forest Service, Northeastern Area State & Private Forestry, Morgantown, WV. 27 P., 1–27.

Welch, R., Madden, M., & Jordan, T. (2002). Photogrammetric and GIS techniques for the development of vegetation databases of mountainous areas: Great Smoky Mountains National Park. ISPRS Journal of Photogrammetry and Remote Sensing, 57(1–2), 53–68.

CHAPTER 3

EXPLORING THE SPATIAL VARIATION AND ENVIRONMENTAL DRIVERS OF BURN SEVERITY IN GREAT SMOKY MOUNTAINS NATIONAL PARK: A CASE STUDY OF THE 2016 CHIMNEY TOPS 2 FIRE[2]

[2] He, Jiaying, et al. To be submitted to *ISPRS International Journal of Geo-Information*

Abstract

Wildland fire is one of the most severe broad-scale disturbances in forest ecosystems. Forest fires can exert strong impacts on climate and ecosystem services and functioning. They can also lead to human deaths and economic losses to human societies. Understanding the spatial distribution of the burn severity and related environmental factors can not only assist post-fire recovery plans, but also help decision makers prepare for future fire management efforts. The Great Smoky Mountains National Park (GRSM) has a long history of fire disturbances. Although fires within GRSM are currently managed under careful monitoring and suppression efforts, the Chimney 2 Tops 2 Fire occurred in November 2016 has led to severe impacts of the forest ecosystems in GRSM and the nearby developed area in Tennessee. In this study we aim to examine the spatial distribution of burn severity within GRSM after the Chimney Tops 2 Fire using the remote sensing imagery. We then identify how this fire affected different vegetation communities. The impacts of environmental factors affecting the distribution of burn severity caused by this fire were also explored with geospatial analysis.

3.1 Introduction

Wildland fire is one of the most severe broad-scale disturbances across many ecosystems in Earth systems (Bowman et al., 2009). Temperate forests in the North America experienced increasing frequency of severe fires during the past few decades (Millar & Stephenson, 2015; Schoennagel et al., 2017). Forest fires can exert strong impacts on climate through the alteration of carbon dynamics and surface radiative forcing (Randerson et al., 2006; Loehman et al., 2014; Seidl et al., 2014). They can also cause severe environmental effects on ecosystem functioning and services, such as destruction of vegetation communities, changes in hydrology and loss of wildlife habitats (Thom & Seidl, 2016). In addition, fire can lead to loss of lives, air pollution, and destruction of homes and livelihoods, thus affecting both health and socioeconomics of human societies (Bonazountas et al., 2007; Liu et al., 2015). Future projections suggest that climatic stresses are likely to increase the long-term fire frequency and severity, enhancing the fire impacts on local ecosystems (Miller et al., 2009; Stephens et al., 2013; van Mantgem et al., 2013; Littell et al., 2016; Parks et al., 2016).

Fire severity, or burn severity, are developed to describe the impacts of wildland fires on ecosystems (Keeley, 2009). Although the two terms are used interchangeably in some studies, their differences exist regarding the post-fire temporal scale and the biophysical properties they describe (Lentile et al., 2006; Keeley, 2009). Compared to fire severity, burn severity represents a broader range of attributes representing both fire severity and ecosystem responses, and considers both short- and long-term fire impacts (Lentile et al., 2006; Keeley, 2009). Contrary to general perception that fire burns evenly through a landscape, the levels of burn severity actually vary across the fire area, with some regions unburned, some lightly burned, and some severely burned. Post fire analysis of the spatial patterns of burn severity contributes to our understanding of fire behavior and ultimate ability to model and predict fire risk (Malmström, 2010; Jenkins et al., 2011; Francos et al., 2016).

The southern Appalachian forests in the southeastern United States (U.S.) have a long history of wildfires. Soil charcoal data suggested that wildfires have occurred regularly across the regions over the past 4,000 years, with an abrupt increase during the past 1,000 years related to the appearance of Native Americans across this area (Delcourt & Delcourt, 1998; Fesenmyer & Christensen, 2010). Fires have become less frequent in the southern Appalachian forests over the recent 250 years, coinciding with the decreased population of Native Americans caused by European settlement (Fesenmyer & Christensen, 2010). In recent decades, fire suppression efforts have significantly reduced fire activities in the forests of the southern Appalachian Mountains (Flatley et al., 2013).

The Great Smoky Mountains National Park (GRSM), located in the subrange of the southern Appalachians along the border of Tennessee and North Carolina, has experienced less fires after the establishment of the park in 1934 because of the federal policies for fire exclusion and suppression (GRSM, 2010). For example, 93 human ignited fires occurred in GRSM between 1931 and 1933 before the implement of vigorous suppression policy with more than 25 km^2 burned. While only 9 fires occurred burned 0.33 km^2 per year within the GRSM during 1960 to 1969 (Dukes, 2001). Since fires serve as the natural recycling mechanism in forest ecosystems for vegetation regeneration and nutrient circulation, both natural and prescribed fires then became allowed within the park with careful monitoring and management (Dukes, 2001). The National Park Service (NPS) further identified three suppression zones: (I) suppression, (II) conditional, and (III) prescribed natural fire zones (Dukes, 2001). Fires along the boundaries of the park and developed areas (Zone I) are immediately suppressed. Fires in Zone II are only allowed when they show no threats to Zone I. While Zone III allows fires burning within certain parameters and staying in the zone within 48 hours (Dukes, 2001).

Currently, the NPS combines the three zones and identifies two types of fire management units “Interface Zone” and “Natural Zone” within GRSM that are delineated for protecting human communities and maintaining fire adapted ecosystems (Figure 3.1; NPS, 2009; GRSM, 2010). The first type “Interface Zone”, covering approximately 17% of the total park area, is established in the regions within and adjacent to the park boundary to protect the safety of human lives, properties and sensitive resources. The remaining 83% of the park is identified as the “Natural Zone”, within which all natural processes are allowed to occur. Particularly, wildland fires occurring naturally in this unit are allowed to burn under proper conditions for the conservation of natural resources under careful monitoring of negative ecological consequences (GRSM, 2010). Within the entire GRSM, approximately 95% of landscape is covered by five fuel groups: non-flammable, grasses, shrubs, timber and slash (Madden et al., 2004). These groups are comprised of various vegetation communities including Spruce-Fir Forest, Northern Hardwood Forest, High Elevation Northern Red Oak Forest, Cove Hardwood Forest, Mesic Oak/ Hardwood Forest, Xeric Oak/ Pine Forest and Woodland, Hemlock Forest, etc. (Madden et al., 2004; GRSM, 2010).

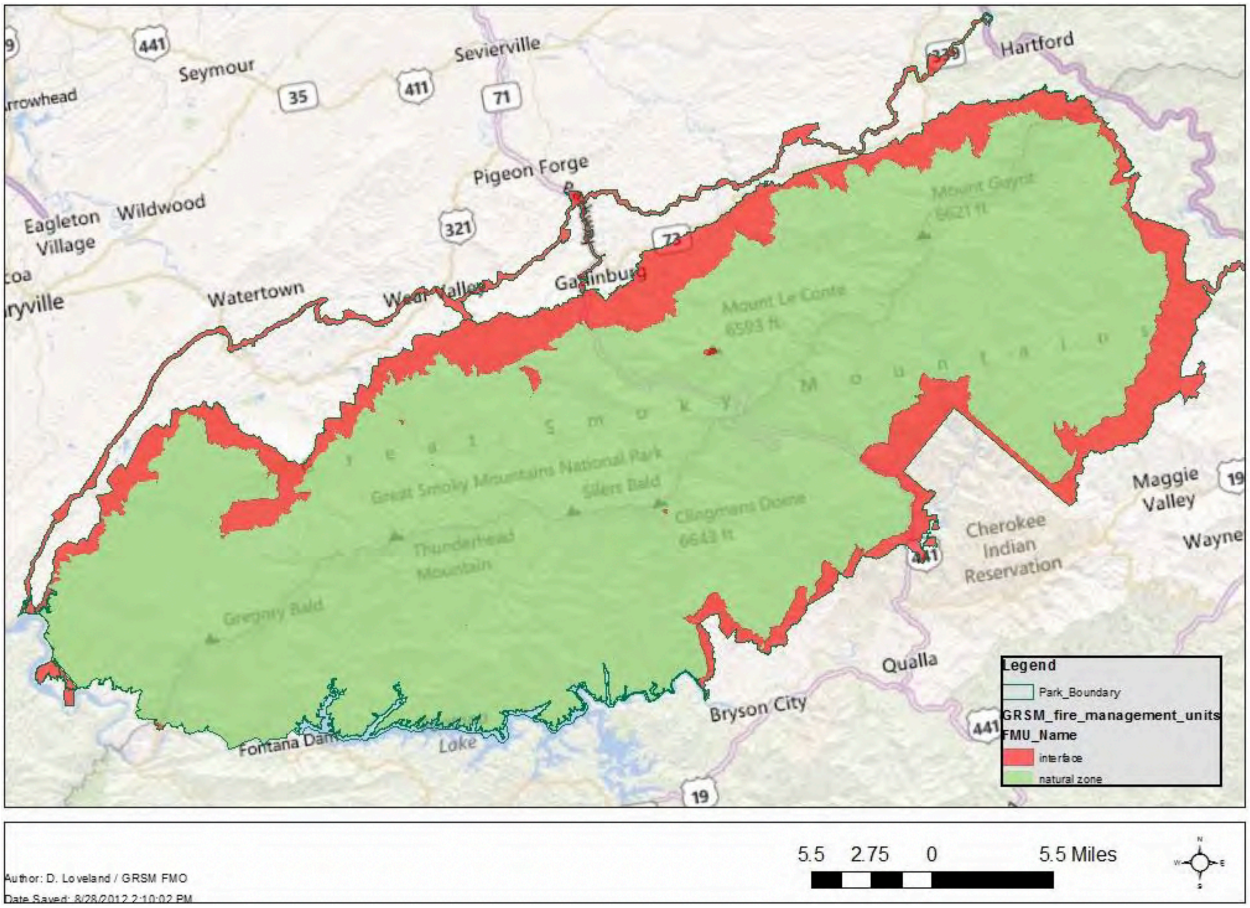

Figure 3.1 GRSM fire management units (GRSM, 2010)

In 2016, a unique combination of events and conditions led to one of the greatest outbreaks of wildfire in the southern Appalachian region. Recorded as one of the largest fires in GRSM, the Chimney Tops 2 Fire occurring in late November of 2016 lasted for six days and burned about 69.36 km^2 in total with 44.37 km^2 inside the park (Klein et al., 2017). Later determined to be caused by arson ignited in the Natural Zone on the slopes of Chimney Tops Mountain, this fire spread rapidly under gale-fore winds and raged across the Interface Zone to Gatlinburg, Tennessee, devastating adjacent developed areas and resulting in 14 deaths and nearly 150 injuries (du Lac et al., 2016; NPS, 2017). Although most wild animals have become adapted to wildfires, the rapid spread of this fire resulted in the wildlife unable to move out of the fire's path. Extensive damage to structures in Gatlinburg and the loss of human life made this one of the deadliest East Coast wildfires in many years (du Lac et al., 2016; NPS, 2016). The rapid spread of this fire was largely caused by the unusually low precipitation and warm temperatures in this region from mid-summer to fall, resulting in a tinder-dry condition for the forests (NPS, 2017). The newly fallen leaves in the autumn of 2016 that accumulated on the forest floor also provided plenty of fuels to support burning. Understanding the spatial distribution of the burn severity and related environmental factors can not only assist post-fire recovery plans, but also help decision makers prepare for future fire management efforts.

Multispectral remote sensing imagery play an important role in broad-scale monitoring and evaluation of burn severity of forest fires (Lentile et al., 2006). Developed to extract properties of land surface features with combinations of spectral bands, vegetation indices such as Normalized Difference Vegetation Index (NDVI) and Normalized Burn Ratio (NBR) have been commonly used because of their strong relationships with field severity measurements (Jensen, 2007; Keeley, 2009). For example, Brewer et al. (2005) identified NBR as the most effective method for mapping burn severity during the 2000 fire season in the Northern Rocky Mountains and Northern Great Plains. Additional indices developed based on the NBR, including differenced NBR (dNBR) and Relative dNBR (RdNBR), also show their efficiency in mapping burn severity (Miller & Thode, 2007; Wimberly & Reilly, 2007). Other metrics such as differenced Soil Adjusted Vegetation Index (dSAVI) and change in leaf area index (LAI) can also capture spatial details of burn severity in forests (Boer et al., 2008; Arnett et al., 2015). Though the values of NBR-based indices may not translate to fire-related biophysical changes accurately (Cocke et al., 2005; Boer et al., 2008), they are still among the most effective methods for assessing broad-scale forest burn severity distribution in many applications (Chang et al., 2016).

Environmental factors including fuel types, topography and weather conditions are major drivers of burn severity distribution across the landscape by controlling fire intensity and duration (Pyne et al., 1996; Dillon et al., 2011; Estes et al., 2017). Fuel types, primarily referred to vegetation fuels for forest ecosystems, affect the flammability and fuel loads that support burning, thus can further influence the fire intensity and duration (Pyne et al., 1996). Topography and weather conditions also exert strong impacts on severity distribution in multiple ways. They can influence the distribution and productivity of vegetation fuels (Barbour, 1999) and control the energy and water balances that impact vegetation development, which then affects the accumulation of fuels for burning (Dillon et al., 2011). In addition, they can control the microclimatic conditions and thus influence the fuel moisture content (Pyne et al., 1996).

The specific relationships between these factors and burn severity vary by sites. Wimberly & Reilly (2007) found burn severity distribution in southern Appalachians was strongly linked to pre-fire vegetation types, topography and changes in species richness. Birch et al. (2015) identified vegetation and topographic features as the major factors driving burn severity in central Idaho and western Montana forests. Kane et al. (2015) also explained the burn severity variance of the Rim Fire in the western US with seven weather and topographic factors. Understanding the spatial distribution of the burn severity and related environmental factors can not only provide resource managers quantitative information for assessing post-fire impacts, but also help decision makers prepare for future vegetation recovery and fire management efforts (Keane et al., 2008).

Although the Burned Area Emergency Response (BAER) team from U.S. Forest Service (USFS) conducted field assessments and classified burn severity levels with Landsat imagery right after the Chimney Tops 2 Fire in December 2016 (Klein et al., 2017), this initial effort simply considered the short-term impacts and failed to capture detailed spatial variation of burn severity. This research aims to evaluate the spatial distribution of burn severity within GRSM one year after the Chimney Tops 2 Fire using the indices derived from remote sensing imagery. Compared to the assessment conducted right after the fire, assessing the data one year after the fire can consider the recovery capability of forest ecosystem in the severity level evaluation. Then we examine how this fire affected different vegetation communities and explore the environmental factors influencing the severity distribution with geospatial analysis. Three research questions are addressed in this chapter: (1) How is the burn severity spatially distributed in GRSM after the 2016 Chimney Tops 2 Fire? (2) How does the fire impact the different vegetation habitats? (3) What environmental factors affected the distribution of burn severity in this fire?

3.2 Data and Materials

3.2.1 GRSM Vegetation Database

The GRSM vegetation database was utilized to identify the distribution of vegetation communities and fuel groups in the study area in this study. Developed by the Center for Geospatial Research (http://www.cgr.uga.edu/) at the University of Georgia in collaboration with NPS (Madden et al., 2004; Welch et al., 2002), this dataset provides detailed information about overstory and understory vegetation species and their distributions throughout the entire GRSM.

The overstory vegetation communities (Figure 3.2) were classified to the Association level, which is the finest division from the National Vegetation Classification System protocol of the U.S. Geological Survey (USGS) NPS Vegetation Mapping Program. Recorded with a Wild RC20 photogrammetric camera, over 1000 color infrared aerial photographs were acquired a 1:12,000 scale from 1997 to 1998 in late October. This is because leaf-on conditions photos acquired in the fall display diverse colors to separate vegetation communities. These photos were then scanned at 800 dpi resulted in digital images, reaching a spatial resolution of 0.4 m (Jordan 2002). These photos were manually interpreted to map the overstory vegetation communities with these data. Supplementary data, including USGS National Aerial Photography Program (NAPP) Air Photos, USGS Topographic Maps, USGS Digital Orthophoto Quarter Quadrangles

(DOQQs) and USGS level-2 Digital Elevation Model (DEM), were also used to generate the GRSM vegetation database.

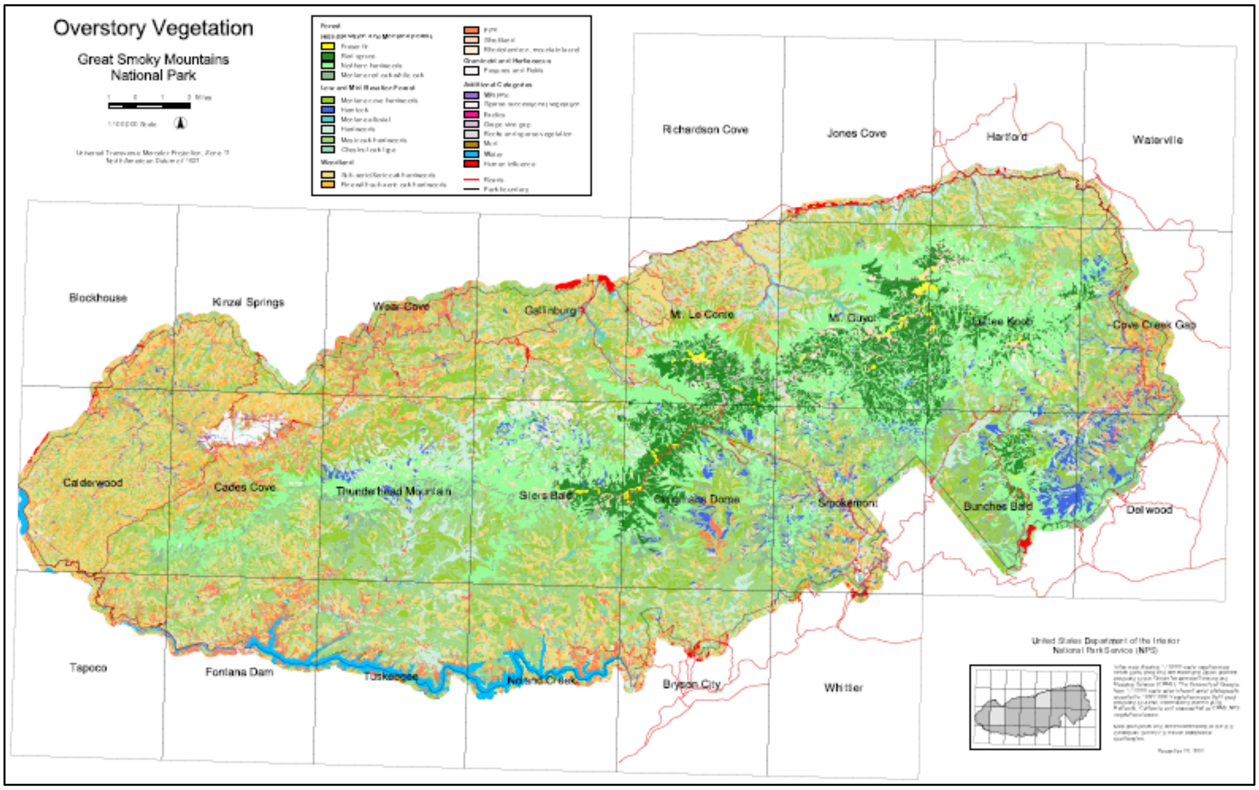

Figure 3.2 GRSM overstory vegetation map (Jordan 2002; Welch et al. 2002; Madden et al., 2004)

3.2.2 Remote Sensing Imagery

Landsat 8 Operational Land Imager (OLI) 30-m Level-2 surface reflectance data provided by U. S. Geological Survey (USGS) are obtained from EarthExplorer (http://earthexplorer.usgs.gov/) to map the burn severity of the Chimney Tops 2 Fire. Processed with the Landsat 8 Surface Reflectance Code (LaSRC), this level-2 product provides surface reflectance values for each reflective spectral band after radiometric calibration, geometric correction and atmospheric correction (USGS, 2018). In this study, the images covering GRSM (Path 19 Row 35) before the fire starts and one year after the fire were selected for data analysis. Specifically, this study selected image pairs collected around similar time period from the beginning of the growing season in May to the end of the growing season in September. Clear images with limited clouds and cloud shadows are preferred when choosing the imagery. Table 3.1 lists the detailed information of the level-2 Landsat 8 OLI images used in this study.

Table 3.1 Landsat 8 OLI Path 19 Row 35 level-2 imagery obtained for this study

State	Landsat 8 Scene ID	Acquisition Date	Date of Year	Cloud Cover
Pre-fire	LC80190352015257LGN01	2015/09/14	257	0.03%
Post-fire	LC80190352017246LGN00	2017/09/03	246	0.24%

3.2.3 The Chimney Tops 2 Fire Dataset

The Chimney Tops 2 Fire data, including fire perimeter and vegetation severity levels (Figure 3.3), were obtained from ArcGIS Online account of GRSM Geographic Information Science (GIS) team (https://www.arcgis.com/home/user.html?user=GRSM_GIS). The Infrared (IR) heat perimeter shapefile for the Chimney Tops 2 Fire was created from thermal infrared scan data obtained from airborne thermal infrared imaging system on Dec. 2, 2016 by USFS. The perimeter data include the main fire polygons, a list of isolated heat sources and potential heat sources. The main fire polygons were generated from the IR data with very few perimeter edits. The vegetation severity data were generated from the Burned Area Reflectance Classification (BARC) image developed with Landsat imagery and field observations collected by the BAER. Specifically, the field observations collected in these data measured the degree of scorch, consumption, and mortality of vegetation and the projected or ultimate vegetative recovery to evaluate the wildfire impacts on vegetative ecosystems.

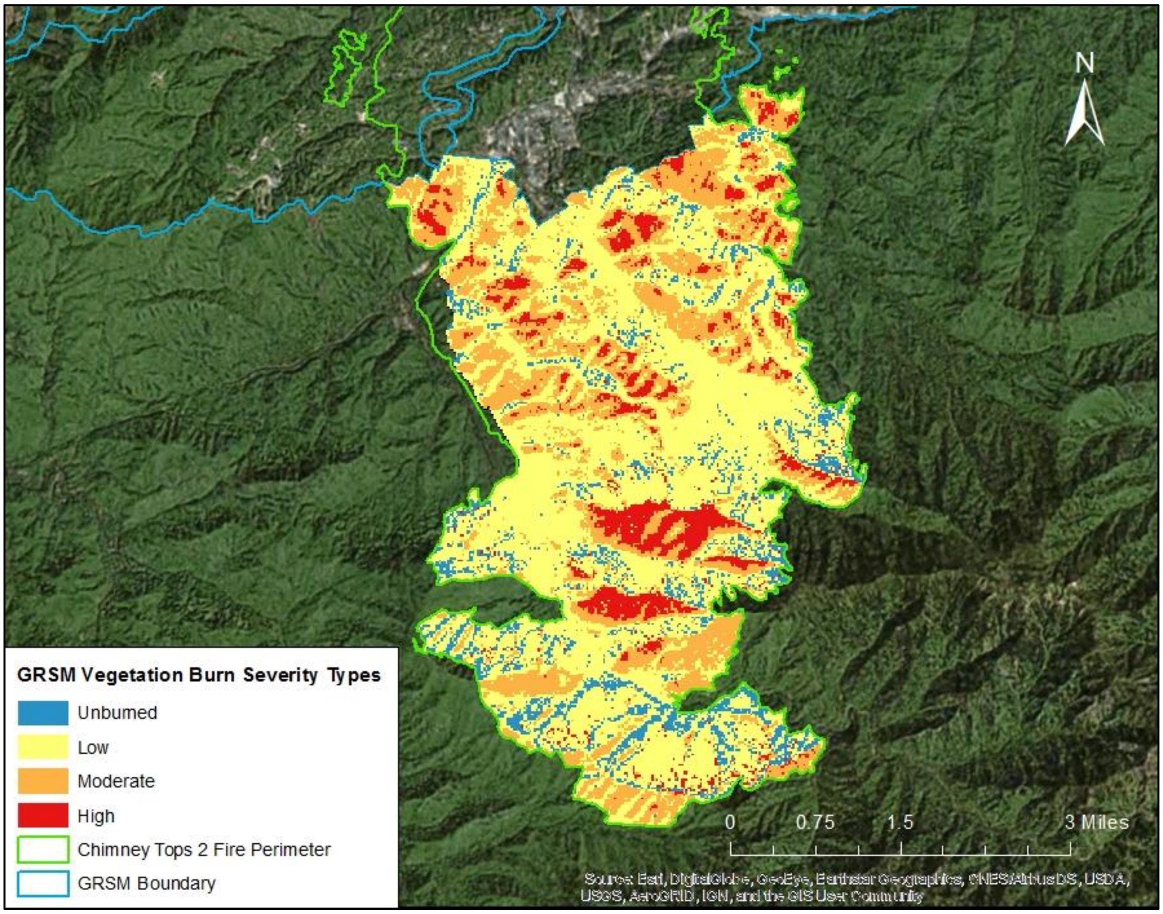

Figure 3.3 Vegetation burn severity levels generated with BARC image by BAER team for the 2016 Chimney Tops 2 Fire within GRSM

3.2.4 Climatic Dataset

To assess the impacts of fire weather conditions on the burn severity, daily surface weather data Daymet were acquired in 2016 through the Oak Ridge National Laboratory Distributed Active Archive Center (ORNL DAAC, https://daymet.ornl.gov). This dataset provides daily, monthly and yearly gridded estimates of weather parameters for the North America since 1980 with 1-km spatial resolution, including minimum and maximum temperature, precipitation, humidity, shortwave radiation, snow water equivalent, water vapor pressure and day length (Thornton et al., 2017). These parameters were generated through an integration of weather station data and spatial interpolation methods. In addition to Daymet, hourly wind speed and wind direction station data in 2016 were downloaded from the NPS Gaseous Pollutant Monitoring Program Database (https://ard-request.air-resource.com). This program provides six weather stations in total in GRSM and four of them have wind data for 2016, including Cades Cove, Clingmans Dome, Cove Mountain, and Look Rock as mapped in Figure 3.4.

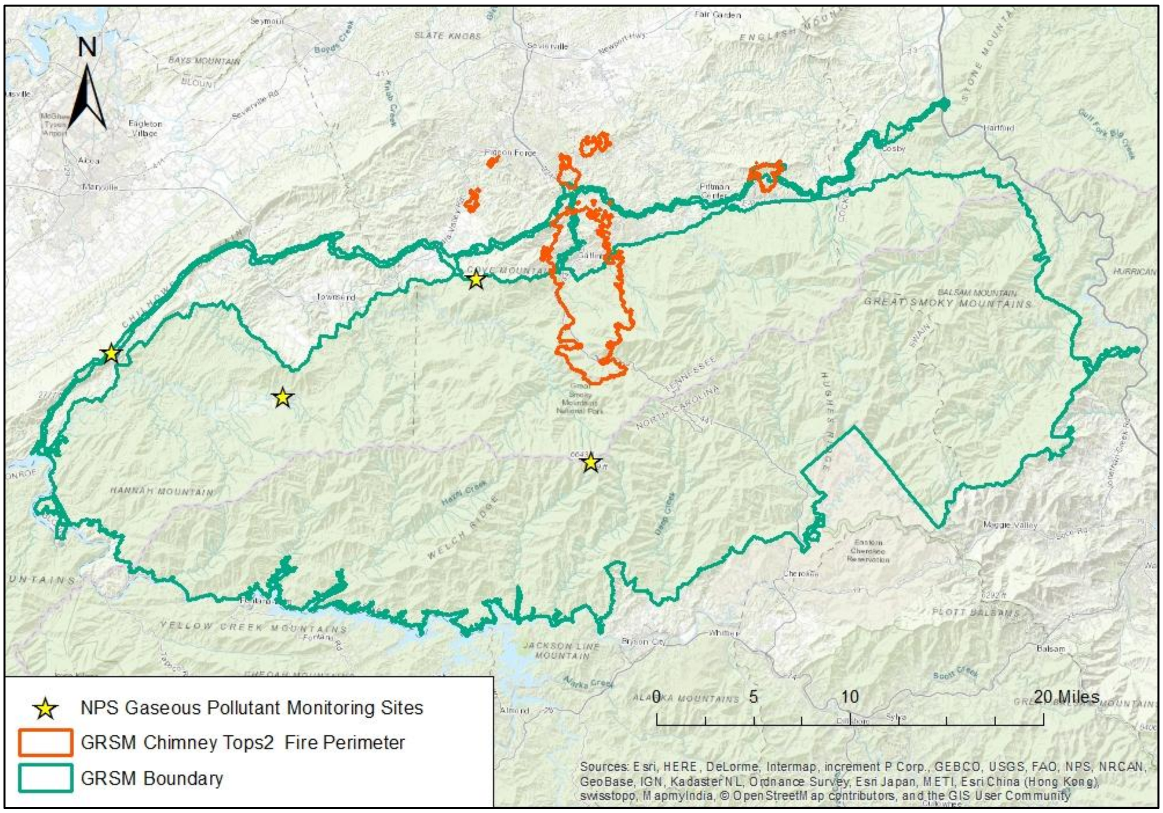

Figure 3.4 The 2016 Chimney Tops 2 Fire perimeter and wind data stations in GRSM

3.2.5 Auxiliary Dataset

To extract topographical features and analyze their impacts on burn severity distribution, the 3-m GRSM Digital Elevation Model (DEM) data published in 2011 was obtained from the Data Store of the Integrated Resource Management Applications (IRMA) Portal for NPS (https://irma.nps.gov/DataStore/). This product was generated using a combination of North Carolina (NC) LiDAR (Light Detection and Ranging), USGS-Tennessee (TN) LiDAR, and National Elevation Dataset (NED) data. Particularly, LiDAR data from the NC Flood Mapping

Program were used to generate DEM for the overlapping area of the park boundary and NC state boundary. In addition, the LiDAR data from a USGS LiDAR mapping contract were used to derive the DEM for the areas located in the intersection of the park boundary and TN state boundary. For all other areas, the DEM data were sourced from the NED. In addition, 30-m resolution products of Topographic Shape Index (TSI; McNab, 1989), Topographic Wetness Index (TWI; Beven et al., 1988), Topographic Position Index (TPI; Guisan et al, 1999), and Topographic Ruggedness Index (TRI; Riley et al., 1999) derived from multisource LiDAR data were also obtained from IRMA to assist the extraction of topographical features.

3.3 Methodology

3.3.1 Estimation of Burn Severity

Although the burn severity classes data generated by GRSM with BARC image and BAER field observations right after the fire can indicate the general burn severity levels, this categorical result cannot capture the detailed spatial variations of burn severity in the local forests or consider the ecosystem recovery when evaluating the impacts of fire. As a consequence, in this study we further extracted a list of commonly used vegetation indices to evaluate the post-fire burn severity for the 2016 fire in GRSM using Landsat 8 OLI images acquired before and one year after the Chimney Tops 2 Fire.

NBR-based vegetation indices have been commonly used in previous studies to estimate the spatial distribution of severity due to their best performance in providing spatial details about the severity levels. First in this study NBR was calculated using with the SWIR and NIR bands for both pre-fire and post-fire Landsat 8 OLI images, as shown in equation (1). dNBR and RdNBR values were then computed based on pre-fire and post-fire NBR images based on equations (2) and (3) as shown below.

$$NBR = (\rho_{NIR} - \rho_{SWIR2})/(\rho_{NIR} + \rho_{SWIR2}) \quad (1)$$

$$dNBR = NBR_{Pre-fire} - NBR_{Post-fire} \tag{2}$$

$$RdNBR = \frac{NBR_{Pre-fire} - NBR_{Post-fire}}{\sqrt{Abs(NBR_{Pre-fire}/1000)}} \tag{3}$$

Additionally, dNDVI and dSAVI were also mapped in this study as previous research also showed strong relationships between these indices and burn severity in forest ecosystems (Arnett et al., 2015; Chang et al., 2016). In particularly, dNDVI can better represent the vegetation loss and dSAVI can better indicate the change of soil conditions caused by forest fires. Pre-fire and post-fire NDVI and SAVI were calculated separately using equations (4) and (5) first. Then equations (6) and (7) were used to generate dNDVI and dSAVI images.

$$NDVI = (\rho_{NIR} - \rho_{Red})/(\rho_{NIR} + \rho_{Red}) \tag{4}$$

$$SAVI = (\rho_{NIR} - \rho_{Red})/(\rho_{NIR} + \rho_{Red} + 0.5)*1.5 \tag{5}$$

$$dNDVI = NDVI_{Pre-fire} - NDVI_{Post-fire} \tag{6}$$

$$dSAVI = SAVI_{Pre-fire} - SAVI_{Post-fire} \tag{7}$$

Next, the results of vegetation indices calculated with Landsat 8 OLI images were compared with the severity classes from BARC data. Box plots were generated to compare the values of vegetation indices and severity classes.

3.4.2 Affected Vegetation Communities

According to the GRSM Overstory Vegetation Database (Madden et al., 2004), the Chimney Tops 2 Fire affected a wide variety of forest species. A full list of related vegetation species was summarized in Appendix II. As different forests could have different or similar fuel loads and moisture content levels, fuel groups were further identified in GRSM based on the vegetation communities to better evaluate the role of vegetation communities on fire severity.

In general, the 2010 GRSM Fire Management Plan identified eight major fuel communities within the national park including Spruce-Fir Forest, Northern Hardwood Forest, High Elevation

Northern Red Oak Forest, Cove Hardwood forest, Mesic Oak/ Hardwood Forest, Xeric Oak/ Pine Forest and Woodland, Hemlock Forest, Successional Hardwood Forest and Others (GRSM, 2010). Here we summarized the detailed vegetation species defined in the GRSM vegetation database (Madden et al., 2004) into these eight fuel communities within the Chimney Tops 2 Fire perimeter. In particular, the category of "Others" is comprised here of vegetation species with very limited coverage in the study area, including Alluvial Forest, Heath Balds, Grassy Balds, Fields, etc. The fuel communities were then summarized into the major fuel groups and classes from (Madden et al., 2004) to better understand their spatial distributions and roles in affecting the burn severity. The fuel communities were also mapped for next-step analysis.

3.4.3 Environmental Variables Influencing Severity Distribution

Extraction of Topographic Features

A list of topographic features was calculated to get independent variables for topographic features. Slope raster in degrees and aspect raster were extracted from the 3-m DEM data first. Then instead of using the original aspect values, an aspect index was calculated using equation (8). Ranging from -1 to 1, higher aspect index values indicate higher potential to receive more downward solar radiation.

$$Aspect\ Index = -cos\ ((Aspect\ \times 2 \times \pi)/360) \tag{8}$$

In addition to slope and aspect, a few more topographic indices, including the 30m resolution TSI, TPI, and TRI provided by GRSM, were used to further evaluate the topographic characteristics in GRSM. Both low TSI and TWI values indicate concave and low gradient regions that are easier to gather water, while high TSI and TWI values represent convex regions with higher steepness, which will shed water and are assumed to be of higher fire risk. The TPI in this dataset is generated by calculating the difference between the elevation value of a cell and the average values of all its neighboring pixels. Positive TPI values indicate that the cell has higher elevation when compared to its surroundings, while negative TPI values mean the opposite. By integrating the TPI and slope values of each cell, it is possible to identify the slope position of that cell, such as at or near the top of a hill or ridge, at or near the bottom of a valley, or at a flat or mid-sloped area. In addition, TRI is calculated by summing the changes in elevation between a grid cell and its eight surrounding neighbors, which can present the ruggedness level of an area. These topographic features were all projected and clipped by the Chimney Tops 2 Fire perimeter.

Calculation of Fire Weather Indices

Fire weather is a dominant factor driving wildfire behavior and thus could affect post-fire burn severity (Bradstock et al., 2010). The U.S. National Fire Danger Rating System (NFDRS) and the Canadian Forest Fire Danger Rating System (CFFDRS) are the two commonly used fire rating systems developed for the North American forest ecosystems. Both systems have provided indices for quantifying fire weather conditions. While CFFDRS mainly uses daily based observations, NFDRS requires more hourly weather parameters. So instead of CFFDRS, Fire Weather Indices (FWI; Stocks et al., 1989) from CFFDRS were used in this study to describe fire weather conditions in the study area. The whole FWI system is comprised of six weather indices as shown in Figure 3.5, including Fine Fuel Moisture Code (FFMC), Duff Moisture Code (DMC), Drought Code (DC), Initial Spread Index (ISI), Buildup Index (BUI) and Fire Weather Index (FWI). Particularly, FFMC is designed to measure the moisture level of cured fine fuels, which indicates the relative ease of ignition and the flammability of fine fuel. The DMC measures average moisture content of loosely compacted organic layers of moderate depth. In addition, DC is designed to estimate the average moisture content of deep, compact organic layers, particularly useful for indicating the seasonal drought effects on forest fuels. ISI combines the effects of wind and the FFMC on rate of spread to rate the expected rate of fire spread. BUI estimates the total amount of fuel available for combustion by integrating DMC and DC. Then FWI evaluates fire intensity in general by combining ISI and BUI.

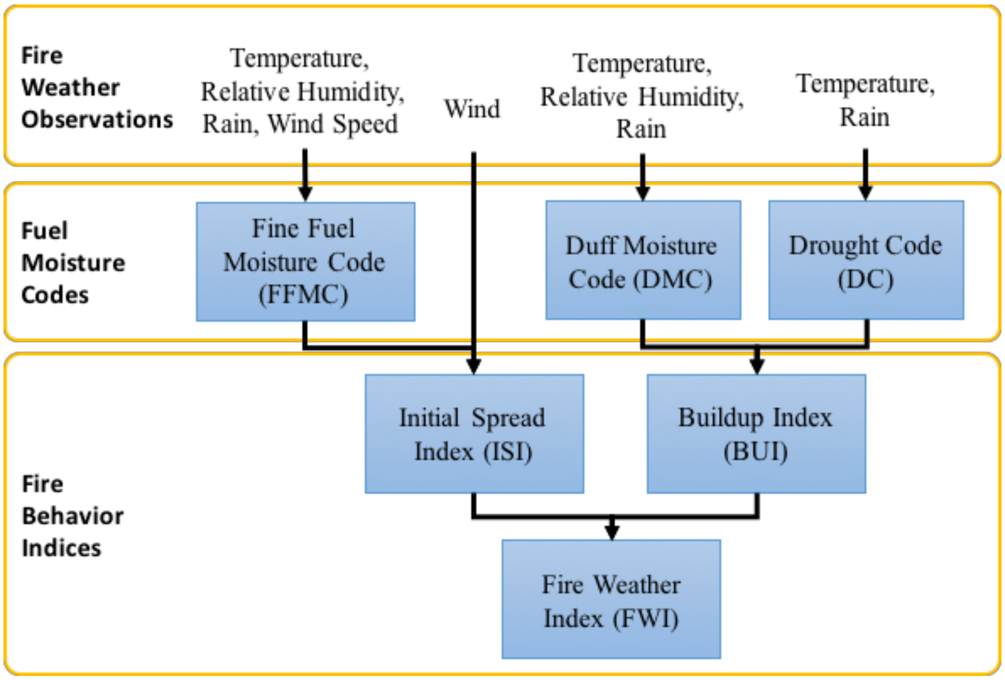

Figure 3.5 Structure of Canadian FWI System (Stocks et al., 1989)

These indices were calculated using 1-km Daymet data and interpolated wind speed data obtained from NPS for 2016 before the fire started. Though the growing season for deciduous species in GRSM could start in early March, we started the FWI calculations from April 19 considering the availability of wind data. We first extracted and projected the daily data for GRSM from April 19 to November 20 in 2016 for precipitation, maximum temperature, vapor pressure (VP), and day length from original Daymet product. As relative humidity data are not provided with Daymet, we then calculated relative humidity (RH) using equations (9) and (10) provided by World Health Organization (WHO) report:

$$Satuation\ Vapor\ Pressure\ (SVP) = 6.112 * e^{\frac{17.62*Temperature}{243.12+Temperature}} \tag{9}$$

$$RH = \frac{VP}{SVP} * 100\% \tag{10}$$

Then Inverse Distance Weighting interpolation method was used to generate daily wind speed distribution for GRSM. After preparing all necessary input weather observations for FWI, six FWI metrics were the computed for GRSM using the "cffdrs" package in R (Wang et al., 2017).

Random Forest Modeling

Random Forest (RF) is a supervised learning algorithm designed for tasks like classification and regression (Breiman, 2001). It is designed to generate an ensemble of decision trees based on the "bagging" method in statistics. Thus, this algorithm could mitigate the overfitting problems from decision tree methods. The RF algorithm typically requires three important parameters that are related to the predictive power: the number of trees that the algorithm constructs before voting or averaging, the maximum number of features for an individual tree, and the minimum number of variables for a split at each internal node. In this study the RF algorithm provided in the Random Forest package in R (Liaw & Wiener, 2002), to model the impacts of different environmental factors on fire severity for the Chimney Tops 2 Fire in GRSM. Environmental factors covering fuel conditions, topographic features and weather conditions were included as independent variables for the algorithm (Table 3.3). Here we utilized both classification and regression methods from RF. Classification was used for modeling the relationship between environmental factors and the severity classes generated with BARC data, while regression was used for modeling the relationship between those factors and the dNBR values generated in previous step. Results were then analyzed to identify the key factors affecting the burn severity variation for this fire.

Table 3.2 Independent environmental variables used for RF classification and regression

Types	Environmental Variables
Fuel Conditions	Vegetation community, NDVI, EVI, NDMI, NBR
Topographic Features	Elevation, Slope, Aspect Index, TPI, TRI, TSI
Fire Weather Conditions	FWI, FFMC, DMC, DC, ISI, BUI

3.4 Results and Discussions

3.5.1 Distribution of burn severity after the 2016 Chimney Tops 2 Fire

To examine the spatial variation of burn severity of the Chimney Tops 2 Fire, four vegetation indices including dNBR, RdNBR, dNDVI and dSAVI were mapped for the study area as shown in Figure 3.6. Within the fire perimeter, the dNBR values range from -0.24 to 1.09, RdNBR range from -12.6 to 40.1, dNDVI ranges from -0.18 to 0.9, and dSAVI ranges from -0.27 to 1.37. These indices show very similar patterns regarding the spatial distribution of burn severity levels. The Chimney Tops, where the wildland fire started, have higher elevation than other areas within the fire perimeter and facing south. It turns out to have the most severe burn severity according to the mapping results. Other regions with lower elevation tend to have lower burned severity levels, although south-facing areas tend to have more severe burning with higher index values in general, when compared to the local neighborhoods. Although normalized indices can usually minimize the impacts of topography, clouds or shadows, the topographical features still have the potential to affect the calculation of metrics for a mountainous region like GRSM. Topographic correction methods can be included in future to further identify the spatial distribution for burn severity.

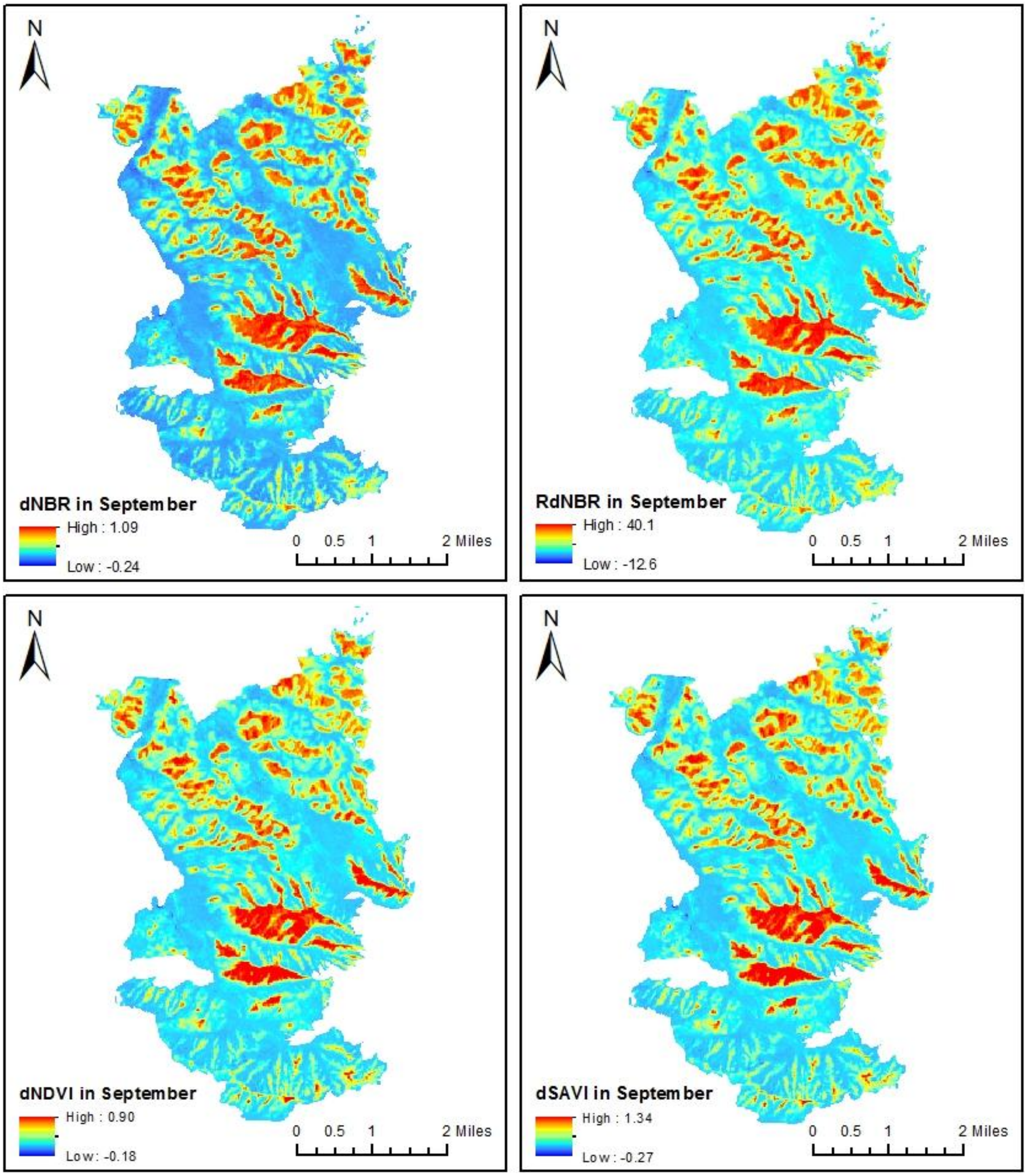

Figure 3.6 Spatial distributions of dNBR, RdNBR, dNDVI and dSAVI in the fire perimeter within GRSM

We also generated boxplots for all four indices by multiple severity levels as shown in Figure 3.7. These indices tested in this study turn out to do a good job in distinguishing moderate and high severity levels from low and unburned, while the values of unburned and low severity levels do not show differences for all indices. The moderate severity level tends to have a wider interquartile range (IQR) when compared to the other three levels. For both unburned and low severity levels, the values of dNBR mainly range from 0 to 0.1 and the RdNBR ranges from 0 to 5. For the moderate severity level, dNBR is primarily within 0.2 to 0.6 and RdNBR values fall within 6 to 24. While high severity level is primarily represented by dNBR values from 0.75 to 0.9 and RdNBR values from 27 to 34.

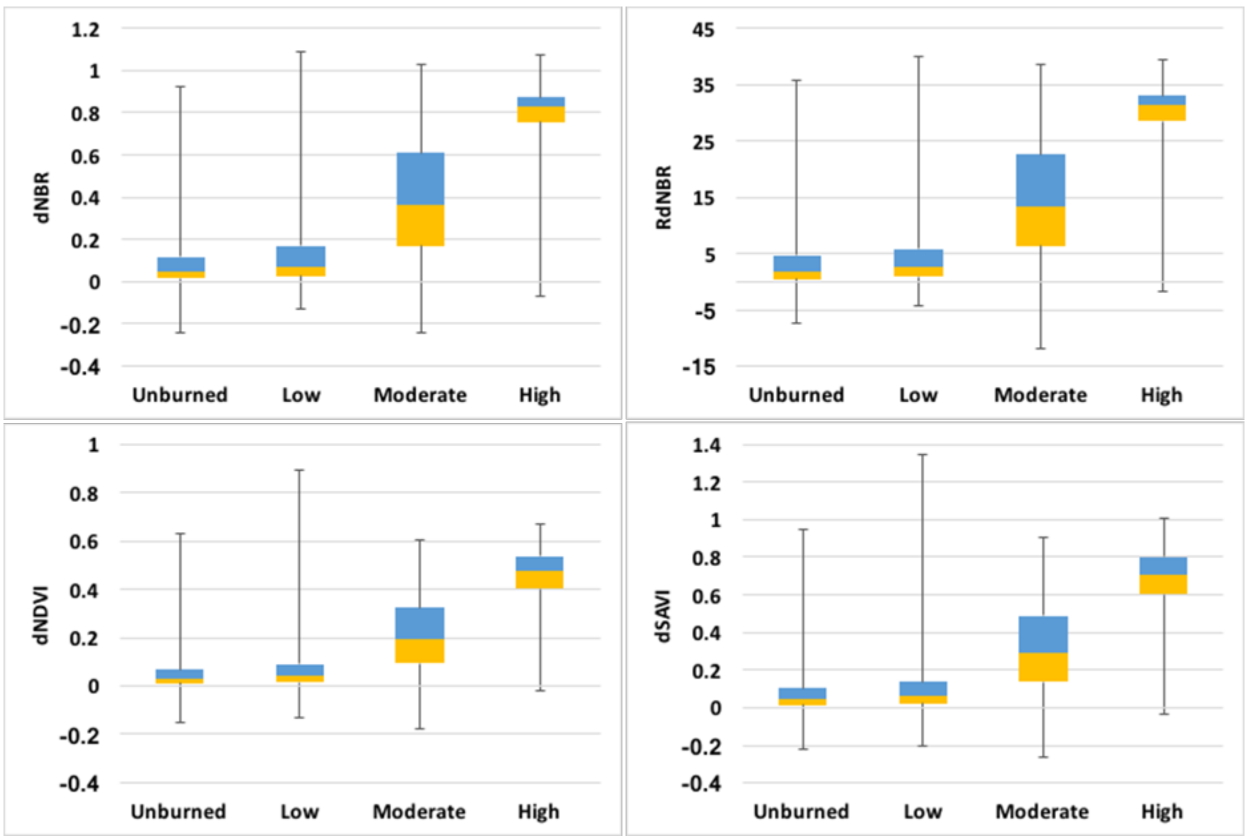

Figure 3.7 Boxplots comparing how vegetation indices distinguish different burn severity levels for the 2016 Chimney Tops 2 Fire

Although, Miller & Thode (2007) previously developed dNBR and RdNBR thresholds for distinguishing different severity levels in the western US, their findings (Table 3.3) are not directly transferrable to this Chimney Tops 2 Fire. This indicates that we not only need to carefully design field measurement strategies for fire severity estimations but also should calibrate the indices derived for western US for describing vegetation fuels and fire impacts in the eastern deciduous forests.

Table 3.3 Ranges of dNBR and RdNBR for different severity levels from Miller & Thode (2007)

Severity levels	dNBR range	RdNBR range
Unburned	< 41	< 69
Low	41 – 176	69 – 315
Moderate	177 – 366	316 – 640
High	>=367	>=641

3.5.2 Severity impacts on the habitats of different vegetation communities

To address the second research question, we first summarized the major fuel groups and vegetation communities according to Madden et al. (2004) in Table 3.4. The distribution of vegetation communities was also mapped in Figure 3.8. We further compared the distribution of vegetation communities and burn severity within the perimeter of the Chimney Tops 2 Fire. Based on Figure 3.8, the burned area percentages for each major vegetation community were first summarized in Figure 3.9. In general, this fire mainly affects the Mesic Oak/ Hardwood Forest, which occupies approximately 42% of the area within the fire perimeter. This community provides habitats for overstory tree species like Chestnut Oak and Red Oak. Following that, both the Northern Hardwood Forest and the Cove Hardwood Forest communities have burned about 16% ~ 17% of the total area for the whole fire site. In addition, about 6% to 9% of the burned area was previously covered by Xeric Oak/Pine Forest and Woodland, Successional Hardwood Forest and Other before the fire started. Communities like Hemlock Forest, Spruce-Fir Forest and High Elevation Northern Red Oak Forest are less influenced by this fire.

Table 3.4 Major fuel classes and overstory vegetation communities within the 2016 Chimney Top 2 Fire perimeter in GRSM

Group	Fuel Class	Description	Vegetation Communities	Overstory Vegetation Dominate Class Code
Non-flammable	0	Non-flammable/Wet	Montane Alluvial Forest	MAL, MAL/T, MALc, MALt
Grass	1	Short Grass	Pasture	P
	2	Timber	Sparse Vegetation	SV
	3	Tall Grass	N/A	N/A
Shrubs	4	Shrub (6 feet tall)	Shrub Understory	K, R
	5	Brush (2 feet tall)	N/A	N/A
	6	Brush/Hardwood Slash	N/A	N/A
	7	Southern Rough	High Elevation Northern Red Oak Forest	MOa, MOr
			Southern Appalachian Health Balds	Hth
Timber	8	Closed Timber Litter	Xeric Oak/Pine Forest and Woodland	OzH, OzH/PI, OzH/PIp, OzHf, PI, PI/OzH, PI-OzH, PIp-OzH
	9	Hardwood Litter	Northern Hardwood Forest	NHx, NHxB, NHxB/S, NHxR, NHx-T, NHxY, S/NHx, S/NHxB, S-NHx
			Cove Hardwood Forest	CHx, CHxA, CHxA-T, CHxR
			Hemlock Forest	T
			Succesional Hardwood Forest	Hx, HxBl/R, HxL
			Mesic Oak/Hardwood Forest	OcH, OmH, OmHA, OmHL OmHp/R, OmHr, OmHR,
			Northern Hardwood Forest	NHx, NHxB, NHxB/S, NHxR, NHx-T, NHxY, S/NHx, S/NHxB, S-NHx
			Cove Hardwood Forest	CHx, CHxA, CHxA-T, CHxR
	10	Timber (Litter and Understory)	Spruce-Fir Forest	S, S/F, S/R, S/T
Slash	11	Light Logging Slash	N/A	N/A
	12	Medium Logging Slash	N/A	N/A
	13	Heavy Logging Slash	N/A	N/A

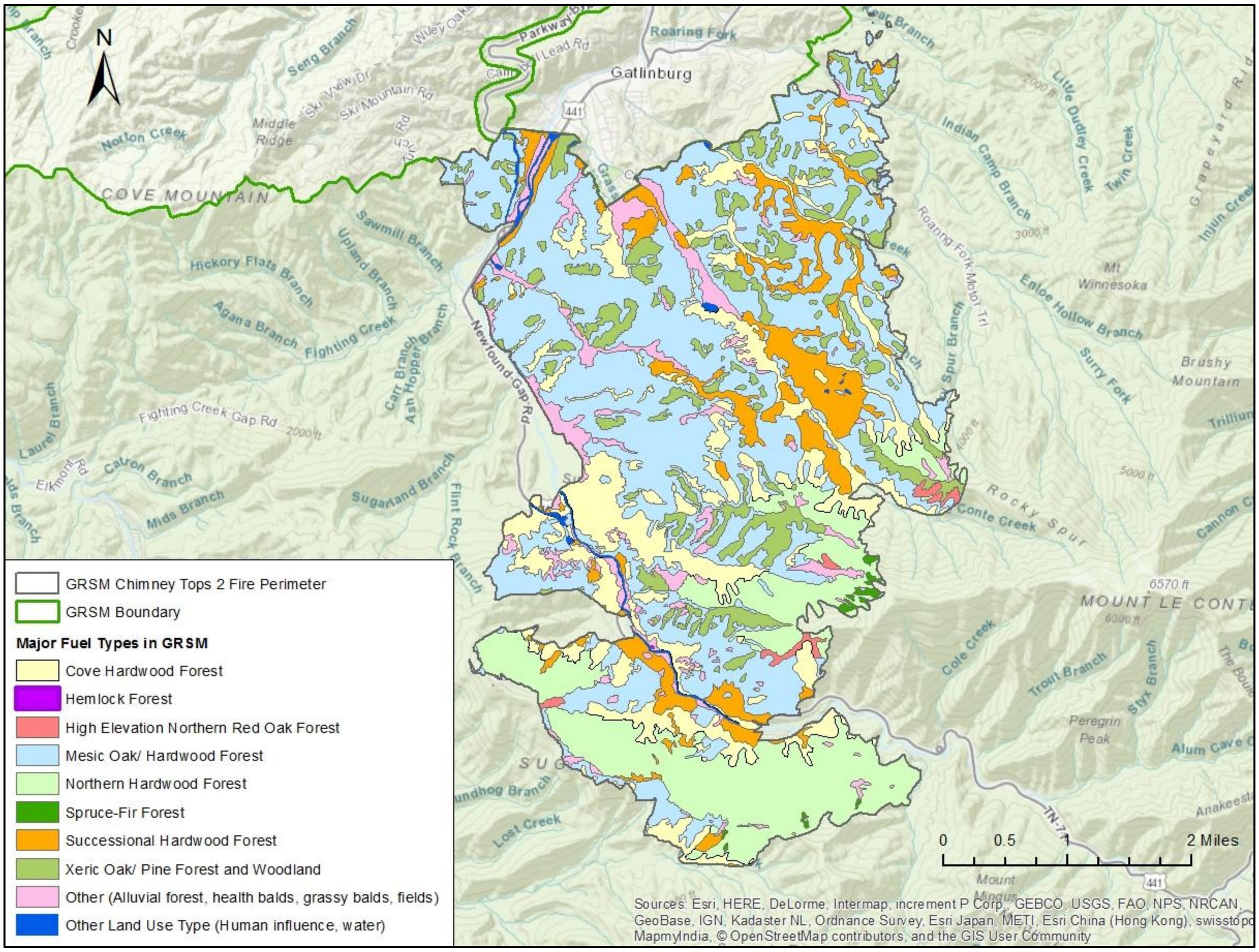

Figure 3.8 Distribution of major vegetation communities within the perimeter of the 2016 Chimney Tops 2 Fire

We then analyzed the burn severity distribution within different vegetation communities affected by the Chimney Tops 2 Fire. The percentages of different severity levels within each vegetation community were plotted in Figure 3.10. Although Mesic Oak/Hardwood Forest has the largest burned area inside the fire perimeter (Figure 3.9), this community is dominated by low to moderate severity levels. More than 50% of the High Elevation Northern Red Oak Forest is burned moderately. Vegetation communities like Hemlock Forest, Successional Hardwood Forest, and Cover Hardwood Forest are less affected by the fire since they are mainly covered by low severity sites. In particular, about 38% of the Xeric Oak/Hardwood Forest habitat is severely burned in this fire, which is the highest among all vegetation communities involved.

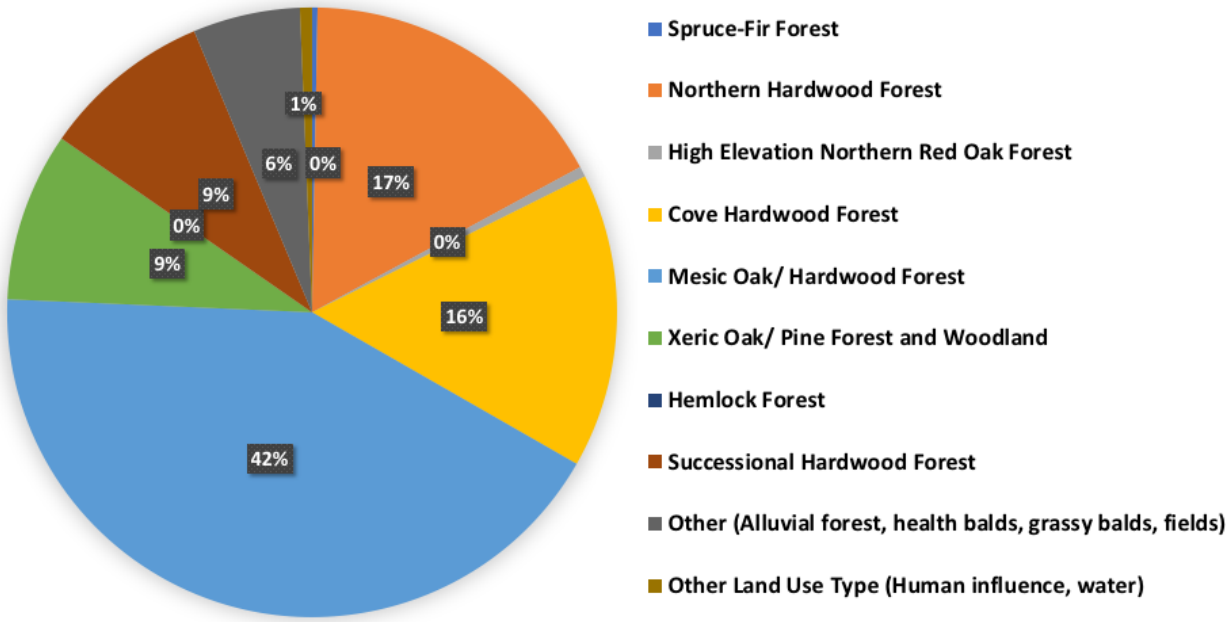

Figure 3.9 Burned area percentages of major vegetation communities affected by the 2016 Chimney Tops 2 Fire

The distribution of dNBR and RdNBR values were also summarized for each community, as shown in Figure 3.11. Similar to the results in Figure 3.10, the Xeric Oak/Pine Forest and Woodland have the highest values of both dNBR and RdNBR, indicating that these communities are most severely burned in this fire. While other communities tend to have much lower burn severity levels with smaller dNBR and RdNBR values in their habitats. This difference also suggests that xeric forest habitats with inadequate moisture content could lead to more severe burns after fire for the local ecosystems when compared to mesic environments in GRSM.

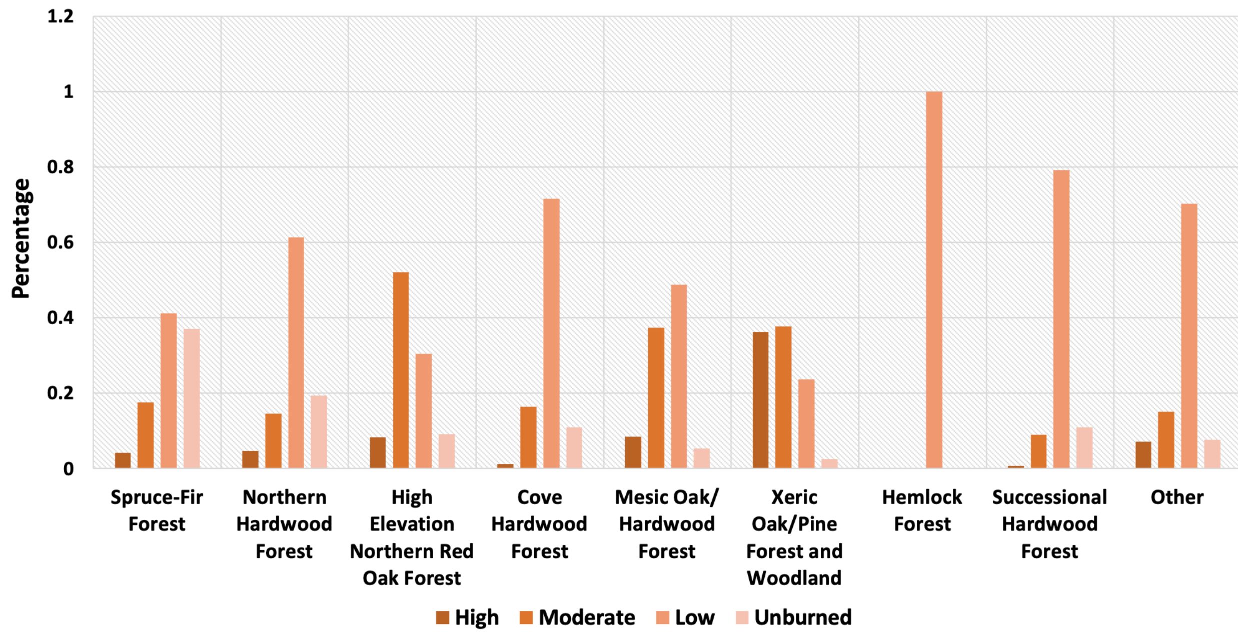

Figure 3.10 Percentages of different burn severity levels for each vegetation community affected by the Chimney Tops 2 Fire

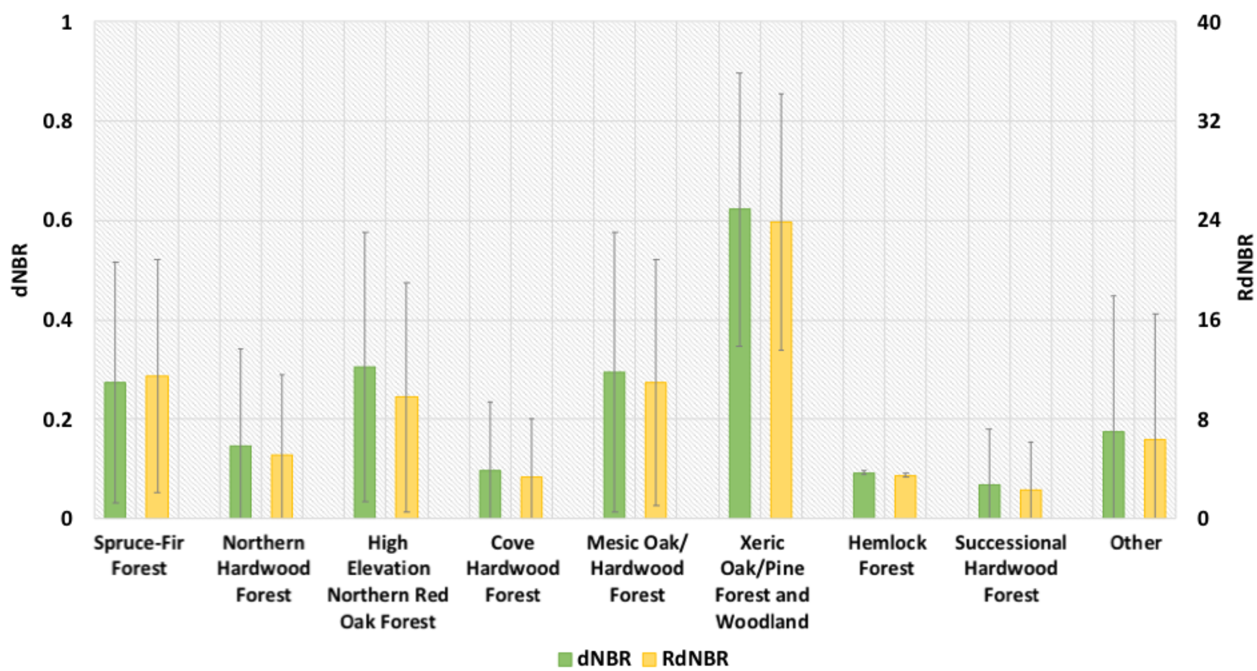

Figure 3.11 Average dNBR and RdNBR values for each vegetation community affected by the Chimney Tops 2 Fire (error bar represents ±1 standard error)

3.5.3 Environmental factors affecting the distribution of burn severity

To explore the environmental factors influencing the burn severity of this fire, we conducted both RF classification with both burn severity classes derived by BARC images, and RF regression with dNBR values calculated using Landsat 8 OLI images. The dNBR index was chosen here mainly considering its good performance in capturing burn severity distribution in previous literature. All independent variables involved are listed in Table 3.3. An overall out-of-bag (OOB) value was generated to evaluate the prediction accuracy of RF algorithm. While regression results with dNBR values for random points did not show strong relationships, classification results turned out to have relatively good estimation of burn severity levels, with OOB estimate of error rate as 25.73%. Table 3.5 shows the detailed classification accuracy for each severity level from the classification results. Low severity level has the highest accuracy, partially because there are more training samples for the low severity class in the classification test. On the other hand, unburned class has the highest error percent, also due to the limitation of training samples generated in this class.

Table 3.5 Confusion matrix of RF classification results

		Classified data				
		Unburned	Low	Moderate	High	Producer's accuracy
Reference data	Unburned	3	31	1	1	8.33%
	Low	2	186	12	0	93.00%
	Moderate	0	23	46	5	62.17%
	High	1	4	8	19	60.38%
	User's accuracy	33.33%	76.23%	68.66%	76.00%	

We further examined the importance of each environmental variable as shown in Figure 3.12. The Mean Decrease of Accuracy value quantifies the importance of a certain variable by measuring how much the classification error reduces when including this variable. The higher the value is, the more importance of the certain variable is. The Mean Decrease Gini coefficient measures the contribution of a variable in generating homogeneous nodes in the output classification forest. Greater Gini decrease suggest a more important role of the variable in data partitioning during the classification process.

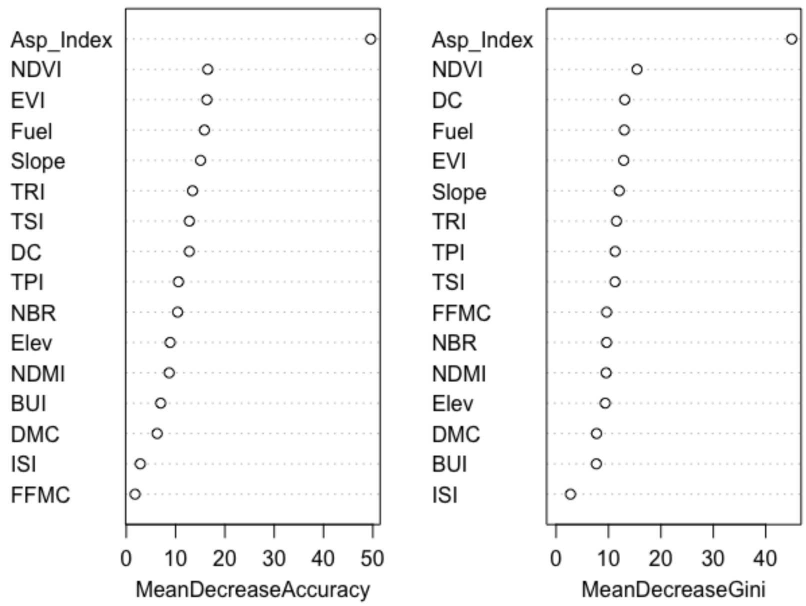

Figure 3.12 Importance of independent environmental variables from RF classification

According to Figure 3.12, the aspect index turns out to be the most important variable that affects the distribution of burn severity in the Chimney Tops 2 Fire site with both Mean Decrease Accuracy and Mean Decrease Gini reaching 50%. Following the aspect index, variables related to vegetation type and greenness including NDVI, EVI and type, also have important influences on the burn severity distribution, with both Mean Decrease Accuracy and Mean Decrease Gini values ranging from 15% to 20%. However, the strong impact of aspect identified here could be related to the complex topography in the study area. The topographical variation also has the potential to affect the spatial distribution of vegetation indices.

Compared to topographic features and vegetation related properties, fire weather conditions show relatively less significances in affecting burn severity distribution in this fire, except the DC index related to moisture conditions. This could be caused by the coarse resolution of

Daymet data and very sparse weather stations for wind data in this mountainous region. Compared to the fire size and the 30m resolution of other variables, the 1-km Daymet data fail to capture the detailed spatial variations of weather conditions throughout the mountainous region. These findings for the 2016 Chimney Tops 2 Fire are also consistent with earlier studies conducted throughout the Appalachian Mountains, which emphasizes the impacts of topography and moisture levels on fire severity (Flatley et al., 2011; Schwartz et al., 2016).

3.5.4 Implications for fire management efforts in GRSM

In recent decades, remote sensing and GIS technologies have played an important role in assisting fire management efforts, such as development of fire risk warning system (Dukes, 2001), active fire monitoring (Yuan et al., 2015), tracking and assessment of post-fire impacts (Miller & Yool, 2002; Lee & Chow, 2015). Efficient fire risk warning requires improvements in accurate monitoring of pre-fire conditions and robust modeling of future fire potential (Thompson & Calkin, 2011). In particular, Dukes (2001) took the initial step towards the systematic assessment and modeling of fire risk throughout the whole GRSM with GIS. Owens (2013) continued the research of fire risk assessment in GRSM, focusing on determining fire frequency and simulating fire spread. Still, relatively fewer studies in pre-fire monitoring have been conducted for the forest ecosystems in the southern Appalachian Mountains when compared to the forests in western United States. This brings up the need for further efforts on developing effective warning systems in future.

Challenges also exist for quantification of fire severity combining field measurements, remote sensing data and modeling efforts (Morgan et al., 2014). Comprehensive assessment of post-fire burn severity could benefit the management policies for long-term ecosystem recovery, such as evaluating the impacts of fuel treatments on prescribed fires, planning and assessing salvage activities, or preparing strategies for controlling post-fire hazards (Beschta et al., 2004). In addition, Jenkins et al. (2011) found that controlling the severity of prescribed fire could lead to regeneration of yellow pine in GRSM. Hutto et al. (2016) also suggested the land managers to keep using severe prescribed fires to maintain the integrity of forest ecosystems. Thus, gaining comprehensive understanding of fire severity and related species could help with targeting certain species for restoring and keeping ecosystem diversity in the southern Appalachian Mountains.

3.6 Conclusions and Future Work

To summarize, this study examines the spatial variations of burn severity and aims to understand environmental factors impacting the burn severity, using the 2016 Chimney Tops 2 Fire in GRSM as an example. We first evaluated the burn severity distribution through mapping of commonly used vegetation indices. We then assessed the impacts of burn severity on local vegetation communities within the fire perimeters. We further explored the impacts of factors related to post-fire severity. All four vegetation indices tested in this study do a good job in distinguishing the burn severity levels, though differences still exist in local regions. From the perspective of the burned area, this fire impacted the Mesic Oak/ Hardwood Forests the most. While from the perspective of burn severity, Xeric Oak/ Hardwood Forests and Northern Hardwood Forests were more severely impacted by the fire. Topographic conditions, vegetation properties as well as habitat moisture levels, tend to have more important impacts on the spatial distribution of fire severity. Particularly, aspect index and vegetation greenness values tend to have the most influences on the severity levels. Due to the complex topographical patterns in the mountainous study area, topographic correction methods can be conducted in future to assist the mapping of burn severity distribution and exploration of environmental drivers.

However, this study is limited by the availability of field data and weather observations. Although BAER team has obtained some measurements of burn severity after the fire and published their BARC map, this is not enough for a detailed and accurate estimation of severity in general. More detailed field measurements should be collected regularly to ensure accurate severity assessment and recovery monitoring in the long run. Also, the lack of high-resolution weather observations within the study area could largely underestimate the roles of weather variables on the fire severity distribution. Weather simulation results generated from numerical weather forecasting models could be other data sources to assist the estimation of fire weather indices in future.

Reference

Arnett, J. T. T. R., Coops, N. C., Daniels, L. D., & Falls, R. W. (2015). Detecting forest damage after a low-severity fire using remote sensing at multiple scales. International Journal of Applied Earth Observation and Geoinformation, 35(PB), 239–246.

Barbour, M. G. (1999). Terrestrial plant ecology. Benjamin/Cummings series in the life sciences. (3rd ed.). Menlo Park, Calif. SE - 1 volume (various pagings): illustrations, maps; 24 cm.: Benjamin/Cummings.

Beschta, R. L., Rhodes, J. J., Kauffman, J. B., Gresswell, R. E., Minshall, G. W., Karr, J. R., Perry, D. A., Hauer, F. R., & Frissell, C. A. (2004). Postfire management on forested public lands of the western United States. Conservation Biology, 18(4), 957–967.

Beven, K. J., Wood, E. F., & Sivapalan, M. (1988). On hydrological heterogeneity – catchment morphology and catchment response. Journal of Hydrology, 100(1–3), 353–375.

Birch, D. S., Morgan, P., Kolden, C. A., Abatzoglou, J. T., Dillon, G. K., Hudak, A. T., & Smith, A. M. S. (2015). Vegetation, topography and daily weather influenced burn severity in central Idaho and western Montana forests. Ecosphere, 6(1), art17.

Boer, M. M., Macfarlane, C., Norris, J., Sadler, R. J., Wallace, J., & Grierson, P. F. (2008). Mapping burned areas and burn severity patterns in SW Australian eucalypt forest using remotely-sensed changes in leaf area index. Remote Sensing of Environment, 112(12), 4358–4369.

Bonazountas, M., Kallidromitou, D., Kassomenos, P., & Passas, N. (2007). A decision support system for managing forest fire casualties. Journal of Environmental Management, 84(4), 412–418.

Bowman, D., Balch, J. K., Artaxo, P., Bond, W. J., Carlson, J. M., Cochrane, M. A., D'Antonio, C. M., DeFries, R. S., Doyle, J. C., Harrison, S. P., Johnston, F. H., Keeley, J. E., Krawchuk, M. A., Kull, C. A., Marston, J. B., Moritz, M. A., Prentice, I. C., Roos, C. I., Scott, A. C., Swetnam, T. W., van der Werf, G. R., & Pyne, S. J. (2009). Fire in the Earth system. Science (New York, N.Y.), 324(5926), 481–4.

Bradstock, R. A., Hammill, K. A., Collins, L., & Price, O. (2010). Effects of weather, fuel and terrain on fire severity in topographically diverse landscapes of south-eastern Australia. Landscape Ecology, 25(4), 607–619.

Breiman, L. (2001). Random forests. Machine Learning, 45(1), 5–32.

Brewer, C. K., Winne, J. C., Redmond, R. L., Opitz, D. W., & Mangrich, M. V. (2005). Classifying and Mapping Wildfire Severity: A Comparison of Methods. Photogrammetric Engineering & Remote Sensing, 71(11), 1311–1320.

Chang, Y., Zhu, Z., Feng, Y., Li, Y., Bu, R., & Hu, Y. (2016). The spatial variation in forest burn severity in Heilongjiang Province, China. Natural Hazards, 81(2), 981–1001.

Cohen, D., Dellinger, B., Klein, R., & Buchanan, B. (2007). Patterns in lightning-caused fires at Great Smoky Mountains National Park. Fire Ecology, 3(2), 68–82.

Delcourt, P. A., & Delcourt, H. R. (1998). The Influence of Prehistoric Human-Set Fires on Oak-Chestnut Forests in the Southern Appalachians. Castanea, 63(3), 337–345.

Dillon, G. K., Holden, Z. A., Morgan, P., Crimmins, M. A., Heyerdahl, E. K., & Luce, C. H. (2011). Both topography and climate affected forest and woodland burn severity in two regions of the western US, 1984 to 2006. Ecosphere, 2(12), art130.

du Lac, J. F., Larimer, S., & Bever, L. (2016, December 8). Two juveniles charged with arson in Tennessee wildfires that left 14 people dead. The Washington Post.

Dukes, R. E. (2001). A geographic information systems approach to fire risk assessment in Great Smoky Mountains National Park. University of Georgia.

Estes, B. L., Knapp, E. E., Skinner, C. N., Miller, J. D., & Preisler, H. K. (2017). Factors influencing fire severity under moderate burning conditions in the Klamath Mountains, northern California, USA. Ecosphere, 8(5).

Fesenmyer, K. a, & Christensen, N. L. (2010). Reconstructing Holocene fire history in a southern Appalachian forest using soil charcoal. Ecology, 91(3), 662–670.

Flatley, W. T., Lafon, C. W., & Grissino-Mayer, H. D. (2011). Climatic and topographic controls on patterns of fire in the southern and central Appalachian Mountains, USA. Landscape Ecology, 26(2), 195–209.

Flatley, W. T., Lafon, C. W., Grissino-Mayer, H. D., & LaForest, L. B. (2013). Fire History and Its Relation to Climate and Land Use in Three Southern Appalachian Landscapes in the Eastern U.S. Ecological Applications, 23(6), 130328164915002.

Francos, M., Úbeda, X., Tort, J., Panareda, J. M., & Cerdà, A. (2016). The role of forest fire severity on vegetation recovery after 18 years. Implications for forest management of Quercus suber L. in Iberian Peninsula. Global and Planetary Change, 145, 11–16.

GRSM. (2010). Great Smoky Mountains National Park Fire Management Plan. National Park Service.

Guisan, A., Weiss, S. B., & Weiss, A. D. (1999). GLM versus CCA spatial modeling of plant species distribution. Plant Ecology, 143(1), 107–122.

Hutto, R. L., Keane, R. E., Sherriff, R. L., Rota, C. T., Eby, L. A., & Saab, V. A. (2016). Toward a more ecologically informed view of severe forest fires. Ecosphere, 7(2).

Jenkins, M. A., Klein, R. N., & McDaniel, V. L. (2011). Yellow pine regeneration as a function of fire severity and post-burn stand structure in the southern Appalachian Mountains. Forest Ecology and Management, 262(4), 681–691.

Jensen, J. R. (2007). Remote sensing of the environment: an earth resource perspective. Prentice Hall series in geographic information science (2nd ed.). Upper Saddle River, NJ SE - xvi, 592 pages, [48] pages of plates: illustrations (some color), maps (some color) ; 29 cm.: Pearson Prentice Hall.

Kane, V. R., Cansler, C. A., Povak, N. A., Kane, J. T., McGaughey, R. J., Lutz, J. A., Churchill, D. J., & North, M. P. (2015). Mixed severity fire effects within the Rim fire: Relative importance of local climate, fire weather, topography, and forest structure. Forest Ecology and Management, 358, 62–79.

Keane, R. E., Agee, J. K., Fulé, P., Keeley, J. E., Key, C., Kitchen, S. G., Miller, R., & Schulte, L. A. (2008). Ecological effects of large fires on US landscapes: benefit or catastrophe? International Journal of Wildland Fire, 17(6), 696–712.

Keeley, J. E. (2009). Fire intensity, fire severity and burn severity: A brief review and suggested usage. International Journal of Wildland Fire, 18(1), 116–126.

Klein, R. N. J., Paxton, E. W., & Wood, J. M. (2017). Southern Appalachian / Piedmont Fire Effects Monitoring Annual Report, 2016. National Park Service.

Lee, R. J., & Chow, T. E. (2015). Post-wildfire assessment of vegetation regeneration in Bastrop, Texas, using Landsat imagery. GIScience and Remote Sensing, 52(5), 609–626.

Lentile, L. B., Holden, Z. A., Smith, A. M. S., Falkowski, M. J., Hudak, A. T., Morgan, P., Lewis, S. A., Gessler, P. E., & Benson, N. C. (2006). Remote sensing techniques to assess active fire characteristics and post-fire effects. International Journal of Wildland Fire, 15(3), 319–345.

Liaw, A., & Wiener, M. (2002). The randomforest package. R News, 2(3), 18–22.

Littell, J. S., Peterson, D. L., Riley, K. L., Liu, Y., & Luce, C. H. (2016). A review of the relationships between drought and forest fire in the United States. Global Change Biology, 22(7), 2353–2369.

Liu, J. C., Pereira, G., Uhl, S. A., Bravo, M. A., & Bell, M. L. (2015). A systematic review of the physical health impacts from non-occupational exposure to wildfire smoke. Environmental Research, 136, 120–132.

Loehman, R. A., Reinhardt, E., & Riley, K. L. (2014). Wildland fire emissions, carbon, and climate: Seeing the forest and the trees - A cross-scale assessment of wildfire and carbon dynamics in fire-prone, forested ecosystems. Forest Ecology and Management, 317, 9–19.

Madden, M., Welch, R., Jordan, T., Jackson, P., Seavey, R., & Seavey, J. (2004). Digital Vegetation Maps for the Great Smoky Mountains National Park. Center for Remote Sensing and Mapping Science, Department of Geography, University of Georgia, US.

Malmström, A. (2010). The importance of measuring fire severity-Evidence from microarthropod studies. Forest Ecology and Management, 260(1), 62–70.

McNab, W. H. (1989). Terrain shape index: quantifying effect of minor landforms on tree height. Forest Science, 35(1), 91–104.

Millar, C. I., & Stephenson, N. L. (2015). Temperate forest health in an era of emerging megadisturbance. Science, 349(6250), 823–826.

Miller, J. D., Safford, H. D., Crimmins, M., & Thode, A. E. (2009). Quantitative evidence for increasing forest fire severity in the Sierra Nevada and southern Cascade Mountains, California and Nevada, USA. Ecosystems, 12(1), 16–32.

Miller, J. D., & Thode, A. E. (2007). Quantifying burn severity in a heterogeneous landscape with a relative version of the delta Normalized Burn Ratio (dNBR). Remote Sensing of Environment, 109(1), 66–80.

Miller, J. D., & Yool, S. R. (2002). Mapping forest post-fire canopy consumption in several overstory types using multi-temporal Landsat TM and ETM data. Remote Sensing of Environment, 82(2–3), 481–496.

Morgan, P., Keane, R. E., Dillon, G. K., Jain, T. B., Hudak, A. T., Karau, E. C., Sikkink, P. G., Holden, Z. A., & Strand, E. K. (2014). Challenges of assessing fire and burn severity using field measures, remote sensing and modelling. International Journal of Wildland Fire, 23(8), 1045–1060.

NPS. (2009). Great Smoky Mountains National Park Fire Management Plan Environmental Assessment.

NPS. (2016). 2016 Wildfire! Smokies Guide, pp. 10–11.

NPS. (2017). Chimney Tops 2 Fire Review Individual Fire Review Report. U.S. Department of the Interior.

Owens, J. B. (2013). Wildfire Risk Assessment and Wildfire Simulation in Southeastern United States Mountainous Areas: Great Smoky Mountains National Park: A Thesis Presented to the Department of Humanities and Social Sciences in Candidacy for the Degree of Master of Science. Northwest Missouri State University.

Parks, S. A., Miller, C., Abatzoglou, J. T., Holsinger, L. M., Parisien, M.-A., & Dobrowski, S. Z. (2016). How will climate change affect wildland fire severity in the western US? Environmental Research Letters, 11(3), 035002.

Pyne, S. J., Andrews, P. L., & Laven, R. D. (1996). Introduction to Wildland Fire (Second Edi). John Wiley & Sons, Inc.

Randerson, J. T., Liu, H., Flanner, M. G., Chambers, S. D., Jin, Y., Hess, P. G., Pfister, G., Mack, M. C., Treseder, K. K., Welp, L. R., Chapin, F. S., Harden, J. W., Goulden, M. L., Lyons, E., Neff, J. C., Schuur, E. A. G., & Zender, C. S. (2006). The impact of boreal forest fire on climate warming. Science (New York, N.Y.), 314(5802), 1130–1132.

Riley, S. J., DeGloria, S. D., & Elliot, R. (1999). Index that quantifies topographic heterogeneity. Intermountain Journal of Sciences, 5(1–4), 23–27.

Schoennagel, T., Balch, J. K., Brenkert-Smith, H., Dennison, P. E., Harvey, B. J., Krawchuk, M.

A., Mietkiewicz, N., Morgan, P., Moritz, M. A., Rasker, R., Turner, M. G., & Whitlock, C. (2017). Adapt to more wildfire in western North American forests as climate changes. Proceedings of the National Academy of Sciences, 114(18), 4582–4590.

Schwartz, N. B., Urban, D. L., White, P. S., Moody, A., & Klein, R. N. (2016). Vegetation dynamics vary across topographic and fire severity gradients following prescribed burning in Great Smoky Mountains National Park. Forest Ecology and Management, 365, 1–11.

Seidl, R., Schelhaas, M.-J., Rammer, W., & Verkerk, P. J. (2014). Increasing forest disturbances in Europe and their impact on carbon storage. Nature Climate Change, 4, 806.

Stephens, S. L., Agee, J. K., Fulé, P. Z., North, M. P., Romme, W. H., Swetnam, T. W., & Turner, M. G. (2013). Managing Forests and Fire in Changing Climates. Science, 342(6154), 41–2.

Stocks, B. J., Lynham, T. J., Lawson, B. D., Alexander, M. E., Wagner, C. E. Van, McAlpine, R. S., & Dube, D. E. (1989). Canadian forest fire danger rating system: an overview. The Forestry Chronicle, 65(4), 258–265.

Thom, D., & Seidl, R. (2016). Natural disturbance impacts on ecosystem services and biodiversity in temperate and boreal forests. Biological Reviews of the Cambridge Philosophical Society, 91(3), 760–781.

Thompson, M. P., & Calkin, D. E. (2011). Uncertainty and risk in wildland fire management: A review. Journal of Environmental Management, 92(8), 1895–1909.

Thornton, P. E., Thornton, M. M., Mayer, B. W., Wilhelmi, N., Wei, Y., Devarakonda, R., & Cook, R. B. (2017). Daymet: daily surface weather data on a 1-km grid for North America, Version 3. ORNL DAAC, Oak Ridge, Tennessee, USA. ORNL DAAC, Oak Ridge, Tennessee, USA.

USGS. (2018). Landsat 8 Surface Reflectance code (LaSRC) Version 4.3 PRODUCT: Product

Guide, (March), 40.

van Mantgem, P. J., Nesmith, J. C. B., Keifer, M., Knapp, E. E., Flint, A., & Flint, L. (2013). Climatic stress increases forest fire severity across the western United States. Ecology Letters, 16(9), 1151–1156.

Wang, X., Wotton, B., M., Cantin, A., Parisien, M-A., Anderson, K., Moore, B., & Flannigan, M. D. (2017). cffdrs: An R package for the Canadian Forest Fire Danger Rating System. Ecological Processes, 6(1), 5.

Welch, R., Madden, M., & Jordan, T. (2002). Photogrammetric and GIS techniques for the development of vegetation databases of mountainous areas: Great Smoky Mountains National Park. ISPRS Journal of Photogrammetry and Remote Sensing, 57(1–2), 53–68.

Wimberly, M. C., & Reilly, M. J. (2007). Assessment of fire severity and species diversity in the southern Appalachians using Landsat TM and ETM+ imagery. Remote Sensing of Environment, 108(2), 189–197.

Yuan, C., Zhang, Y., & Liu, Z. (2015). A survey on technologies for automatic forest fire monitoring, detection, and fighting using unmanned aerial vehicles and remote sensing techniques. Canadian Journal of Forest Research, 45(7), 783–792.

CHAPTER 4

CONCLUSIONS

Forest ecosystems are suffering from increasing frequency and intensity of biotic and abiotic disturbances related to climate change, such as insect outbreaks, fires, droughts and wind storms (Dale et al., 2001). GRSM forests have long been affected by natural or human disturbances (Harmon et al., 1985; Pyle, 1988). In recent decades, the development of remote sensing technologies has played an important role in ecological applications, particularly large-scale forest monitoring caused by either natural or human disturbances (Kerr & Ostrovsky, 2003; Hansen et al., 2013). This manuscript-style thesis demonstrated an example of applying remote sensing technologies and NASA Earth Observations to understand vegetation disturbances in space and time through two case studies of insect outbreak and wildfire in GRSM.

Chapter 2 examined the spatiotemporal patterns of hemlock defoliation caused by HWA infestation. We constructed a 20-year time series with 30m Landsat imagery and applied a temporal segmentation algorithm "LandTrendr" to map the significant disturbance events in hemlock forests. We developed maps of onset year, magnitude and duration of significant disturbance and recovery events for hemlock forests in GRSM. Based on these maps, we identified the key regions and temporal periods of hemlock defoliation. In particular, majority of the hemlock decline were found to start from 2003 and 2006 in GRSM. We also compared the similarities and differences in disturbance patterns between hemlock dominant forests and hemlock mixed forests. In addition to the abrupt disturbance caused by HWA infestation, we observed gradual forest decline within hemlock dominant or mixed forests, which might be caused by other disturbance factors or data inconsistency. Our study provides an initial effort of monitoring the consistent hemlock change across the entire GRSM in the long term. However, due to the lack of historical field measurements, Chapter 2 simply applied relative methods to assess the results of this study, which might not be enough to quantify the overall performance of our methods and outputs. In addition, although we identified the defoliation caused by 2011 tornado outbreak in eastern GRSM, this study didn't examine the impacts of other potential factors that might drive gradual loss of hemlock forests in in detail.

Chapter 3 evaluated the burn severity distribution for the 2016 Chimney Tops 2 Fire in GRSM and explored the impacts of related environmental factors on the severity. We mapped the spatial distribution of four indices one year after the fire, including differenced Normalized Burn Ratio (dNBR), Relative dNBR (RdNBR), differenced Normalized Difference Vegetation Index (NDVI) and differenced Soil Adjusted Vegetation Index (dSAVI). All four indices derived from 30m Landsat imagery data have shown good performances in distinguishing multiple burn severity levels, although differences still exist in local regions. Among all the vegetation communities affected by this fire, the Mesic Oak/Hardwood Forests have the largest burned area and the Xeric Oak/Hardwood Forests and Northern Hardwood Forests have the most severe burn severity when compared to other communities. We also found that the topographic and vegetation conditions showed more significant impacts on the spatial distribution of burn severity when compared to weather conditions. In particular, aspect index and vegetation greenness values tended to have the most influences on the severity levels.

Although the Burned Area Emergency Response (BAER) team has obtained some measurements of burn severity within one month after the fire, this is not enough for accurately mapping the detailed burn severity distribution. Field measurements like Composite Burn Index (CBI) should be collected consistently to assess the severity pattern and to monitor the recovery trend in the long run. In addition, despite the fact that weather conditions were not identified as significant factors in our burn severity modeling results, this could be caused by the coarse weather observations from 1-km Daymet product and very limited weather stations inside the study area. Weather simulation results generated from numerical weather forecasting models could be another data source to assist the estimation of fire weather indices with higher spatial resolution in the mountainous GRSM.

Based on our current results and analyses in this thesis, we see some future opportunities for monitoring GRSM disturbances in the long run. The launch of Landsat 8 satellite in 2013 and Sentinel-2 satellites in 2015 and 2017 has enable the next stage of moderate resolution observations for global forest ecosystem in the long run. With improved performances in spatial resolution, temporal coverage and radiometric resolution, large spatiotemporal scale monitoring of abrupt or gradual disturbance events in GRSM and preparation of management policies will certainly benefit from these new missions. In addition, understanding the roles of environmental factors in driving HWA infestation on hemlock trees is of great importance in assisting the HWA control efforts in HWA. Koch et al. (2006) previously modeled the infestation risks of hemlock trees in GRSM through the analysis of field sites and found the connectivity provided by road or trail networks and riparian corridors to be the most importance factor that lead to HWA infestation. The relationships between environmental factors and HWA infestation could be further evaluated and explored in large scale with hemlock decline maps developed in this study. Moreover, we should also examine historical fires in GRSM to understand the drivers of burn severity in GRSM and their impacts on local communities.

References

Dale, V. H., Joyce, L. A., Mcnulty, S., Neilson, R. P., Ayres, M. P., Flannigan, M. D., Hanson, P. J., Irland, L. C., Lugo, A. E., Peterson, C. J., Simberloff, D., Swanson, F. J., Stocks, B. J., & Wotton, B. M. (2001). Climate Change and Forest Disturbances: Climate change can affect forests by altering the frequency, intensity, duration, and timing of fire, drought, introduced species, insect and pathogen outbreaks, hurricanes, windstorms, ice storms, or landslides. Bioscience, 51(9), 723-734.

Hansen, M. C. C., Potapov, P. V, Moore, R., Hancher, M., Turubanova, S. A. a, Tyukavina, A., Thau, D., Stehman, S. V., Goetz, S. J., Loveland, T. R., Kommareddy, A., Egorov, A., Chini, L., Justice, C. O., & Townshend, J. R. G. (2013). High-Resolution Global Maps of 21st-Century Forest Cover Change. Science, 342(November), 850–854.

Harmon, M. E., Bratton, S. P., & White, P. S. (1985). Disturbance and vegetation response in relation to environmental gradients in the Great Smoky Mountains. Plant Community Ecology: Papers in Honor of Robert H. Whittaker, 55(3), 129–139.

Kerr, J. T., & Ostrovsky, M. (2003). From space to species: Ecological applications for remote sensing. Trends in Ecology and Evolution, 18(6), 299–305.

Koch, F. H., Cheshire, H. M., & Devine, H. A. (2006). Landscape-Scale Prediction of Hemlock Woolly Adelgid, Adelges tsugae (Homoptera: Adelgidae), Infestation in the Southern Appalachian Mountains. Environmental Entomology, 35(5), 1313–1323.

Pyle, C. (1988). The type and extent of anthropogenic vegetation disturbance in the Great Smoky Mountains before National Park Service acquisition. Castanea, 53(3), 183–196.

APPENDIX I

LIST OF ACRONYMS

	Acronym	Full description
A	AVHRR	Advanced Very High Resolution Radiometer
B	BARC	Burned Area Reflectance Classification
	BAER	Burned Area Emergency Response
	BUI	Buildup Index
C	CBI	Composite Burn Index
	CFFDRS	Canadian Forest Fire Danger Rating System
D	DC	Drought Code
	DEM	Digital Elevation Model
	DMC	Duff Moisture code
	DN	Digital Number
	dNBR	differenced Normalized Burn Ratio
	dNDVI	differenced Normalized Difference Vegetation Index
	dSAVI	differenced Soil Adjusted Vegetation Index
	DOQQs	Digital Orthophoto Quarter Quadrangles
E	EOS	Earth Observing System
	ETM+	Enhanced Thematic Mapper Plus
	EVI	Enhanced Vegetation Index
F	FFMC	Fine Fuel Moisture Code
	FWI	Fire Weather Index
G	GIS	Geographic Information Science
	GRSM	Great Smoky Mountains National Park
H	HRG	High Resolution Geometrical
	HWA	Hemlock Woolly Adelgid
I	IQR	Interquartile Range
	IRMA	Integrated Resource Management Applications
	ISI	Initial Spread Index
L	LAI	Leaf Area Index
	LaSRC	Landsat 8 Surface Reflectance Code
	LEDAPS	Landsat Ecosystem Disturbance Adaptive Processing System
	LiDAR	Lightning Detection and Range
M	MODIS	Moderate Resolution Imaging Spectroradiometer
N	NAPP	National Aerial Photograph Program
	NASA	National Aeronautics and Space Administration
	NBR	Normalized Burn Ratio
	NDMI	Normalized Difference Moisture Index
	NDVI	Normalized Difference Vegetation Index
	NED	National Elevation Dataset
	NFDRS	National Fire Danger Rating System

	NIR	Near Infrared
	NPS	National Park Service
O	OLI	Operational Land Imager
	OOB	Out-of-bag
P	PCA	Principle Component Analysis
R	RdNBR	Relative differenced Normalized Burn Ratio
	RH	Relative Humidity
S	SARVI	Soil and Atmospheric Resistant Vegetation Index
	SAVI	Soil Adjusted Vegetation Index
	SLC	Scan Liner Corrector
	SVP	Saturation Vapor Pression
	SWIR	Shortwave Infrared
T	TC	Tasseled Cap
	TM	Thematic Mapper
	TOA	Top-of-atmosphere
	TPI	Topographic Position Index
	TRI	Topographic Ruggedness Index
	TSI	Topographic Shape Index
	TWI	Topographic Wetness index
U	UNESCO	United Nations Educational, Scientific and Cultural Organization
	USDA	United States Department of Agriculture
	USGS	United States Geological Survey
	UTM	Universal Transverse Mercator
V	VP	Vapor Pressure
W	WHO	World Health Organization

APPENDIX II

OVERSTORY VEGETATION COMMUNITIES AND RELATED CODE IN GRSM

MENTIONED IN THIS THESIS

Code	Main Class	Sub Class
CHx, CHx-T	Southern Appalachian Cove Hardwood Forests	Southern Appalachian Cove Hardwoods, Typic (with Hemlock)
CHxA, CHxA-T	Southern Appalachian Cove Hardwood Forests	Southern Appalachian Cove Hardwood, Acid type (with hemlock)
CHxL-T	Southern Appalachian Cove Hardwood Forests	Southern Appalachian Cove Hardwoods, Liriodendron dominated, lower slope (with Hemlock)
CHxR	Southern Appalachian Cove Hardwood Forests	Southern Appalachian Cove Hardwood, Rich type
HI	Human Influence	Human Influence
Hth	Southern Appalachian Heath Balds	Southern Appalachian Heath Balds
Hx	Southern Appalachian Early Successional Hardwoods	-
HxA-T	Southern Appalachian Mixed Hardwood Forest, Acidic	Red Maple-Sweet, Yellow Birch-Fraser Magnolia-Blackgum-Sourwood / Rhododendron Submesic
HxB-T	Southern Appalachian Early Successional Hardwoods	Broad Valley Sweet Birch Type (may have Hemlock) Shared association with Southern Appalachian Acid Cove Hardwoods
HxL-T	Southern Appalachian Early Successional Hardwoods	Tuliptree-Red Maple-Sweet-Birch-(Black Locust), Liriodendron Successional Type (may have Hemlock)
HxBl/R	Southern Appalachian Mixed Hardwood Forest, Acidic	Southern Appalachian Sweet Birch/ Rhododendron
HxL	Southern Appalachian Early Successional Hardwoods	Tuliptree-Red Maple-Sweet Birth-(Black Locust)
K	Shrub Understory	Kalmia latifolia (mountain laurel)
MAL, MAL/T, MAL-T	Montane Alluvial Forest	Montane Alluvial Forest
MALc	Montane Alluvial Forest	American Hornbeam Thicket
MALt	Montane Alluvial Forest	Sycamore-Tuliptree- (Yellow, Sweet Birch)/ Alder-American Hornbeam; Large River Type
MOa	Montane Xeric White Oak/ Kalmia-Deciduous Ericaceous Woodland	Montane Xeric White Oak/ Kalmia-Deciduous Ericaceous Woodland
MOr	Montane Northern Red Oak	Montane Northern Red Oak
NHx, NHx-T	Southern Appalachian Northern Hardwoods	-
NHxA-T	Southern Appalachian Northern	Southern Appalachian Mixed Hardwoods/

	Hardwoods, Acidic	Rhododendron, Acid type
NHxB, NHxB/S, NHxB-T	Southern Appalachian Northern Hardwoods	Southern Appalachian Northern Hardwoods, Yellow Birth type
NHxR, NHxR-T	Southern Appalachian Northern Hardwoods	Southern Appalachian Northern Hardwoods, Rick type
NHxY	Southern Appalachian Northern Hardwoods	Southern Appalachian Northern Hardwoods, Typic type
OcH	Submesic to Mesic Oak/ Hardwoods	Chestnut Oak type
OmH	Submesic to Mesic Oak/ Hardwoods	Submesic to Mesic Oak/ Hardwoods
OmHA	Submesic to Mesic Oak/ Hardwoods	White Oak- (Red Oak-Chestnut Oak)-Hickory, Acid type
OmHL	Submesic to Mesic Oak/ Hardwoods	Red Oak-Red Maple type, Liriodendron co-dominant
OmHp/R	Submesic to Mesic Oak/ Hardwoods	Chestnut Oak-(Red Maple-Red Oak)/ tall Rhododendron
OmHr	Submesic to Mesic Oak/ Hardwoods	Red Oak-Red Maple-Mixed Hardwoods Type
OmHR	Submesic to Mesic Oak/ Hardwoods	Red Oak-(White Oak, Chestnut Oak, Scarlet Oak)-Hardwoods/ Herbaceous, Rich type
OzH	Chestnut Oak/ Hardwoods	Chestnut Oak-Red Maple-Scarlet Oak
OzH/PI, OzH/PIp	Chestnut Oak/ Hardwoods	Chestnut Oak-Red Maple-Scarlet Oak/ Mountain Laurel Xeric Ridge/ Slope Woodland
OzHf	Chestnut Oak/ Hardwoods	Chestnut Oak-Red Maple/ Sourwood/ Herbaceous Forest
P	Cultivated/ pasture/ old-field	Cultivated/ pasture/ old-field
PI	Southern yellow pine species in xeric woodlands	Southern yellow pine species in xeric woodlands
PI/OzH, PI-OzH	Southern yellow pine species in xeric woodlands	Blue Ridge Pitch Pine-Table Mountain Pine Woodland
PIs-T	Eastern Hemlock – Eastern White Pine/ Rhododendron	-
R	Shrub Understory	Rhododendron sp., generally R. maximum
RD	Road	Road
S	Red Spruce	Red Spruce
S/F	Red Spruce - Fraser Fir	Red Spruce - Fraser Fir
S/NHx, S/NHxB	Red Spruce-Yellow Birch- (Northern Hardwood)	Red Spruce-Yellow Birth- (Northern Hardwood)/ Shrub/ Herbaceous
S/R	Red Spruce	Red Spruce/ Rhododendron
S/T, S-T, S-T/R, T/S	Red Spruce-Hemlock/Rhododendron	Red Spruce/ Hemlock
SV	Sparse vegetation	Sparse vegetation
T, T/R, T/K	Eastern Hemlock	-
T/NHxA	Eastern Hemlock/ Southern Appalachian Mixed Mesic Acid Hardwoods	-
T/NHx, T/NHxB	Eastern Hemlock/ Yellow Birch/	-

	Rhododendron-(Northern Hardwoods)/ Rhododendron	
T/MAL	Montane Alluvial Forest	Hemlock/ Montane Alluvial Hardwoods and Broad Valley Acid Code Hardwoods
T/CHx	Southern Appalachian Cove Hardwoods	Southern Appalachian Cove Hardwoods, Typic (with Hemlock)
T/CHxA, T/HxL	Southern Appalachian Cove Hardwoods	Southern Appalachian Cove Hardwoods, Acid Type (usually with Hemlock)
T/PIs	Eastern Hemlock - Eastern White Pine/ Rhododendron	-
V	Montane Grape Vine Opening	Montane Grape Vine Opening
W	Water	Water